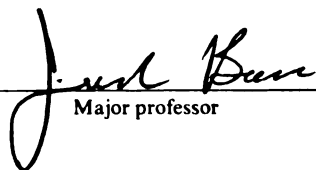This is to certify that the

dissertation entitled

AN EXPERIMENTAL INVESTIGATION OF THE ELECTRONIC
TRANSPORT PROPERTIES OF MOLTEN PURE METALS AND ALLOYS

presented by

Harold Scot Schnyders

has been accepted towards fulfillment
of the requirements for

___Ph.D.___ degree in ___Physics___

_____
Major professor

Date _12 - 18 - 97_

LIBRARY
Michigan State
University

PLACE IN RETURN BOX
to remove this checkout from your record.
TO AVOID FINES return on or before date due.

DATE DUE	DATE DUE	DATE DUE

AN EXPERIMENTAL INVESTIGATION OF THE ELECTRONIC TRANSPORT
PROPERTIES OF MOLTEN PURE METALS AND ALLOYS

By

Harold Scot Schnyders

A DISSERTATION

Submitted to
Michigan State University
in partial fulfillment of the requirements
for the degree of

DOCTOR OF PHILOSOPHY

Department of Physics and Astronomy

1997

ABSTRACT

AN EXPERIMENTAL INVESTIGATION OF THE ELECTRONIC TRANSPORT PROPERTIES OF MOLTEN PURE METALS AND ALLOYS

By

Harold S.Schnyders

A complete description of the nature of chemical ordering and it's effects on the conductivity and thermopower in molten metals has not been developed, in part due to an incomplete body of experimental evidence. In our studies, we seek to augment and verify existing electronic transport property data for molten pure metals and alloys, and to examine our results in light of recent experimental results and theoretical considerations. Our experiments have revealed a previously unseen peak in the conductivity in the liquid semiconductor Ag-Te near Ag_2Te, comparable to similar features seen in Ag_2Se and Ag_2S, and also possibly associated with the persistence of local ordering that enhances electronic conduction. We have also measured the metallic resistivity and thermopower of the weakly covalent pure liquids silicon and germanium, and have developed a successful containment technique for the former, highly corrosive liquid. Finally, we have found low resistivity, but negative temperature coefficient, in liquid Cu-Ce near the congruently melting solid compound Cu_6Ce; further interpretation with neutron diffraction suggests that crystalline-like short range order decomposing with temperature leads to this effect. The latter two studies are especially important in that they demonstrate that weak ordering is not incompatible with metallic conduction.

ACKNOWLEDGEMENTS

TABLE OF CONTENTS

LIST OF TABLES

LIST OF FIGURES

INTRODUCTION

This dissertation will explain our experimental determination of the resistivity and

thermopower of several pure liquid metals and alloys of current interest, and will also

explain our atomic structural study of one of the alloys (liquid Cu_6Ce). The last several

decades of research have revealed that the liquid is a far more ordered environment than

thought earlier. Ionic bonding has in some cases been shown to result in atomic clusters,

some as large as 10 Å. Such strong ordering powerfully influences the electronic

behavior, often resulting in behavior commonly associated with conduction near an

energy gap in the density of states (see Enderby and Barnes [1] for a complete review).

The liquids chosen for study in this work are meant to elucidate the effects of *weak*

ordering on the electronic properties; the lifetimes of the associations that we describe as

weakly bonded are perhaps shorter, and fewer atoms at any particular time participate.

The bonding in the solid compounds that melt to these liquids is more covalent than

ionic, in most cases. It is expected that the effects on the electronic or atomic structural

properties will be weaker and harder to detect in these systems, and therefore represent a

class of liquids perhaps inadequately experimentally characterized, and not at all

completely explained theoretically. Although the materials we've studied come from

various areas of the periodic table, and as a whole do not comprise a systematic study of

one narrow family of compounds, the various metals and alloys in this thesis have all

1

proven to be at the fringes of our understanding of liquids.

Some of the earliest attempts to understand liquid metals had at their roots Nearly Free Electron theory, and the associated assumption that the potentials felt by plane wave like electrons in metals are weak enough to be treated by perturbation theory. In this case, the plane waves are disrupted by the disorder in a material, and the resistivity and thermopower are directly related to the structure. In fact this formalism, first proposed by Ziman [2], has successfully described many simple pure liquid metals, and the extension of the theory by Evans [3] has been adequate in some cases presumed far more difficult, such as the pure liquid transition metals and rare earths, whose semi full shells of d and f electrons made it far from apparent that weak scattering theory was appropriate. The success of the theory in practice, however, is certainly influenced by the application of accurate structural data and suitable pseudopotentials. Binary alloys of the simple metals with one another have largely been correctly described by the theory as well, by expanding the formula to involve the three partial structure factors in such cases. The theory has even correctly predicted the observed negative temperature coefficient in divalent liquid metals and alloys.

Another class of liquids exists, however, for which weak scattering is clearly unsuitable, namely liquid semiconductors and liquid semi-metals, of which the ionic alloys are a part; for these one must retreat to the Kubo Greenwood (KG)[4] formalism. Such formalism dates to approximately the time of Ziman's formulation, but is far more general, and may be used carefully in cases where the large resistivity would suggest that the Fermi Energy is near or in an energy gap in the density of states. This theory incorporates an energy dependant conductivity, $\sigma(E)$, and the energy derivative of the

Fermi function (a more complete description is given in the Ag-Te section of this thesis). The shape of $\sigma(E)$ is subject to some debate, but the metallic approximation $\sigma(E) \propto N(E)^2$ is often used, and the density of states at the edge of a band is often assumed to be free electron like, and proportional to $E^{1/2}$. Some early attempts at the conductivity and thermopower integrals of this theory result in analytic expressions for conductivity and thermopower, but these use the Boltzmann approximation for the electron energy distribution, and render these results of limited validity (for example, they are not to be used in cases where the Fermi energy is near the band edge). Enderby and Barnes have recently relied on numerical integration to evaluate the integrals using the full Fermi distribution and a linear dependance of $\sigma(E)$ near the band edges. This has led to a highly successful and much referenced method of wide applicability for calculating the transport properties of liquid semiconductors.

As suggested earlier, there remain liquid metals that fall in between these explanations, and several of the subject materials of this thesis are a sampling of this group. However, Ag_2Se and Ag_2S are semiconducting solids that melt into liquids with even poorer conductivity, and one might expect that the Kubo Greenwood equations could adequately characterize these liquids. Surprisingly, at the stoichiometric concentration in these liquids, the conductivity is enhanced with respect to surrounding concentrations of Ag and chalcogenide, and a metallic (negative) temperature dependance of the conductivity is observed. This anomalous behavior is confined to a narrow region around the stoichiometric compound; it has never been observed in the chemically very similar Ag_2Te, which we systematically examine in a similar concentration range. We add our results to the considerable recent experimental work that exists on the

connection between ionic mobility and the enhanced electronic conductivity in these materials.

The transition in liquid Si and Ge from the crystalline semiconducting state to metallic liquid is a poorly understood topic of great current interest. During this transition, the number of nearest neighbors for an average Si only changes from 4 to roughly 5.8, and the liquid structure as measured by neutron [5] and X-ray [6] scattering reveals evidence for ordering strongly reminiscent of the tetrahedral networks in the crystalline materials. In the liquids context, ordering does not mean long lived molecules, but rather short lifetime associations of atoms, where lifetime is measured in terms of the frequency of random thermal motions. Significant progress has been made in the area of ab-initio calculations; the bond lifetimes in liquid Si have been estimated in computer simulations to be about 0.1 ps, and approximately 30% of Si atoms are bonded at any one time. In spite of recent computational insight into these liquids, considerable difficulty surrounds the containment of liquid Si, which has hampered actual physical measurements. We have successfully developed a new containment technique for this material, and utilize it to measure accurately the resistivity and thermopower.

Finally, liquid Cu_6Ce shows signs of ordering in neutron diffraction experiments, with a diffraction peak at low momentum transfer corresponding to correlations on a length scale as large as 4.4 Å; yet the resistivity is curiously featureless, except for the temperature coefficient of the resistivity, which is sharply negative at the concentration Cu_6Ce, a concentration corresponding to a crystalline compound which exists up to the melting point. Cu-Ce and Ag-Ce appear to be alloys in which Chemical Short Range Order (CSRO) and metallic conduction coexist, and in this way are members of a still

very small, largely unexplored class of alloys.

Early characterization of the pure metals and alloys in this thesis has often been limited to the conductivity, and our studies improve the accuracy and quantity of the data for this important property. However, in many cases, the thermopower has not been measured, because of the inherent difficulty. High temperature thermopower standards for measurements have been in existence for decades, but were often extrapolated from lower temperature data. Recent measurements at high temperature (1500 C°) of the thermopower of Pt by Roberts [7], utilizing the measurement of Thompson heat, has established a reliable standard. The thermopower is very important in liquid semiconducting systems, as theory indicates that the positive-negative transition in the thermopower seen in many such systems provides a direct way to measure the width of the energy gap. Thermopower is also readily calculated for weak scattering pure metals and alloys from the Ziman theory. We present new experimental results for thermopower for the liquid copper lanthanides and for silver cerium, as well as for pure liquid silicon. We also present data for liquid Ag-Te, including thermopower in the immiscible region below 31 at. % Te.

All of the results presented in this thesis are discussed in light of the current theories, and where possible, calculations have been done to test the applicable theories. Liquid Si and Ge have been treated with Ziman formalism, using a recent pseudopotential to calculate resistivity and thermopower; Ag-Te has been modeled with the Kubo Greenwood formula. Cu-RE and Ag-Ce are discussed in light of recent experimental evidence of the subtle effects of CSRO on the transport properties. It will be seen throughout this work that significant gaps exist in the theoretical description of liquids; it

is our hope that this work will provoke fresh thought on these subjects.

This thesis includes both a descriptive section for each of the studies undertaken, and a copy of the publication or manuscript (as accepted for publication) of the same study. In each case, the descriptive section is provided to augment the information available in the publication. Both should be read, however, to provide the full picture of each study.

I. Silver-Tellurium alloys

A. Review of the Silver Chalcogenides

Liquid chalcogens have been of long term interest because of the unusual

properties they possess. Se and S are semiconducting liquids, while liquid Te has quite

metallic conduction. Scattering experiments on the pure liquids have revealed evidence

that may be interpreted as short lived structural units like short chains (Se, Te) [8]; the

presence of these units is intimately tied to the rich behavior of the electronic transport

and atomic structural properties as the chalcogenides are alloyed with each other, and

with other elements of the periodic table. Of particular recent interest are the electronic

and atomic structural properties of the chalcogens alloyed with the noble metals; the pure

noble metals are well described structurally by hard sphere packing of atoms, and are

very fine metallic conductors, and are considered in pure form to be monovalent. Ab

initio studies of liquid Ag-Se alloys [9], for example, have demonstrated the gradual

change from non bonding liquid to bonded networks as Se content is increased from 33

to 65 at. %, and have provided new understanding of the transition from metallic

conduction to semiconducting behavior as chalcogenide is added.

The electronic transport properties of liquid alloys of Ag with the chalcogens

around the composition Ag_2X, where X = S, Se, are particularly surprising, and

significantly different than, for example, the compounds around Cu_2X . In the latter

compounds the conductivity, σ, is clearly semiconducting ($\sigma < 500 \ \Omega^{-1} \ cm^{-1}$), with $\sigma=40$

$\Omega^{-1} \ cm^{-1}$ and $160 \ \Omega^{-1} \ cm^{-1}$ for S and Se compounds, respectively, and is at a minimum at

stoichiometry [1]. This behavior, as well as a positive temperature coefficient of the

conductivity, is rather typical of a liquid semiconducting alloy. In contrast, systematic

7
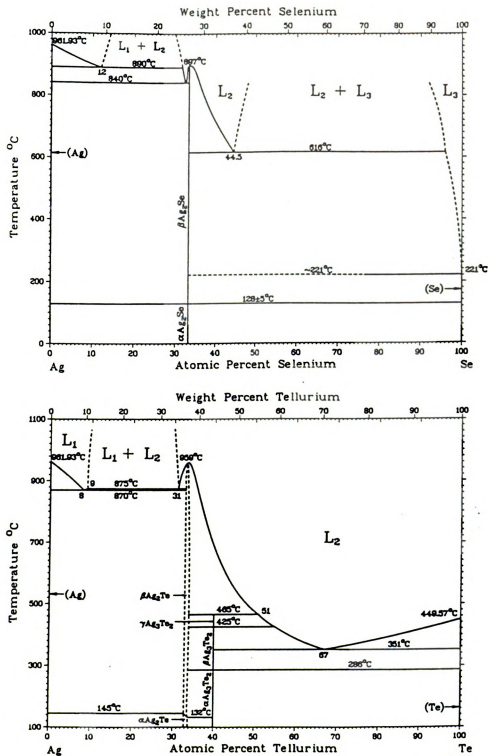
Figure 1 - The phase diagrams for Ag-Te and Ag-Se alloys, from [59].

studies in the neighborhood of Ag_2X [10,11] (The phase diagram shows a peak in the

melting curve and a congruently melting solid compound at this concentration (Figure

1).) have revealed an unexpected rise in the conductivity to a sharp peak that is about

200 $\Omega^{-1}cm^{-1}$ in height at 900°C and approximately 4 at. % wide, and centered on

stoichiometry (Figure 2); this peak decreases to 100 $\Omega^{-1}cm^{-1}$ in height by 1000° C. The

peak in conductivity is accompanied in this narrow concentration range by a negative

temperature coefficient, which becomes positive further from stoichiometry on either

side. According to earlier electronic transport studies on Ag-Te [12,13,14], Ag_2Te

behaves in the former more common fashion. We note, however, that in the earliest

study of liquid Ag-Te, Dancy [12] lacked the ability to stir the alloy, and further was

unable to probe the presumed immiscible region immediately below stoichiometry

(Figure 2). The more recent re-examination of Ag-Te by Okada et.al. [13] was conducted

over a broad and widely spaced range of concentrations, even in the critical neighborhood

of stoichiometry. The data of the final study by Ohno et.al.[14], while covering a finer

grid of points than in [13], is still sufficiently sparse to have missed narrow and small

features; furthermore, no details are given as to the measurement of properties within the

previously mentioned immiscible region.

Recent structural studies by Price et al. [15] on liquids Ag_2Se and Ag_2Te revealed

a remarkable similarity between the structure factors of the liquids, although a prepeak at

about 1.8 $Å^{-1}$ in the structure factor of Ag_2Se was not seen in the Te compound. (This,

however, was attributed to the similarities in the scattering lengths of Ag and Te.)

There was no noticeable change in the positions or widths of the first coordination peak

in Ag-Se as temperature was varied, or as Se content was varied from 30-36 at. %,
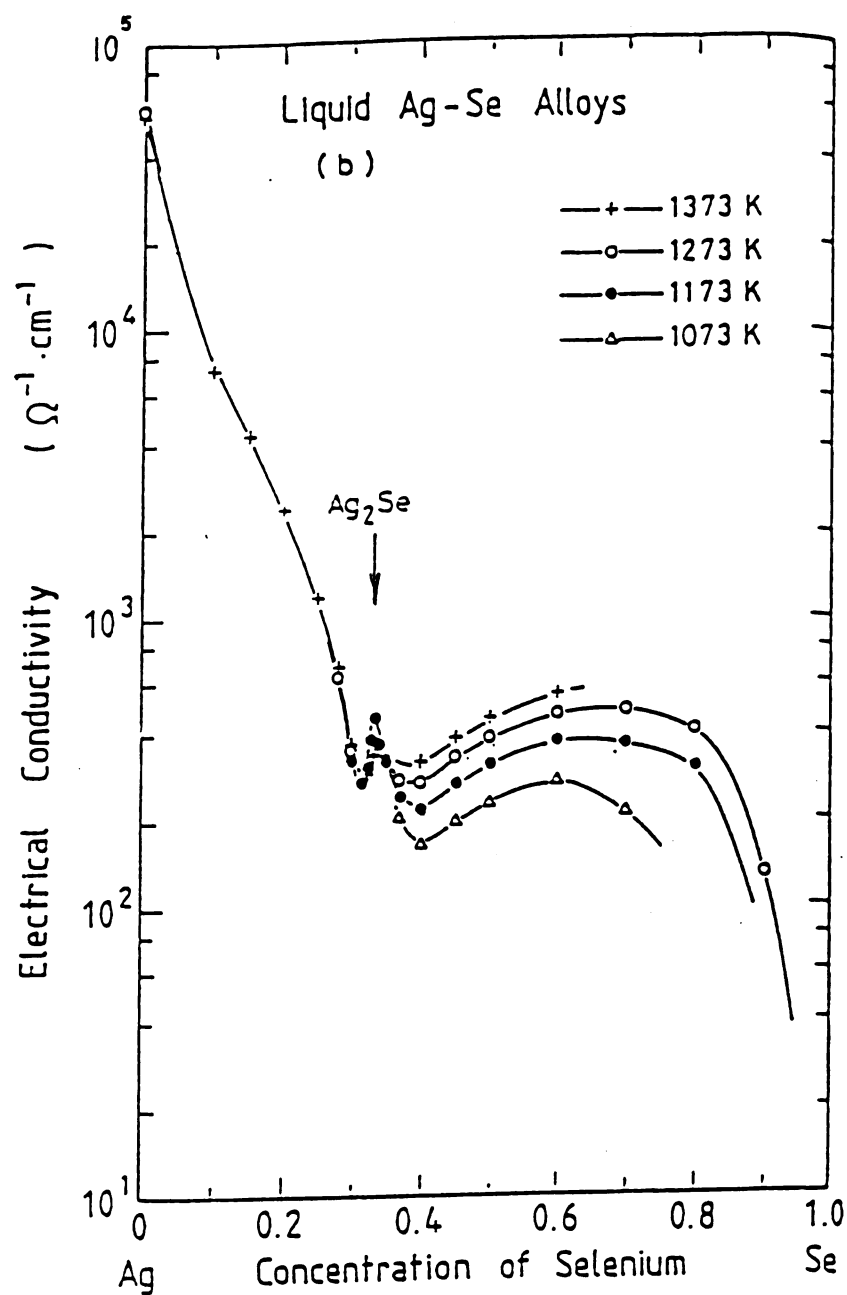
Figure 2 - The conductivity of liquid Ag-Se alloys, from Ohno *et.al* [11]

although a significant change was noted in coordination of Se around Ag. According to

the x-ray attenuation density measurements by Tsuchiya [16], however, it is possible

that an incorrect number density was used to calculate coordination. It has been

concluded that no sudden structural change with temperature or concentration causes

the anomalous electrical conductivity behavior.

Stoichiometric compounds of Ag with S, Se, and Te are all fast ion conductors in

the high temperature solid phases of the alloys; the ionic conductivity reaches values of

5-7 $\Omega^{-1}cm^{-1}$ for these solids [17]. Ionic conduction is by way of the Ag ions, which are

proposed to move by jumping between tetrahedral sites within a chalcogen lattice. A

picture of Ag jumping between chalcogen ion cages is used to describe the liquids as

well, since the ionic conductivity decreases by only ~30% upon melting [17], although Te

cages in Ag-Te had been thought to break up quickly with increasing temperature due to

the negative temperature dependence of the ionic conductivity in liquid Ag_2Te. Only very

recently has a full partial structure factor analysis of liquid Ag_2Se been completed by

Barnes et.al. [18] by the method of isotopic substitution and neutron diffraction. The

results show what was earlier postulated; that the Se-Se correlations are largely

responsible for the prepeak, and further that these distances are really quite similar to

those in the b.c.c. crystal from which the alloy melts.

The extreme asymmetry of the p-n transition of the thermopower revealed in the

data of Ohno et.al., and the variation of the conductivity with concentration make it clear

that the rigid band model is unsuitable for this system, as was similarly shown for Ag-Se

and Ag-S. In light of the structural similarities, and the comparable ionic conductivities

between solid and liquid Ag_2Se and Ag_2Te it is a serious question why AgTe should

behave so differently electronically near stoichiometry from the other silver

chalcogenides. We have therefore reexamined the well stirred liquid in fine concentration

steps.

B. Experimental Details

Our samples were contained in alumina (Al_2O_3) tubes, 24" long and closed on

one end. The tube is 0.315" outer diameter, and between 0.180" and 0.220" inner

diameter, the variation due to the nature of the casting process. Four holes were drilled

with a diamond drill bit into each tube, the first 7/8" above the closed end, and the others

spaced evenly from this hole 1 7/8" apart. The tubes were cleaned after drilling with a

brush in water to remove debris from the drilling process, and were then rinsed with

acetone. They were then calibrated at room temperature by tightly binding 0.002"

molybdenum foil over the holes, fastening four wires, one to each hole, and filling the

tube to a depth of ~6" with double distilled Hg. Current for the measurements is supplied

by an Hewlett Packard 6267B constant current supply, and to measure the current, the

voltage across a 0.01Ω standard resistor is measured. All voltages are read by a Kiethley

181 nanovoltmeter, with channel selection by a Kiethley 705 scanner and an external

computer. The resistance, R, of the mercury sample between the center holes was

measured using the conventional 4 probe DC resistance technique. The room

temperature resistivity of pure Hg is well known, and the tube constant is readily

calculated from the formula

$R = \rho L/A$

where ρ is the resistivity of the sample, and L and A are the effective length and cross

sectional area of the volume between the center holes, respectively. The tube constant

at high temperature was later computed accurately knowing the coefficient of thermal

expansion of alumina, $\kappa = 8.1 * 10^{-6} / C°$.

After calibration, the holes were plugged with machined cylinders of high density

Aeromet grade graphite, supplied by Electronic Space Products International (ESPI).

Typical impurities for this grade graphite are as follows, in ppm: Fe-100, V-100, Al-20,

Cu-5, Si-80, Ti-15, Ni-10. The plugs are held in place only by tight fit; however, we

have had no difficulty with cracking of the tubes or leaking due to the difference in

thermal expansion of the materials (Aeromet grade graphite $\kappa = 10.34 * 10^{-6} / °C$). Typical

tube preparation involves the sanding down of the fitted plugs until they stand < 0.004"

proud of the alumina, and encircling the tube over the plugs with molybdenum bands,

which serve as additional protection against leakage. The bands are made of 0.002" Mo,

and are secured by stainless steel screws, nuts, and clamps. The wires are held against

the Mo by one further band of 0.005" stainless steel, held by the same clamps, and chosen

for it's strength and resistance to corrosion.

The sample tube, and it's placement with respect to the various furnace coils, is

shown in Figure 3. The lifetime of the coils is affected by the surface loading

limitations (in watts/cm^2) of the heater wire (0.032" Kanthal$^○$ A-1 wire), and this

ultimately limits the highest temperature this furnace may achieve, about 1200°C, even

though the melting point of Kanthal is 1510°C. Kanthal is well suited to application in

air, as heating in this environment creates a protective oxide layer. Higher temperatures

can be attained in the same furnace with Mo wire, although much greater care with

regards to oxidation of the coils must be exercised. A 2" i.d. alumina tube surrounds the
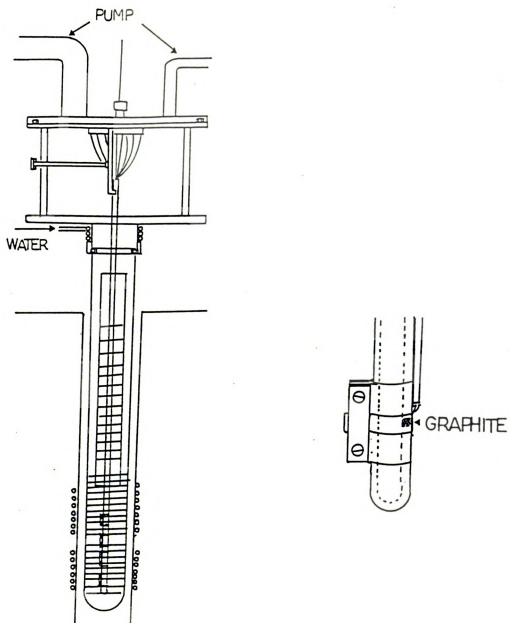
Figure 3 - A diagram of the furnace and sample tube.

sample tube, and is held in place by a water cooled brass collar and an O-ring. This tube has been threaded on the outside lower portion for easy and consistent placement of the supplementary heating coils, which are used to control the temperature during thermopower measurements. An IBM computer controls the duty cycles of the power supplies for the upper and lower coils, and can control the temperature of the bottom and top of the sample to ~0.1 C°. The bulk of the power delivered to the sample is from the main furnace, also of Kanthal, and divided into upper and lower coils. This is raised to surround the furnace tube during operation.

The resistivity measurements were done using the four probe DC technique. The upper and lower thermocouples are under normal circumstances 0.010" chromel-alumel from Omega Engineering, Inc. Under especially arduous experimental conditions, diameters as high as 0.020" have been used for greater temperature and corrosion resistance. The temperature of the upper and lower thermocouples are controlled to be the same during the resistivity measurement, but slight variations in the thermocouple material result in a small error in the temperature measurement (Omega, the manufacturer of the chromel and alumel wire, specifies that the temperature measured by these thermocouples is good to ±0.75%). A difference in temperature between the electrodes during a resistivity measurement would introduce an additional thermal emf to the measured voltage; contributions to the resistivity measurement are eliminated by reversing the current during the measurement, measuring the voltage in both directions, and taking the appropriate difference, thereby eliminating the thermoelectric emf.

Thermopower measurements are conducted in the following manner. The upper and lower portions of the sample are equilibrated in temperature , and the thermal voltage

is measured using chromel electrodes of the thermocouples . The temperature of the

upper portion of the sample is then ramped upward at a constant rate ($\sim 1\,°C/min$) while

the lower temperature is kept constant. At periods throughout the ramping, the thermal

voltage is measured and recorded. When 10-15 points have been taken, during which

time the temperature difference ΔT has reached $\sim 30\,°C$, a quadratic fit of the thermal

voltage as a function of ΔT is conducted, from which $S_{Relative}=dV/dT$ is extracted. The

thermopower of the sample may be calculated using the formula

$$S_{sample}= S_{chromel} \pm dV/dT$$

where the $\pm$ is determined only by the arrangement of the counterelectrodes at the input of

the voltmeter. The thermopower of Chromel has been measured in our lab [19] against

Cu and Pt, and is in excellent agreement with previous measurements [20]. This method

of thermopower measurement yields accurate results because of the smoothing effect of

the fit over numerous points, and allows the measurement of thermopower very near to

phase transitions.

The high vapor pressure of Tellurium did not appear to affect our measurements;

no condensed Te was found in the cooler regions of the sample tube. Samples are usually

stirred with 0.040" Mo wire; however, significant attack was noted on Mo stirring wires

for Te concentrations >34 at. %. For these concentrations, we changed to alumina stirring

rods. Ag and Te were of 99.99% and 99.999% purity, respectively (metals basis), and

were supplied by Aesar-Johnson Matthey Co. The sample concentration was not varied

continuously during the experiment to avoid even the possibility of progressive

contamination. The majority of the samples were independently prepared in separate

tubes from the pure materials, making most data points completely independent of all

others.

C. Results

Our results for the conductivity of Ag-Te are shown in Figure 4 , including for comparison the previous results for the higher Te concentration region by Ohno et al. [14]. Our data are in excellent agreement with those of Ohno et.al., except as stoichiometry is approached from the Te rich side, where our data fall noticeably below his for concentrations between roughly 36 and 45 at. % . An extrapolation of the curve fit to this data and the higher Te concentration data of Ohno et.al. reveals a peak in the conductivity in the neighborhood of stoichiometry; this peak is shown in Figure 5, and is about 60 Ω^{-1}-cm^{-1} in height at 960°C, which is comparable to but less than the ~100 Ω^{-1}-cm^{-1} at 1000°C seen in Ag$_2$Se. As with the other silver chalcogenides, dσ/dc is significantly steeper on the Ag rich side than on the Te rich side; however, the temperature coefficient of the conductivity is positive at stoichiometry, in contrast to the unusual negative temperature coefficient seen in Ag$_2$S and Ag$_2$Se. A positive temperature coefficient of the conductivity is expected in liquid semiconducting alloys, because the broadening of the Fermi distribution with temperature introduces more electrons into the conduction process.

We have extended the resistivity measurements into the immiscible region; an examination of the phase diagram marks 31 at. % to 9 at. % Te as the boundaries of the phase separation, with a sharply concentration dependent temperature boundary. One concentration, the liquid 30 at. % Te alloy, proved amenable to examination above and below the miscible-immiscible phase boundary. No time dependance of the conductivity
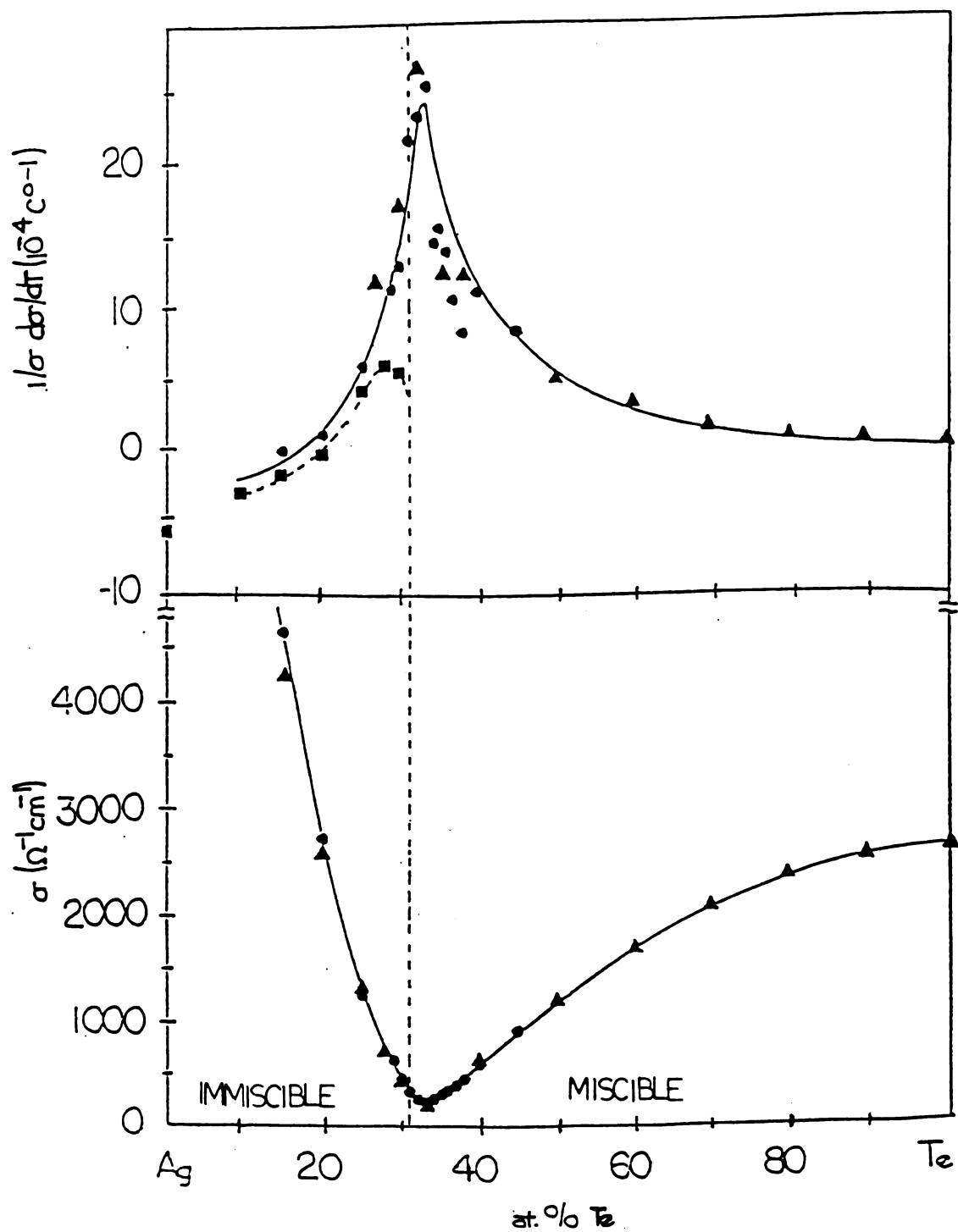
Figure 4 -   Current data for the conductivity of liquid Ag-Te at 950 C° - ●;
recent data for liquid Ag-Te at 1000 C°- ▲, from Ohno *et.al.* [14];
data for liquid Ag-Se from Ohno *et. al.* [11] - ■ .
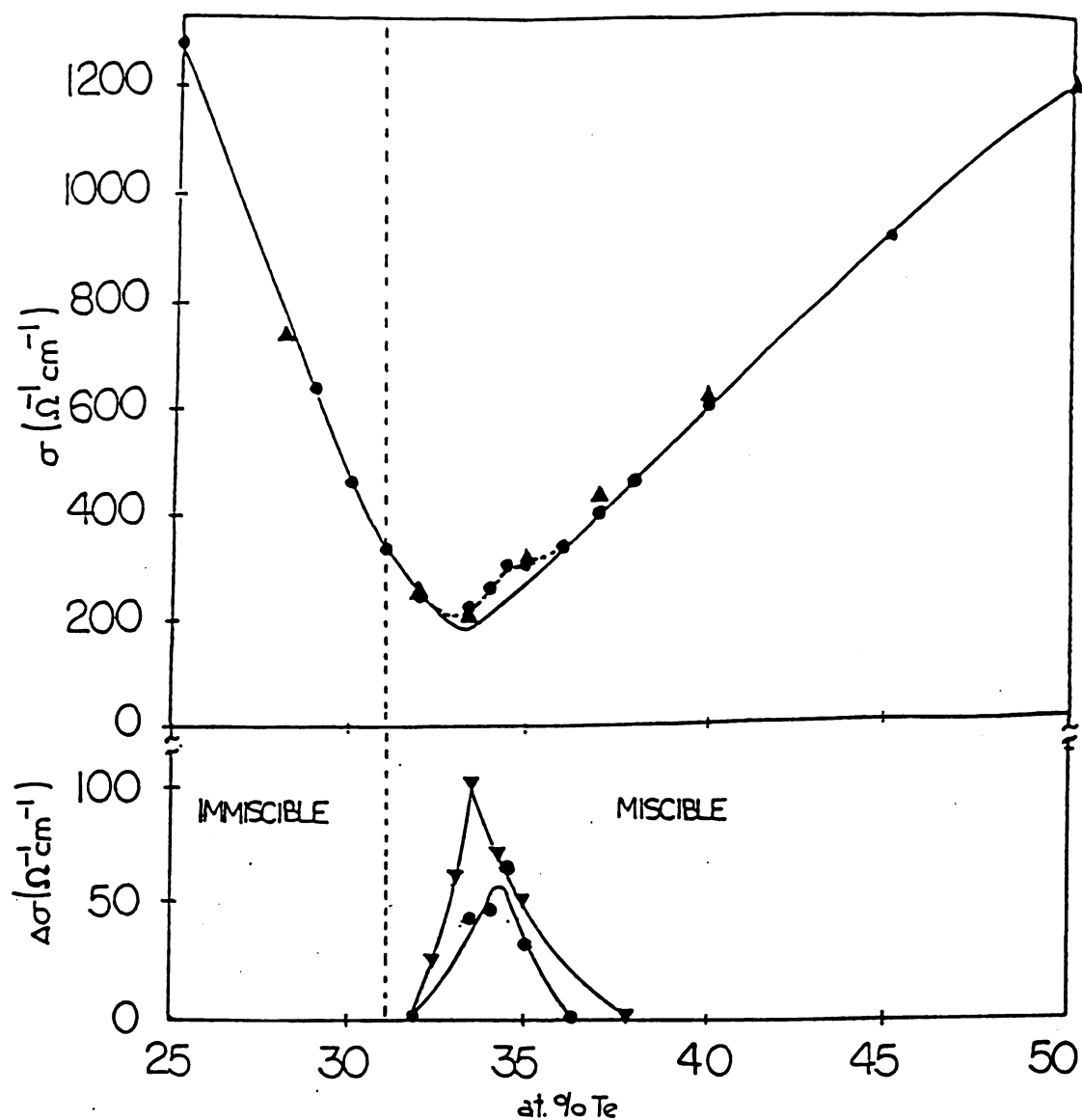
Figure 5 - Present data (●) and data of Ohno *et.al.* (▲) for the conductivity of Ag-Te in a narrow range of concentrations around stoichiometry. An extrapolation of our data and that of Ohno *et.al.* from outside the stoichiometric region drawn toward Ag₂Te demonstrates the presence of a peak in conductivity. In the lower half of the figure, the current peak data is compared to the peak seen by Ohno et.al. [11] in Ag-Se (▼). The boundary of the immiscible region is clearly marked to demonstrate that the peak is not a result of phase separation.

was seen in measurements taken at temperatures below the boundary of the immiscible region during a time period of up to 1 hr after the sample had been vigorously stirred and allowed to settle. In addition, no evidence for a sharp change in conductivity occurs at ~1075°C, or at any temperature up to 1150°C; such a change was taken as an indication of the immiscible-miscible transition in Ag-S and Ag-Se alloys (Figure 6). Nevertheless, we stir all of the samples at intervals of less than 1 hr to ensure homogeneity, although we believe that Ag-Te alloys are perhaps more stable than Ag-Se or Ag-S.

We also have measured the thermopower, including in the immiscible region (Figure 7). In Ag-Te, it is found that the thermopower never descends below -13 $\mu V/C°$ on the silver rich side of stoichiometry, in contrast to the highest extent that it reaches on the Te rich side, +120 $\mu V/C°$. In addition, the dramatic dip of the thermopower in Ag-S and Ag-Se that precedes the rapid change from negative to positive S is absent in Ag-Te. The steeply sloped, rapidly increasing conductivity σ(c) on the Ag rich side of stoichiometry and the shallow dS/dc and small |S| in the same range of concentration are very similar to the combination seen below 28 at.% Ag in Ag-S and Ag-Se. The temperature coefficient of the thermopower is positive in the silver rich region and at stoichiometry, as it is in Ag_2Se and Ag_2S, and it changes to negative as concentration passed to the Te rich side of stoichiometry.

Our thermopower data agree well with Ohno et.al. , except at concentrations in the neighborhood of the peak in the conductivity. Whereas in other regions the data of Ohno et.al. [14] fall consistently below ours by 4 $\mu V/C°$, in this region they exceed ours by as much as 25 $\mu V/C°$, a far greater difference than the estimated error of Ohno et.al., about 10 $\mu V/C°$, and also greater than the 3-5 $\mu V/C°$ we estimate for our data. (This estimate
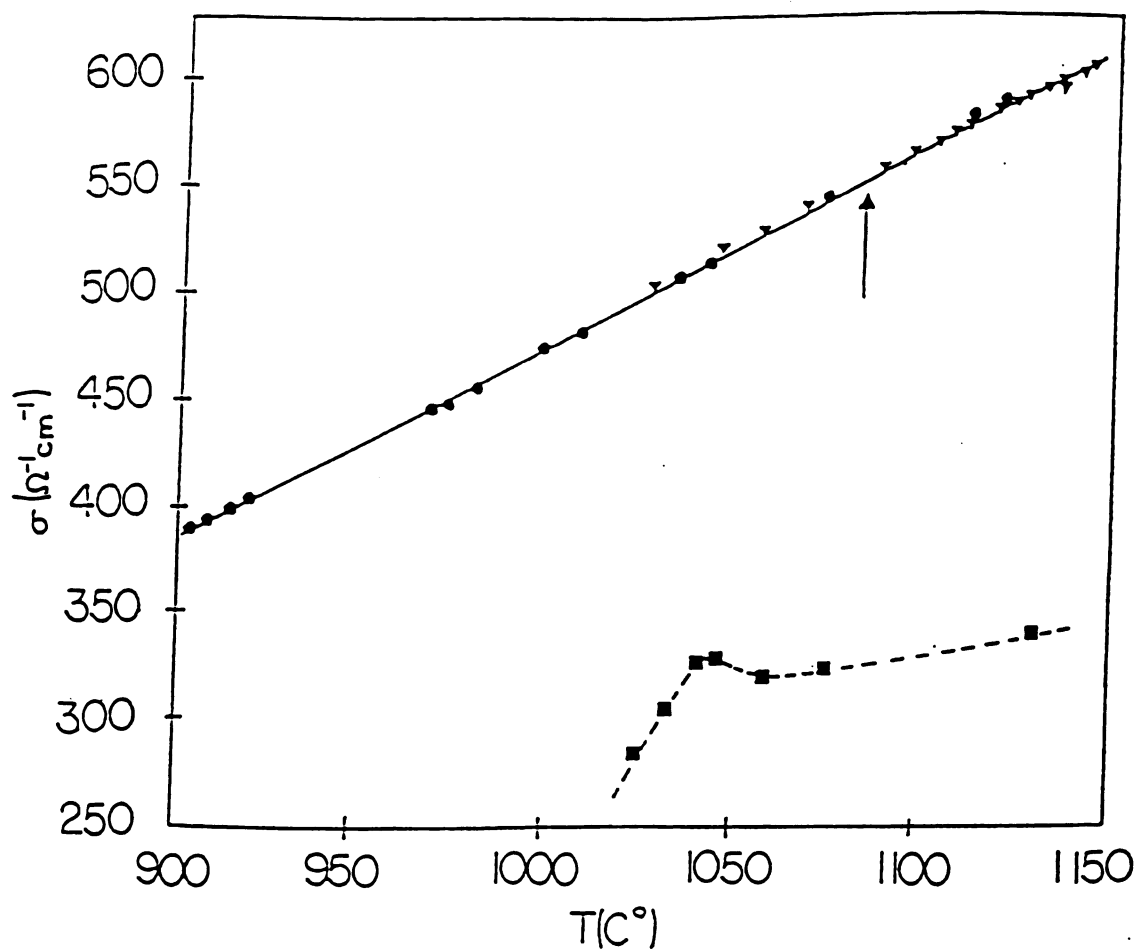
Figure 6 - Conductivity of two samples of $Ag_{.70}Te_{.30}$ as the temperature boundary
(arrow) of the miscible- immiscible region is crossed (current data for
two independent measurements on two samples of $Ag_{.70}Te_{.30}$- ● ▼), as
compared to the results of Ohno et.al. [10] for $Ag_{.705}S_{.295}$- ■ . (The
comparable miscible-immiscible boundary for $Ag_{.705}S_{.295}$ is at 1050°C.)
This demonstrates the apparent stability of liquid Ag-Te at temperatures
and concentrations within the immiscible region.
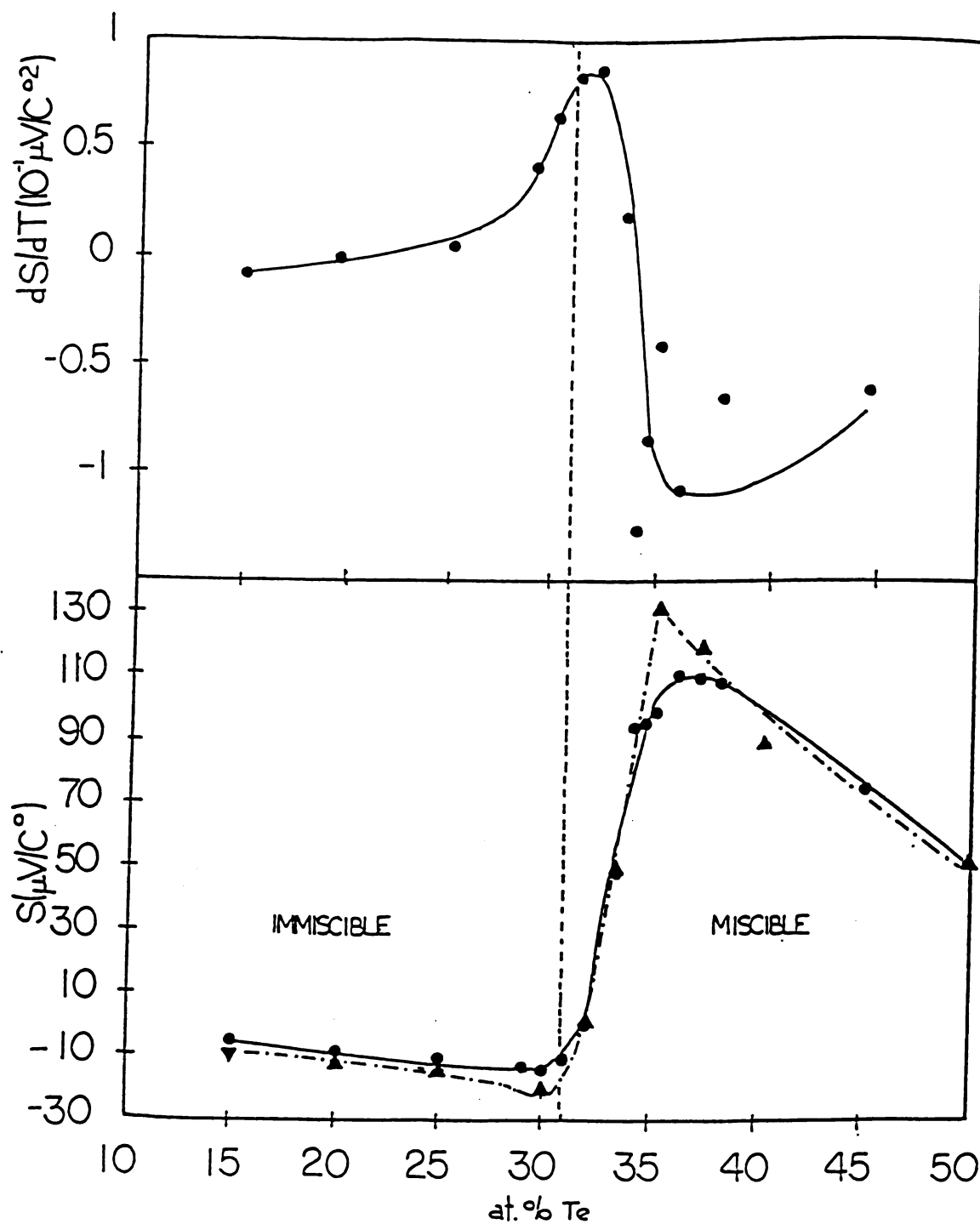
Figure 7 - Current results for the thermopower of liquid Ag-Te -● evaluated at
960°C, compared to the data of Ohno et.al [14]-▲at 950° C.
Significant differences greater than either experimental error exist in
the concentration range where the peak in the conductivity is seen.

is based on our experience with repeatability of measurements on separate samples of the

same concentration, and also on the scatter seen in a set of measurements on a given

sample.) The conductivity data in this concentration region are crucial to the

identification of the peak in the conductivity.

D. Discussion

For the majority of liquid semiconductors, numerical integration of the Kubo

Greenwood equations using the full Fermi function, as demonstrated by Enderby and

Barnes [1], can yield a good qualitative agreement with experimental data. The

equations are

$$\sigma = \int_0^\infty \sigma(E) \ \frac{\delta f(E)}{\delta E} \ dE$$

$$S = \frac{k}{e} \int_0^\infty \frac{\sigma(E)}{\sigma} \ \frac{E - E_f}{k_B T} \ \frac{\delta f}{\delta E} \ dE$$

In these equations, $\sigma(E)$ is the energy dependent conductivity , k_B is Boltzmann's

constant, and f is the Fermi function. The Fermi function is

$$f(E) = \frac{1}{exp^{\frac{-(E - E_f)}{k_B T}} + 1}$$

with E_f being the Fermi energy and T the absolute temperature of the material. It is

assumed that the shape of the bands is constant even as the concentration of the alloy is

changed, or in other words, that the bands are rigid. Early treatments using these basic

equations make two assumptions, the first of which is that near the energy gap $\sigma(E) \propto$

σ_0, a constant, but also that $\sigma(E)$ drops sharply to zero at the gap. A second assumption is that the Boltzmann approximation is valid ,

$$f(E) \approx \exp \frac{-(E - E_F)}{kT}$$

Both of these assumptions together lead to the recognized result

$$S = \frac{k}{e} \left[\frac{E_V - E_F}{kT} + 1 \right].$$

where E_V is the energy of the valence band edge. While the Boltzmann approximation is justifiable in situations where $E_f\text{-}E_V \gg k_BT$, it is not good for calculations near a conductivity edge, where the full Fermi function should be used, and results gained in this manner are of limited applicability.

Enderby et.al.[1] differ from these early attempts by making the reasonable assumption that $N(E) \propto E^{1/2}$ near the edge of the band, and that $\sigma(E) \propto (N(E))^2 \propto E$. An appropriate a choice of a simplified $\sigma(E)$ for valence and conduction bands is of the form

$$\sigma_c(E) = a_c[E - E_c]^\nu$$

$$\sigma_V(E) = a_V[E - E_V]^\nu$$

with E_V and E_c the valence and conduction band edges, respectively, and $\nu = 1$ in this case. Here, we use the following relation for band gap, $\Delta E = E_c\text{-}E_V$, and the variables a_c and a_V may be calculated using the band width, the atomic separation, and the total number of electron states per unit volume in the band [21].

Enderby and Barnes have shown that in liquid semiconductors where rigid band

formalism is applicable, the magnitude of $\Delta S = S_{max} - S_{min}$, where S_{max} and S_{min} are the

maximum and minimum observed thermopower, is directly related to the width, ΔE, of

the energy gap. Our data indicate $\Delta S = 130 \ \mu V/K$, which at 1233 K corresponds to $\Delta E \sim 0$

eV. Using the Kubo Greenwood formulas with $\Delta E \sim 0$ eV as a starting point, we have

done several tests to gauge the effects on the conductivity and thermopower of varying

the slope of the (linear) valence and conduction band edges, a_c and a_v. Some results of

numerical integration of the Kubo Greenwood formulas are shown in Figure 8, along

with the energy dependant conductivity used for each calculation. The conductivity is

given by

$$\sigma = \sigma_e + \sigma_h$$

where σ_e and σ_h are the contributions from electrons and holes, respectively. The

thermopower is calculated by a conductivity weighted average

$$S = \frac{\sigma_e S_e + \sigma_h S_h}{\sigma_e + \sigma_h}$$

with S_e and S_h the thermopower from electrons and holes. Quite apart from

reproducing the peak in the conductivity, we have found that there is no choice of a_c and

a_v that can simultaneously reproduce even the general features of conductivity and

thermopower together. Our tests, using a value of $a_c \sim 1300 \ \Omega^{-1} \ cm^{-1} \ eV^{-1}$, and a choice of

$a_c = 2a_v$ (This choice of asymmetry between conduction and valence bands is comparable

to that chosen for a similar calculation on Ag-Te [14].) can indeed roughly reproduce the

magnitude and asymmetry of $\sigma(c)$ in the concentration range around stoichiometry, and a

thermopower that rises to a maximum of roughly 150 $\mu V/C°$ on the Te rich side.

However, with this choice of $\sigma(E)$, the minimum of $\sigma(c)$ and the p-n transition of S(c) is
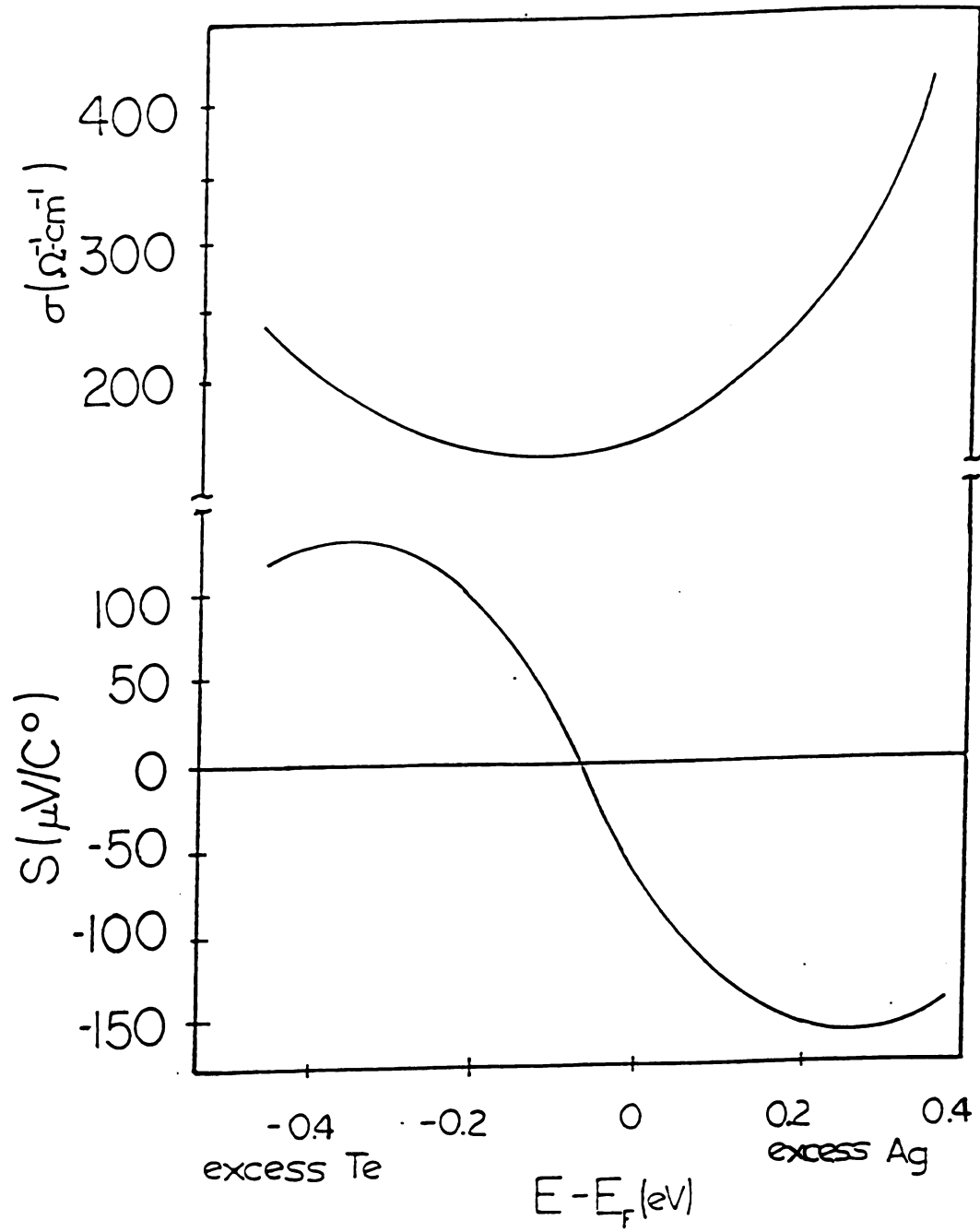
Figure 8 - The thermopower and conductivity calculated using the Kubo
Greenwood formulas with $a_c = 2a_v = 1300 \ \Omega^{-1} \ cm^{-1} \ eV^{-1}$

shifted several atomic percent to the tellurium rich side of stoichiometry; in addition, the p-n transition is broadened, and S(c) also descends far below 13 $\mu V/C°$.

Although the peak in the conductivity appears to be unique to the silver chalcogenides, there are other liquids that are also poorly modeled by this formalism. In particular, in the concentration neighborhood of the fast ion conducting system liquid Mg_3Bi_2, σ experiences a steep and sudden drop as stoichiometry is approached from either side [22]. However, the thermopower maintains very small values ($|S|<10$ $\mu V/C°$), even through stoichiometry. It has been suggested that this is a result of a rapid opening of an energy gap as a result of rapidly changing mobility within 1 at. % of stoichiometry, where previously there had been perhaps a pseudogap. Such an explanation is not unlike that advanced by Ohno et. al. [11] to explain Ag_2Se, where it is supposed that $d\sigma(E)/dE$ changes very rapidly at concentrations near the peak in conductivity.

Significant experimental evidence for a tie between ionic and electronic mobility has now been accumulated, although theoretical considerations are still sparse (the possibility of a connection between ionic conduction and the energy gap has been explored by Ramasesha [23]). In crystalline NaSn and CsPb [24], for example, the electronic conductivity jumps when a phase boundary is crossed from the higher symmetry, lower temperature β phase, to the lower symmetry, high temperature ionic conducting α phase. The lowering of the symmetry would typically result in the narrowing of the energy bands, and perhaps the widening of the band gap; the increase in the conductivity is contrary to this. Indeed, a similar transition in the ionic and electronic conductivity is seen in the solid Ag_2Se and Ag_2S compounds as the β to α phase boundary is crossed [25], and apparently also in crystalline Mg_3Bi_2 [26]. (We have

already noted that these are ionic conductors in the liquid as well as the high temperature solid.)

It is significant, however, that recent ab-initio calculations on liquid Ag-Se [9] have revealed that an energy gap in $N(E)$ does exist at stoichiometry; further muffin tin [27] calculations have verified the presence of this gap, and have shown the presence of a gap in Te and S compounds at stoichiometry as well. The ab-initio calculations have shown that the gap disappears as Se concentration is increased from 33.3 at. % to 65 at. %, and it may not be ruled out that at least for these systems, the anomalous conductivity may depend as significantly on changes in $N(E)$ as changes in the mobility $\mu(E)$. It is unfortunate that no ab-initio results exist for Te or S alloys with silver, or for any such system in fine concentrations steps around stoichiometry; it is clear that the present results warrant all of these calculations.

II. Liquid Si and Ge

A. Introduction

Pure liquid Ge and Si have for decades been the subject of theoretical and experimental inquiry because of the similarities and differences between their solid and liquid phases. Both are semiconductors in the solid, but in each the resistivity drops enormously upon melting to metallic values ($\rho < 200\mu\Omega$-cm); at least for liquid Ge, experiment has shown that this decrease in the resistivity is associated with the disappearance of the energy gap in the density of states [28]. Remarkably, the structure apparently remains open and far from the hard sphere packing normally associated with metallic conduction, which often correspond to coordination numbers of 10-12. The shoulder observed in numerous x-ray and neutron scattering experiments on the high Q side of the main peak of the structure factor is unreproducible by even more sophisticated hard sphere modeling [29]. The fourier transformed structure factor has an ill defined first minimum, which makes estimation of coordination number from the area under the first peak of g(r) difficult; coordination has been found to be as small as 5.8 and 6.1 for liquid Si and Ge, respectively [30]. Estimates range as high as 9.5 for both liquids depending on the definition of the upper boundary of the first peak.

The shoulder in the experimental structure factor S(Q) is excellently reproduced by Reverse Monte Carlo (RMC) modeling [31]. (The RMC method has been used to analyze our liquid Cu-Ce data, and a full account of this technique will be delivered in that section.) It is interesting that the same method has demonstrated that requiring progressively more atoms within the simulation to be coordinated as they are in the

covalently bonded crystal results in the splitting of the first peak in the structure factor, and that even weak covalency can result in a shoulder like the one seen in liquids Ge and Si. In addition to this, this technique can yield the experimentally unobtainable bond angle distribution, although it must be emphasized that the configuration achieved by the RMC method is not the only configuration that can yield a particular S(Q). (It is not unique.) For Ge, the bond angle distribution shows a peak at around $\cos \theta = 0.65$,which suggests that the structure is weakly diamond like, with significant overlap of the first and second coordination shells.

Evidence for remaining covalent bonding in the liquid has also been noted through the recent development of ab initio molecular dynamics. These simulations, in a series of steps, calculate the interatomic forces through full quantum mechanical considerations, and then allow the ions to move according to classical equations of motion. (See, for example, Stich et.al. [32].) The method has been used with success for several pure liquid metals [33] and alloys [9]. A consideration of the electronic wave functions of liquid Si by this method has shown a transient accumulation of charge between neighboring atoms, which amounts to more than effects due merely to the proximity of the atoms. The excess charge is in fact interpreted as covalent bonds in the liquid. These experimentally inaccessible results are grounded in experiment; good agreement exists between simulated and experimental atomic structure, density of states, and bulk modulus for liquid Si. However, the experimental resistivity, also valuable for comparison to simulation, varies by as much as 20 % from one experiment to another, and an improvement in the accuracy of these data is clearly necessary.

B. Procedure and results.

Liquid Ge is completely compatible with Alumina; all measurements were done in the same way as the Ag-Te alloys, and no special care was needed to isolate the material from the air during preparation. The experiment, however, was still done in an argon atmosphere with 1-2 psi overpressure after baking the system under vacuum. Ge of purity 99.9999% was supplied by Aesar-Johnson Matthey Co.

Si was also supplied by Aesar-Johnson Matthey , and was of 99.99% purity. Liquid Si presents unique containment problems, as our own tests showed that it vigorously attacks alumina and quartz. A survey of the literature showed that a number of previous measurements had been conducted in containers of this sort, and were therefore to be treated with caution.

Earlier workers [34] had shown that high density graphite could contain liquid Si with minimal corrosion, although none had characterized graphite electronically for the purpose of transport measurements; this early work had also shown that conventional machined graphite rods immersed in l-Si experience a change in radius due to corrosion of only about 1.02×10^{-3} cm hr^{-1}. In the same tests, neither x-ray diffraction nor light microscope inspection of the boundary could reveal evidence of the formation of silicon carbide, an electric insulator. We have performed our own test of this by measuring the resistance of a graphite-(liquid-Si)-graphite junction over a time period as long as 12 hours, with the result that no increase of resistance was measured, suggesting that no appreciable amount of SiC was formed. Our tests were performed on Aeromet grade graphite supplied by ESPI, their hardest, least porous graphite. ESPI has confirmed that
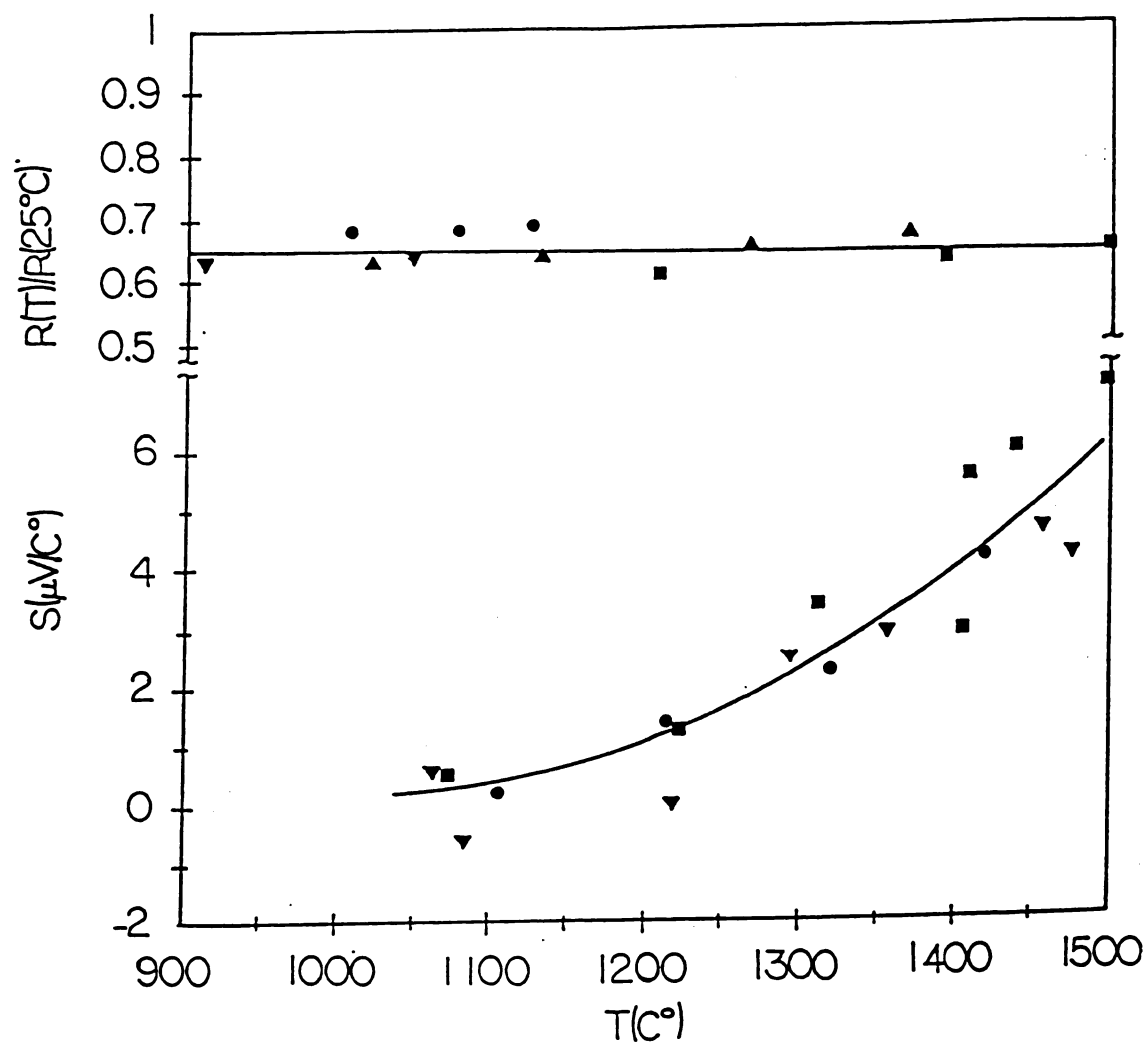
Figure 9 - The electronic characteristics of high density graphite. The various symbols indicate separate experiments done on samples of different material manufacturer batch number, and on samples of the same batch number with different thermal histories.

additional ingredients are not responsible for the different grades of graphite, but that the difference lies only in the individual steps of the preparation process.

For measurements to be made using a conductive graphite container, a complete knowledge of the electronic characteristics of the high density graphite is necessary for the extraction of the sample resistivity and thermopower. We have characterized numerous samples of the graphite through the full range of temperatures necessary for the liquid measurement, and have further examined several samples through numerous temperature cycles. The results of our calibration are shown in Figure 9 . Although the resistivity of the graphite may vary from one rod to the next by as much as 10%, the ratio of R(T)/R(room temperature) was highly reproducible. The thermopower of the rods was measured against W-Re 26% electrodes, and was highly consistent from one rod to the next, being within $\pm 1\mu V/C^\circ$ on all the rods tested, and also independent of the thermal history of the material.

The graphite containers for our measurements were not available commercially, but were prepared from .375" dia. × 6 " rods of graphite by drilling with a special hollow core drill that allowed compressed air to expel the graphite powder, thereby maintaining a smooth machined inner surface . The wall thickness was about 0.76 mm. Triangular grooves were machined on the outside for accurate and consistent placement of contact wires. Voltage leads for the resistivity measurements were Mo wires nominally of 0.102 mm diameter; these were placed in the grooves and held in place by semi-circular Al_2O_3 clamps. The uncertainty introduced to the measurement of sample resistivity by the effect of the grooves on the cross sectional area of the tube was estimated at below 0.1%.

The thermoelectric voltage was measured sufficiently far away from the ends of the tube so that end effects in the thermopower were negligible [35]. The counter electrodes were too thick (0.010") and inflexible to be bound under the alumina clamps, and were therefore affixed with 0.015" molybdenum wire in such a way as to minimize the longitudinal area in contact with the tube, to avoid as much as possible the addition of a third parallel component to the thermopower measurement. Figure 10 is a diagram of the arrangement.

The tubes were calibrated in a slightly different fashion than the method for the alumina tubes used in the Ag-Te experiment. The first step was to measure the resistance of the empty tube, wired as it would be for the actual experiment. The tube was then filled with Hg, and the resistance of the parallel arrangement measured. After calculating by the parallel resistors formula the resistance of the Hg, $R=\rho L/A$ was used to extract the tube constant, A/L, using the well known resistivity of Hg at room temperature, 95.7 $\mu\Omega$ cm. With the room temperature resistance of each tube known, the resistance of the tube at high temperature was calculated using the calibration curve for graphite described earlier. Resistivity of the sample was calculated by considering the graphite tube and the sample to be resistors in parallel. As in all of our resistivity measurements, the current is reversed midway through the measurement to eliminate thermal voltages.

The thermocouples used for temperature measurement were of W-5% Re and W-26% Re. These component wires were supplied in matched lengths by Omega Engineering Inc., and thermocouples formed of these matched lengths were quoted to be accurate to ±1%. The W-26% Re leg also served as the counterelectrode for
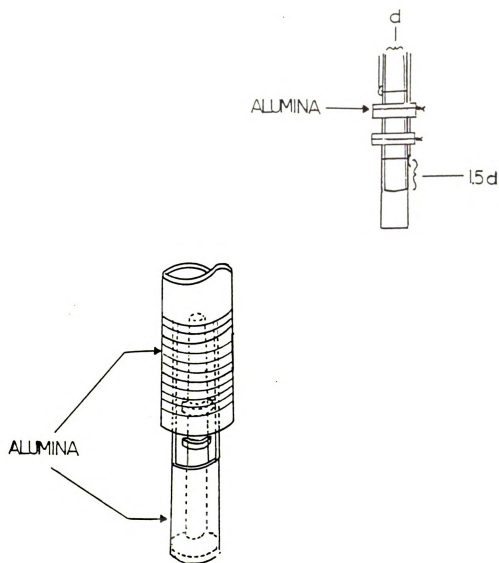
Figure 10 -   Diagram of graphite sample container, support tube, and gradient coil.

measurement of S, and its thermopower was measured to above 1500°C against Pt. (The thermopower of pure platinum by Roberts et.al. [7] was measured using the Thompson heat method.) In addition, a calibration up to 1200°C was conducted against chromel; the Pt calibration data was used in conjunction with our lower temperature chromel calibration data to extract the absolute thermopower of W-26%Re. We estimate the uncertainty in S for W-26%Re to be ±0.5 μV/C°. It is worth noting that another calibration of W-26% Re against molybdenum, using the early calibration of Cusack and Kendall (1958) [36] , differed from results gained from Pt and Chromel in temperature region above 1250°C; we expect the most recent high temperature standards to be more accurate.

The furnace is different than the one described for Ag-Te alloy, and capable of much higher temperatures. Kanthal Super elements (made of $MoSi_2$ sheathed in a thick layer of SiO_2) were used; this material has a maximum operating temperature of 1700°C in air. The maximum surface load, 12.5 W/cm², is again the limiting factor for temperature, and this is achieved with 140A at 1500C°. At these high temperatures the efficient radiative transfer of heat makes the delicate maintainance of the constant lower temperature during thermopower measurements described earlier difficult. Instead, a supplemental coil with Molybdenum windings supplying ~300 W was hung around the uppermost part of the sample within the external furnace tube. A temperature gradient was established by lowering the main furnace current, and by increasing the supplemental coil current. When conducted properly, the lower temperature dropped steadily, and the upper temperature rose steadily, such that the average temperature would remain the

same. The thermoelectric voltage was measured for numerous temperature differences ΔT_i, all with the same average temperature, and the "small thermal gradient method" [37] was used to calculate the relative thermopower using the following formula,

$S_{rel} = (\epsilon_i - \epsilon_j) / (\Delta T_i - \Delta T_j)$

where ϵ_i is a thermoelectric voltage and ΔT_i is the associated temperature difference. This yields a relative thermopower free from errors in the thermocouple calibration, with the assumption that the parasitic voltages remain constant over small temperature intervals of the same average temperature, and may be subtracted out. The absolute thermopower of the sample is extracted using the W-Re 26 % thermopower calibration data S_x, the thermopower of the graphite S_{tube}, and the following formula

$S_{liquid} = (1+B)(S_x + dV/dT) - BS_{tube}$

where

$B = \rho_{liquid} A_{tube} / \rho_{tube} A_{liquid}$

with ρ being the material resistivity and A the cross sectional area of the material. The dimensions chosen for the tube, and it's nearly ideal electronic properties, render B of minimal importance to the calculation; the value of B in these experiments was only about 0.02, and the contribution of the BS_{tube} term to the measured thermopower only about 0.12 μV/C°. Therefore, uncertainties in the tube parameters contributed minimally to the final values obtained for S for liquid Si.

C. Experimental Results and Discussion

Liquid Si has been seen to melt very slowly [38], passing through a semi solid phase before becoming completely liquid; the slow destruction of order could result in
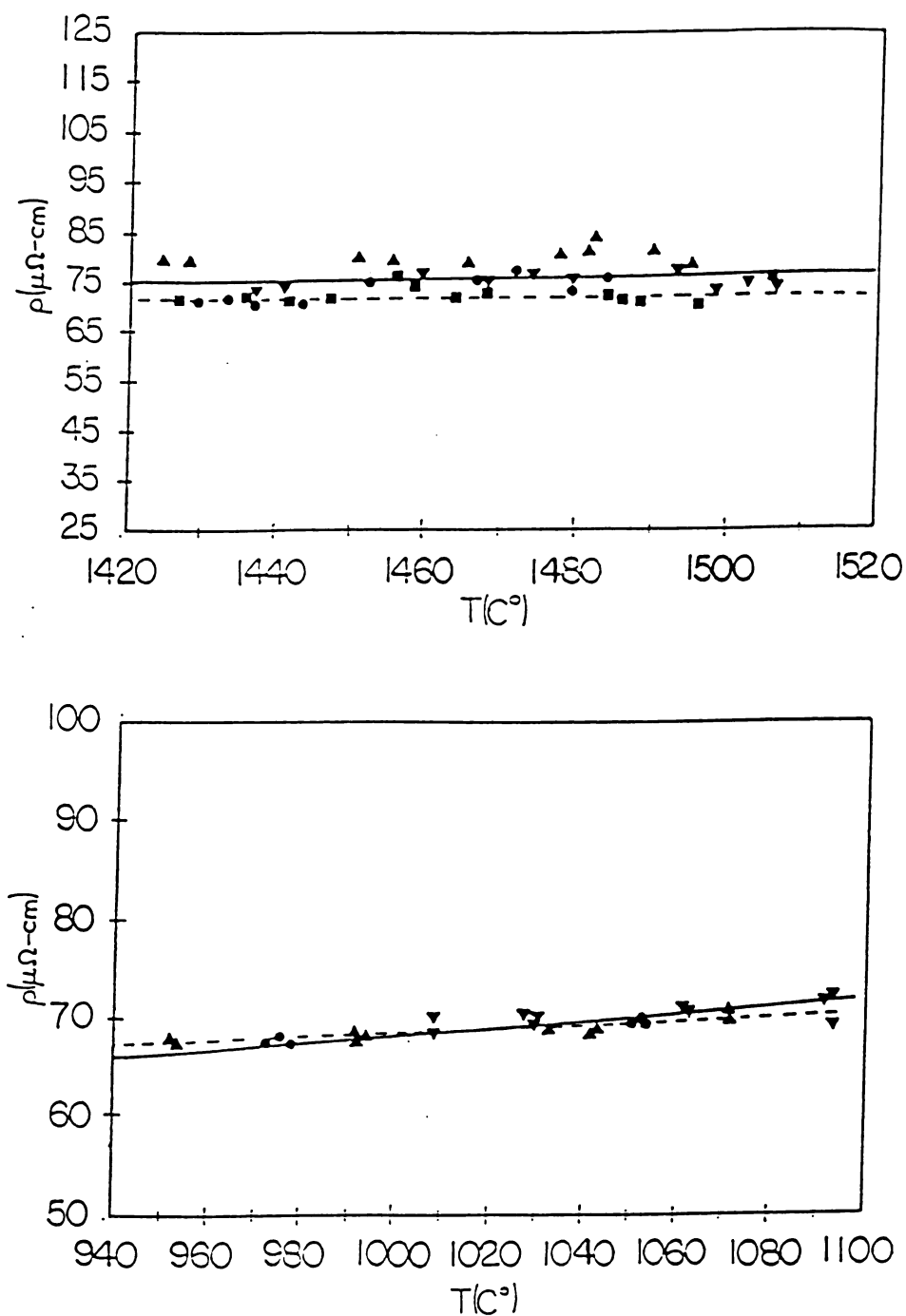
Figure 11 - The resistivities of liquids Si (top) and Ge. All of the data shown
are our own, the different symbols being separate experiments on
different samples. A random selection of 1/3 of the data accumulated
is displayed, for graphical clarity. The solid line is a fit to all of the
current data, including data points not shown, and the dashed lines are
the results of Sasaki et. al.[39] and Koubaa *et.al.* [38] for Si and Ge,
respectively.
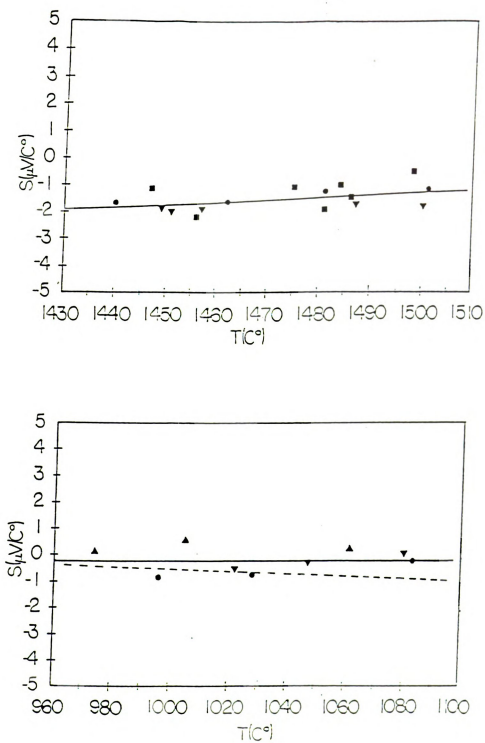
Figure 12 -   The thermopower, S, of liquids Si (top) and Ge. The lines and data points
are as described previously in Figure 11.

time dependent electronic properties before the material is fully melted. To investigate

this possibility, we have measured the resistivity at constant temperature for periods of

up to 30 minutes at $T_{melt}+50\,^{\circ}C$, and have seen no discernible change. Furthermore,

results at the beginning and the end of an experiment were consistent, and further suggest

that the liquid state is achieved quite immediately at temperatures above the melting

point.

The results for the resistivity and thermopower of liquids Si and Ge are shown in

Figures 11 and 12. We find that our results for the 3 separate samples of Ge are very

consistent, and further agree very well with the recent results of Koubaa *et. al.* [39], who

also contained their sample in alumina. Our measured thermopower of Ge also agrees

well with the same workers. Our resistivity results for liquid Si are very similar to those

of Sasaki et. al. [40], who contained their sample in boron nitride containers and used a 4

probe measurement technique. Unfortunately, these workers have made no attempt to

measure thermopower. Our results for thermopower differ significantly from those of

Glazov et.al [41] , and we attribute this to our vastly improved containment technique.

(The containment for the earlier measurement was Al_2O_3.)

Because the resistivities of liquid Si and Ge are comparatively low, one might

expect that an analysis according to Ziman formalism is appropriate. Ziman theory

emerges from perturbation theory, and is often used to explain the so called weak

scattering metals, that is, cases when the electron interaction with the ionic cores is not

strong. The Ziman formulas for resistivity and thermopower are shown here

$$\rho = \frac{3\pi}{e^2 \hbar v_F^2} \frac{N}{V} \frac{1}{4k_F^2} \int_0^{2k_F} Q^3 \cdot S(Q) \, |u(Q)|^2 dQ$$

$$S = \frac{\pi^2 k_B T}{3|e|} \left[\frac{\delta(\ln[\rho(E)])}{\delta E} \right]$$

where $S(Q)$ is the structure factor of the material, $u(Q)$ is the fourier transform of the

scattering potential, and v_f and k_f are the Fermi velocity and Fermi wavevector,

respectively. The Fermi wavevector may be calculated using Nearly Free Electron

techniques and the conduction electron density, n, using the formula

$$k_F = (3\pi^2 n)^{1/3}$$

The structure factor, which will be seen again in the following section, is defined for pure

liquids as

$$S(Q) = 1/N \langle \sum_j \sum_k \exp[-iQ \cdot (r_j - r_k)] \rangle$$

where N is the number of atoms, and r_j is the position of an atom. Also, $\mathbf{Q} = \mathbf{k}_i - \mathbf{k}_f$,

where $\hbar k$ is the momentum of the scattered particle, and ($|k_i| = |k_f|$) for elastic scattering.

The isotropy of the liquid allows Q in $S(Q)$ to be a scalar quantity.

The earliest attempts to calculate the electronic properties of l-Si and l-Ge using

this theory used by necessity hard sphere structure factors for the materials. Hard sphere

packing routines typically have as input only the density, packing fraction, and

concentration of constituents (for binary alloys). No hard sphere structure factor,

including the more sophisticated softened hard sphere structure factor employed by

Rahman [29], can adequately model the shoulder on the high Q side of the main peak of

the experimental $S(Q)$ of both liquids Ge and Si. It is interesting to test this weak

scattering theory using the experimental structure factors against our current, accurate experimental results, to examine its success with regards to weakly ordered liquids.

Ziman theory also involves a sufficiently weak scattering potential to satisfy the assumptions of perturbation theory. Although the full, all electron potential can in principle be calculated with the Dirac equations, we are left with potentials for the conduction electrons that are strong in the core region of the atom. A solution is the creation of a pseudopotential, a potential that is not strong in the core region, but maintains the same energy dependent scattering properties to first order as the true potential. This potential may be used in weak scattering Ziman theory.

For this purpose we have employed the highly versatile Bachelet, Hamann, and Schluter (BHS) pseudopotential [42]; versions of this potential suitable to various computing situations are regularly seen in current molecular dynamics studies. This pseudopotential is constructed in a series of steps from the fully relativistic atom, but at distances outside the core region may be used in normal Schroedinger equations. The accuracy of the BHS pseudopotential has been demonstrated by agreement of calculations to within several percent of experiment for lattice constants, cohesive energies, bulk moduli, and phonon frequencies. It has also been used in several recent molecular dynamics simulations [31,43].

The total bare ion average pseudopotential is assembled from the expanded parts as follows

$$V_{ps}^{ion}(r) = \sum_l \langle l \mid [V_l^{ion}(r) + \mathbf{L.S}\ V_l^{spin\ orbit}(r)] \mid l \rangle$$

with

$\mathbf{L.S} = \frac{1}{2} \, J^2 - \frac{1}{2} \, (L^2 + S^2)$

where $V_l^{ion}(r)$ is the additional potential felt by electrons with different angular momenta.

Each l component is then weighted according to the fraction of total electrons present in

each l orbital. For example, for both Si and Ge, there are 2 s-electrons and 2 p-electrons,

and the potentials would be added

$V^{ion}(r) = .5 \, V_{ps,l=0}^{\ ion} + .5 \, V_{ps,l=1}^{\ ion}$

For ease of tabulation, the BHS pseudopotential is separated into a long range l-

independent Coulomb part, and into short range l-dependent parts

$V_l^{ion} = V_{core}(r) + \Delta V_l^{ion}$

All of the components added together merge to the all electron coulombic potential

outside of a radius R_{core} . Both l-dependant and l-independent parts are expanded in terms

of Gaussian like functions

$\Delta V_l^{ion} = \sum_i \ (A_i + r^2 A_{i+3}) \exp(-\alpha_i \, r^2)$

yielding a set of expansion coefficients A_i and decay constants α_i. An additional set of

coefficients is created by a similar expansion to describe the spin orbit interaction. Some

of the values for the coefficients are quite large and have many significant figures, and

are not easily tabulated. Bachelet et.al. have published the coefficients A_j in terms of

different, less numerically ponderous coefficients C_i , related by a matrix multiplication to

A_j. The 6×6 matrix was required to be generated to 100 bit accuracy by integrals of the

form

$$S_{im} = \int_0^\infty r^2 \, \Phi_i(r) \, \Phi_m(r) \, dr$$

with

$\Phi_i(r) = \exp(-\alpha_i r^2)$ for i = 1,2,3

$\Phi_i(r) = r^2 \exp(-\alpha_i r^2)$ for i = 4,5,6

The vectors C_i were multiplied with this matrix to the same accuracy to attain the

original A_i's with the intended number of significant figures. We were able to

accomplish this conversion using *Mathematica*. As a check that our matrix inversion

program was correct, we compared our calculated A_i's to the one set provided in the

BHS paper for this purpose (for Si), and found complete agreement.

The l dependant potentials for Ge are shown in Figure 13. We notice that in

each, the singularity at r=0 has been removed. The fourier transform to generate V(Q)

was accomplished within a program by successively fitting portions of the curve with a

least squares method, and numerically integrating the fourier integral. V(Q) was then

screened,

V(Q)=V'(Q)/ϵ(Q)

where V'(Q) is the transform of the (unscreened) BHS potential, and ϵ(Q) the calculated

screening function; the resulting screened potential is suitable for input into the Ziman

integral. The screening of Vashishta and Singwi (VS) [44] and of Itchumaru and Utsumi

(IU) [45] were used; Figure 14 is a comparison of the squares of the screened potentials

for liquid Si, and a fairly constant difference between them is seen along the full range
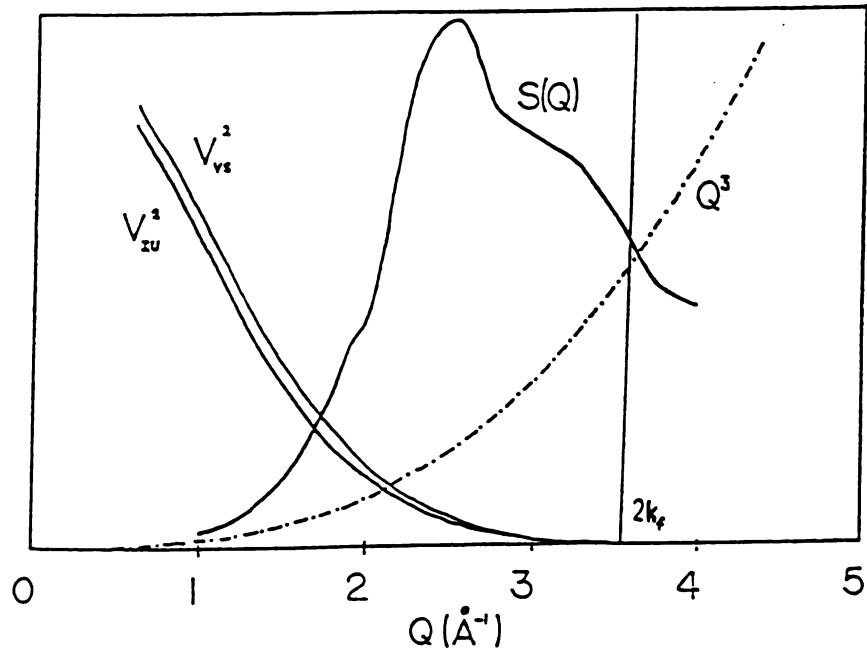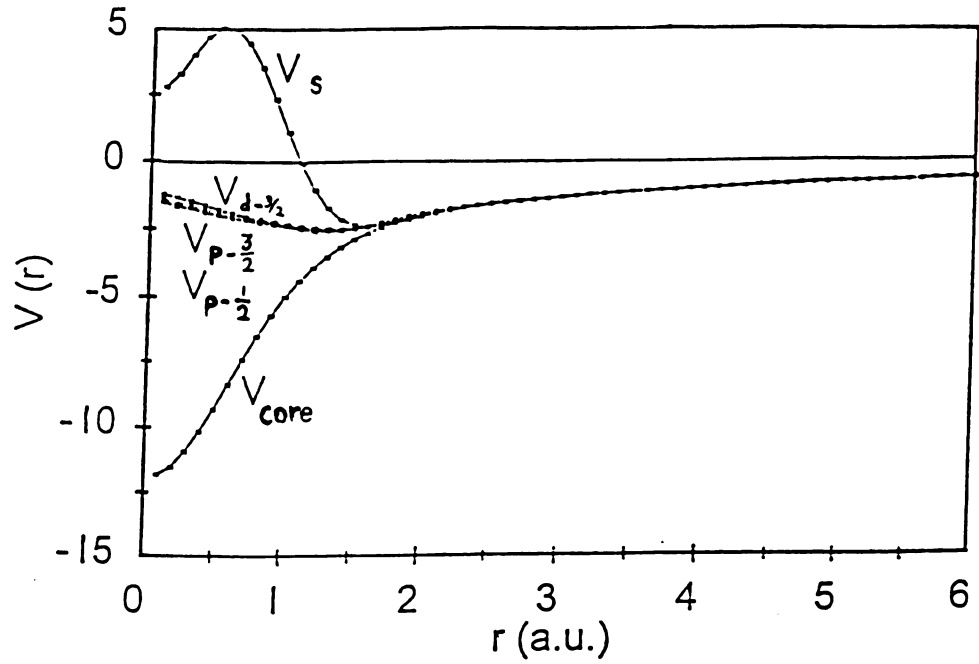
Figure 13 -   (Top) The l-dependent parts of the BHS pseudopotential for
              Germanium. $V_{p-3/2}$ and $V_{p-1/2}$ are both pictured, but lie nearly
              on top of one another.

Figure 14 -   (Bottom) The various parts of the integrand of the Ziman formula
              for liquid Si. S(Q) is the structure factor, from Waseda [46], Q is the
              scattering vector, k_f is the Fermi energy, and V_{IU} and V_{VS} are the
              screened potentials, using the screening function of Ichumaru and Utsumi
              [45] and Vashishta and Singwi [44], respectively.

of Q values considered by the integral. The structure factor of the liquids, measured by Waseda [46] by X-ray diffraction, was also entered; it should be noted that the data of Waseda for liquid Si agrees well with the recent x-ray results of Kita *et. al.* [30] and with the neutron results by Gabathuler *et. al.* [5].

The computation of V(r), the fourier transformation of V(r) to V(Q), the calculation of the screening function, and finally the numerical integration of Ziman's formula to yield resistivity were all done with BASIC programs that were written for these express purposes.

The value that we calculate for ρ for liquid Si using VS screening, 66.6 $\mu\Omega$ cm, is rather close to the experimental value, but the result for liquid Ge using similar screening is not nearly so good (41.2 $\mu\Omega$ cm). Furthermore, we found that if we used IU screening in this calculation, we obtained a value for ρ for liquid Ge that was even lower by about 15 $\mu\Omega$ cm. These screening functions are very similar, but for both liquids the small differences between them occur in the Q range where the contribution of S(Q) to the resistivity integral is significant (Figure 14).

It is interesting that a calculation that completely ignores bonding, such as Ziman theory, produces a value of the resistivity close to what is actually observed. The results of the computationally far more complex ab-initio simulations of liquid Si [32] are marginally worse than the results of Ziman theory. It seems to be more than good fortune, however, that the recent ab-initio results for liquid Ge by Kulkarni et. al.[47], who have extended the simulation to several temperatures and have extracted the temperature coefficient of the resistivity, are in excellent agreement for both ρ and dρ/dT

with our experimental results. It is our hope that our new, reliable data for ρ of liquid Si will provoke similar simulations, and that perhaps thermopower calculations will be considered by these methods. We also look to the very recent development of more effective containerless methods to explore the structure and transport of this corrosive liquid material at extremely high temperature and in the supercooled state. Preliminary results on levitated liquid Si [48] shown good agreement with our results for the resistivity.

IV. Liquid Cu-Rare Earth and Ag-Rare Earth Alloys

A. Introduction

The electrical resistivities of the alloys of copper with the light rare earths (RE= La, Ce, Nd, Pr) were experimentally studied about 25 years ago by Busch et.al. [49]; there was no attempt made to measure the thermopower. At the time, the transport properties of the pure liquid rare earths were of significant interest because of the quite linear variation of the resistivity across the series of pure liquid metals from La to Er , which defied explanation in terms of a continuously varying spin disorder resistivity across the series as a result of the continuous filling of the f shell. Furthermore, the resistivities of dilute (<20 at. %) RE alloys with Cu were nearly identical, and the temperature coefficient always small and positive, further suggesting that the f-electrons were of little importance , and were likely significantly below the Fermi level, and close in energy to the core electrons of the RE atoms. The resistivity data of the alloys of the rare earths with monovalent (Cu) elements, and even polyvalent (Sn) elements, were satisfactorily described by considering the trivalent RE's to have 2 electrons in a virtual d band, and the 3rd in an s like state, and free to conduct. Alloying of RE with monovalent copper resulted in a liquid that had positive temperature coefficient; the alloy with tetravalent Sn also had positive TC, except near the equiatomic concentration, where the valence of the alloy was near 2, and the temperature coefficient negative. A theory describing these alloys would build on the modification of Ziman theory by Evans [3] which extended coverage to the more complicated, partially full d-shell pure transition metals, by the incorporation of a t matrix in the place of the potentia. (Recall a

pseudopotential was used in the calculations done in the present work for liquid Si and Ge.) A t-matrix formulation has successfully described stronger scattering liquid Ba (ρ=320 μohm cm [50]). In addition, in the place of a total structure factor, there would be a weighted sum of the partial structure factors of the constituents in the alloys. We are not aware that any calculations were ever done by this method for comparison to experiment.

Recent interest in Cu-Ce has focused on the stoichiometric *solid* compound Cu_6Ce, in both crystalline and amorphous forms; crystalline Cu_6Ce was one of the first Heavy Fermion (HF) compounds discovered [51]. Perhaps an even more compelling reason for a reexamination of the liquid is the recent discovery of HF behavior in the amorphous solid [52]. This is evidenced by a -log(T) dependance of the resistivity in the disordered solid at very low temperatures (<10K), which is also seen in crystalline Cu_6Ce in the same temperature range, as well as in other HF compounds, and is rather a signature of HF behavior. The amorphous compound also shows continued negative temperature coefficient of the resistivity to 300K, the highest temperature surveyed. No such effect is seen in amorphous Cu_6La; crystalline Cu_6La has not been reported as HF compound, as the source of the HF behavior is almost certainly the Ce-contributed localized f electron in the alloy, and it's detailed interaction with the itinerant electrons.

With the evidence that disorder does not destroy the interesting electronic effects, we have therefore measured the electronic properties of liquid Cu-La and Cu-Ce alloys in a range of concentrations that encompass the stoichiometric composition Cu_6RE. For comparison, we have also examined the Ag-Ce system; to our knowledge no liquid alloy

Ag-RE has been systematically studied for either ρ or S, and a comparison to Cu-Ce would be of certain interest. The measurements on Cu-RE and Ag-Ce were done in aluminum oxide containers in a fashion very similar to the measurements on Ag-Te . Owing to the reactivity of the rare earth materials with oxygen and water vapor, the samples were prepared in an evacuable glovebox which was backfilled with argon to several psi overpressure. Sample materials entered the glovebox through an airlock; both the box and the airlock are evacuable to 20 microns. The inert atmosphere over the sample was preserved for the short trip to the furnace by simply fastening a clamped rubber fitting over the end of the tube before exiting the glovebox; the clamp was loosened by a feedthrough in the furnace vacuum system after the system had been evacuated. The rubber fitting was several inches above the water cooled O-ring (see Figure 3) , in a relatively cool portion of the furnace. Pressures of $\sim 10^{-4}$ torr were achieved in the furnace system before backfilling with Argon. The sample was stirred with 0.040" Mo wire to ensure homogeneity, and to eliminate bubbles. No attack was noted on the Mo for any Cu-RE or Ag-RE alloys. Neither was any attack noted on the alumina or the graphite plugs; the post experiment solidified samples were seen to be uniform and well stirred, devoid of bubbles, and were separated from the alumina tube without difficulty. Materials were supplied by AESAR/ Johnson Matthey; lot analyses of La and Ce yielded impurity levels of 60 and 200 ppm (wt), respectively; Ag and Cu, from the same supplier, were of 99.99% and 99.999% purity, respectively.

B. Results

The results for the resistivity measurements on liquid Cu-RE and Ag-Ce alloys

are shown in Figure 15. In all of alloys, the resistivity, ρ, rises smoothly and quickly as RE is added, with the $\rho(c)$ curves of the different alloys being essentially indistinguishable until ~30 at. % RE. At no time does the resistivity exceed ~200 $\mu\Omega$-cm, even in the neighborhood of the compounds Cu_6RE or Cu_2RE, which correspond to solid crystalline compounds that exist up until the melting point. Our results for ρ are in excellent general agreement with the previous results of Busch et.al. [49] for lower RE concentrations, being uniformly increasing with increasing RE content, although they appear to be consistently ~5% above his values. We do note, however, that the unnamed ceramic material that Busch et.al. used for containment was subject to some corrosion, and that the RE materials used in the study were of lower purity than our own.

The thermopower (Figure 16) is as featureless as the resistivity, and remains small and metallic in magnitude at all concentrations studied. The temperature coefficient of the resistivity, however, displays sharp structure in the neighborhood of Cu_6RE, dropping in both Ce and La alloys to a narrow minimum, which furthermore is negative in Cu_6Ce (Figure 17). It is highly unusual to see such a small resistivity (95 $\mu\Omega$-cm) along with a Negative Temperature coefficient (NTC). NTC was also seen in a comparatively broad range of concentrations surrounding the congruently melting compound Ag_3Ce, although the same magnitude of NTC as is seen in Cu_6Ce was only reached when ρ had exceeded 140 $\mu\Omega$-cm (in comparison to 95 $\mu\Omega$-cm for Cu_6Ce).

For both Cu_6La and Cu_6Ce, an attempt was made to measure the properties of the high temperature solid material as well as the liquid, as current data for the solid extends to only roughly 300°K. Visual inspection of the solidified sample revealed that it was a
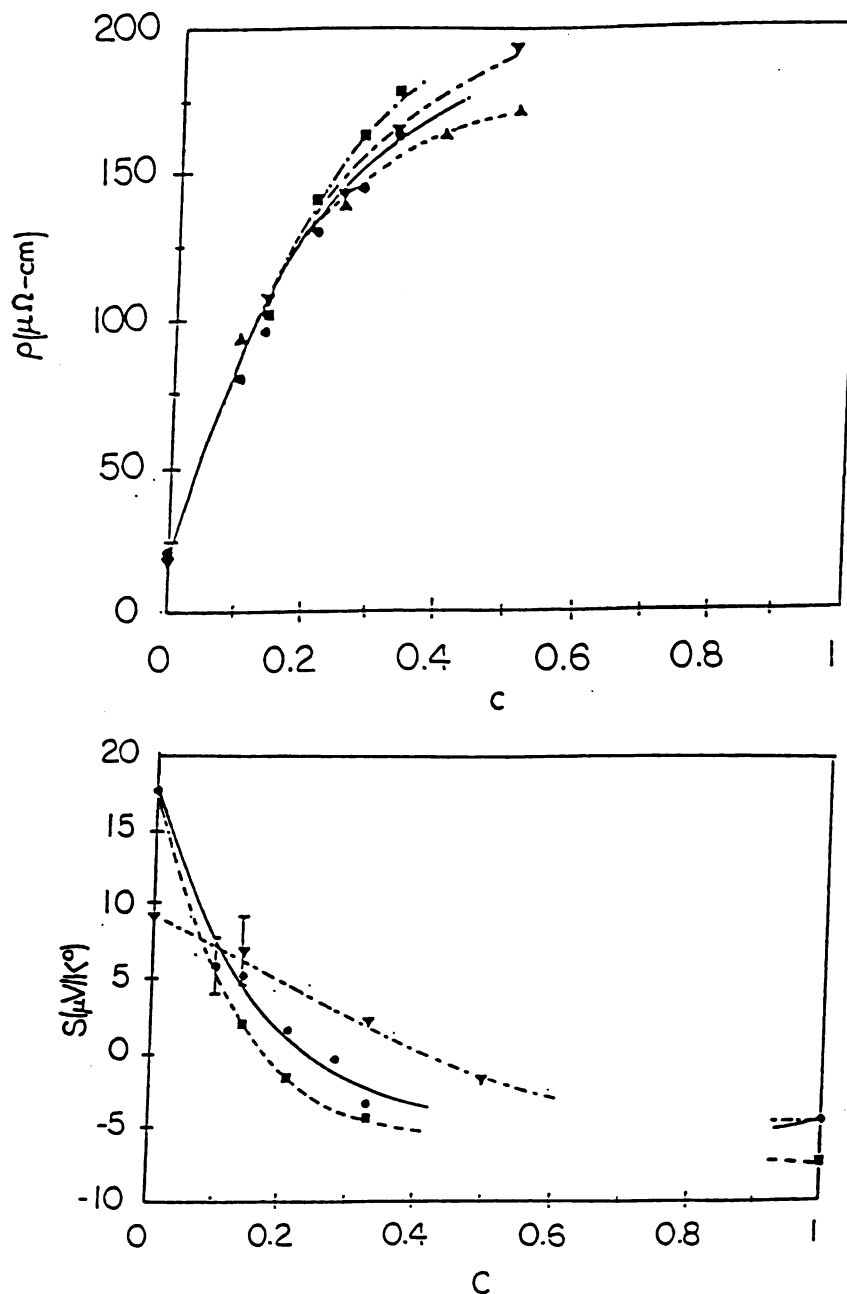
Figure 15 -   (Top) Current data for resistivity, ρ, of Cu-Rare Earth alloys, evaluated at 950°C for Cu-La (■) and Cu-Ce (●) , and at 1050°C for Ag-Ce (▼). Cu-Nd (▲) (Busch et.al. [48]) is at 1000°C.

Figure 16 -   (Bottom) The thermopower, S, of Cu-Ce, Cu-La, and Ag-Ce. The symbols and temperatures are the same as for Figure 15. Error bars are calculated from a linear fit to all of the data for each concentration, and unless shown are smaller than the extent of the point.
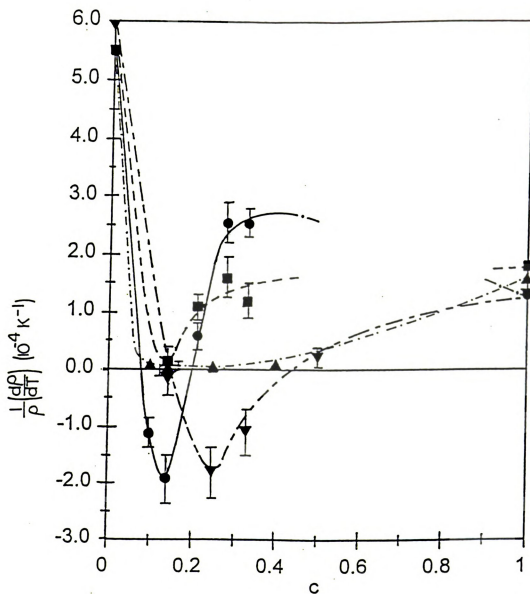
Figure 17 - $\alpha= 1/\rho \ d\rho/dT$ for Cu-Ce, Cu-La, and Ag-Ce. Temperatures and symbols are the same as for Figure 15.

highly uniform polycrystalline sample. Because of differing expansion coefficients, we were unable to establish contact with the entubed solidified sample. In several instances, we were able to remove the sample from the tube in one ~ 6" cylindrical rod, and directly fasten wires to it, but our measurements were not reproducible for either Ce or La samples. Interestingly, amorphous Cu_6La was noted by Suzuki et.al. [52] to be extremely brittle and prone to cracking; in fact, microcracks were blamed for unusual electrical properties in samples of this material.

C. Discussion of Transport Measurements

The NTC's in Ag-Ce and Cu-Ce are in both cases of the same order of magnitude seen in the pure divalent liquids Sr and Zn, and in the divalent alloy SnCe. One of the great successes of Ziman theory [53] is the explanation of NTC in divalent liquid metals and alloys, which occurs as a result of the temperature dependance of the main peak in the structure factor, $S(Q)$, and it's proximity to $2k_f$ (where k_f is the Fermi wave vector). In pure metals and in alloys, the structure factor generally exhibits temperature dependence in the form of both lowering and broadening of the main peak, a result of modification of the interatomic distances with temperature. In divalent metals, the upper limit of the resistivity integral, $2k_f$, is located in such a position that the contribution of the lowered and broadened main peak is lessened as the temperature increases, leading to NTC. The valence of an element is often inferred from the oxidation state of a material; for example, the rare earths, except for Eu and Yb, are thought to be trivalent. In Cu_6Ce and Ag_3Ce, however, a concentration weighted average of the valence of the constituents, using 3 for Ce and 1 for Cu and Ag, yields a valence of 1.3 and 1.5 respectively, rather

too far from divalence to be explained by Ziman formula. (It should be noted that divalent metals considered with t-matrix formalism are affected in the same way by the location of $2k_f$ with regards to the main peak as materials able to be considered in the original theory using pseudopotentials.) The early suggestion of t-matrix treatment by Busch et.al. appears inadequate for this situation.

Quite recently, several studies of the dilute transition metals with the noble metals, (for example, liquid Au-Fe [54] and Cu-Fe [55]) have revealed an overall concentration dependance of the resistivity very similar to that seen for Cu-RE, and have for Au-Fe revealed that the temperature coefficient becomes negative at roughly 8 at.% Fe, reaching a minimum at about 15 at. %. Here, as in Ce-Cu, the minimum temperature coefficient is associated with an unusually small resistivity, about 90 $\mu\Omega$-cm, although the minimum seen in both noble metal-iron compounds appears to be significantly wider in concentration than in Cu-Ce. A calculation has been done using t-matrices, assuming the adequacy of hard sphere structure factors of Ashcroft and Langreth , and making the assumption that Fe is monovalent , and has found that Evans theory has significantly underestimated the resistivity at all concentrations, and was unable to reproduce the observed NTC. Further analysis revealed that the NTC may be tied to the spin disorder resistivity, as the transition metal atoms appear from magnetic susceptibility measurements to retain a significant moment due to their d electrons even in the alloy. Susceptibility measurements on liquid alloys of Ce with Cu, and with La and Pr have indeed shown that the magnetic moment changes nearly linearly with concentration, and that the source of the moment is f-electrons [56]. However, if spin disorder effects from

the filling f band were significant to transport in the Cu-RE systems, the resistivity of dilute Cu-RE alloys would vary greatly with differing RE; for our data, the concentration curves of the various RE alloys are nearly indistinguishable in this regime.

NTC's are also expected and observed for liquid and amorphous metals and alloys for which E_f falls approximately at a fairly deep minimum in the Density of States (DOS). Fresard, Beck, and Itoh [57] have considered an elastic scattering model, and have used the full Fermi Dirac distribution to calculate the temperature dependance of the resistivity. They have found that their model does indeed reproduce NTC at high temperature, but only in cases where $\rho >400$ $\mu\Omega$-cm. They also note an extreme sensitivity in the thermopower to the features in the DOS. Neither property describes our experimental data.

NTC may also result for liquids from the release of electrons from ionic or covalent bonds into the conduction band as temperature increases. These NTC's tend to be quite sharply concentration dependent and occur most frequently at maxima in the melting curves where congruently melting solid crystal structures exist. In fact, extrema in $\rho(c)$ and evidence for bonding in the structure factor S(Q) are so often seen together, that some workers have defined new stoichiometric compounds by the concentration positions of these extrema in cases where diffraction studies are difficult, and have even qualified the strength of the bonding by the relative heights of the peaks in the resistivity [58]. No feature is apparent in $\rho(c)$ at stoichiometry in either Cu-Ce or Ag-Ce, and the resistivity in the neighborhood of these compositions is quite low (~100 $\mu\Omega$-cm) to be associated with strongly bound electrons.

The nature of the phase diagram of Cu-RE and Ag-RE alloys (Figure 18), especially the presence of a congruently melting solid compound at Cu_6RE, suggest that it is possible that short range order exists in the liquid. According to Massalski [59], no compound Ag_3Ce has been identified, although the highest point of the melting curve is centered precisely at this concentration; an intermetallic compound $Ag_{51}Ce_{14}$ is located in this area. It is worth noting, however, that phase diagrams have incompletely identified solid compounds before, so much so as to make Xu [58] comment, "Evidently the results of thermodynamic and crystallographic investigations are almost incongruous." Many of the liquid compounds identified in the work of Xu were not signaled by recorded congruently melting solids, but were discovered in part by extrema in the electronic properties of the liquid.

D. Neutron Diffraction Procedure and Results

To pursue the notion of CSRO further, we have undertaken a neutron scattering study of liquid Cu_6Ce at the Glass, Liquid, and Amorphous Diffractometer (GLAD) at the Intense Pulsed Neutron Source at Argonne National Lab. Sample preparation was conducted in our lab, the pure ingredients being melted and stirred in an alumina tube, following glovebox preparation similar to the samples used in the electrical measurements. The mixed sample was then transferred in the glovebox from alumina to a vanadium tube, and the tube was sealed under argon atmosphere by TIG welding vanadium plugs into the ends. There was concern of the solubility of the vanadium container in Ce, as a thin band of concentrations with comparatively low melting temperature exists for dilute V in Ce. However, immersion of a known mass of V in
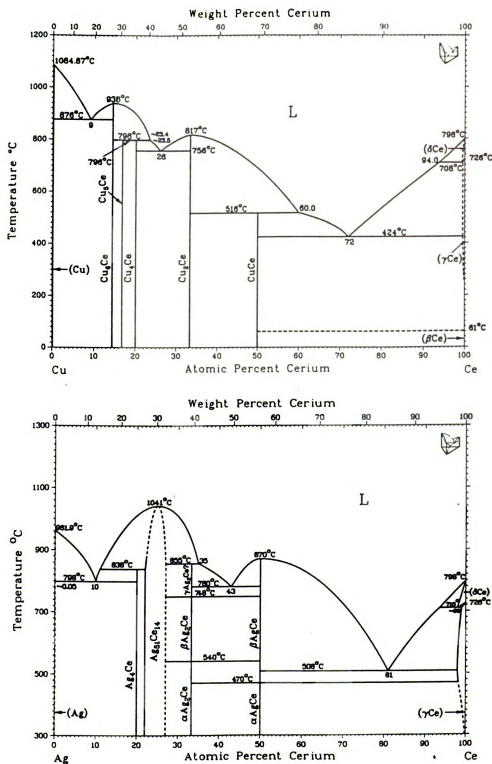
Figure 18 -   The phase diagrams of Cu-Ce and Ag-Ce. All of the Cu-RE
compounds considered here have a congruently melting crystalline
compound at Cu$_6$RE (From [59]) .

liquid Cu_6Ce for an extended time period, and dissolving away of the post experiment

solidified Cu-Ce with *aqua regia* (50% HCl, 50% H_2NO_3; vanadium is immune to this)

and subsequent re-weighing, revealed no significant dissolving of the V by the liquid.

Another empty tube of the same dimensions, also sealed on both ends, was prepared so

that a separate scattering experiment might be done on it, and the tube scattering might be

subtracted from the total sample plus tube signal. On each tube, one of the end pieces had

a threaded hole to support the tube in the hanging position when it was in the neutron

beam. This also allowed for the very precise positioning of both the empty and full tubes,

which is essential for proper subtraction of the tube contribution. The tube was

sufficiently long that the neutron beam, which at position of incidence measures roughly

1cm wide by 5 cm high, would impinge only on the smooth length of the cylindrical

container, and would not strike the welded ends, which were not uniform from one tube

to the next. The temperature was controlled to within ± 1 C° by a furnace consisting of

several concentric, cylindrical vanadium sheets; the container holding the furnace was

evacuated to $\sim 10^{-3}$ torr while the measurements were being taken. Finally, the scattering

of the empty furnace had to be measured, as it also is subtracted in the analysis. All

scattering experiments were conducted in the so called "downstream position", meaning

the sample is several meters closer to the detector than in the upstream position. In the

downstream position, the detectors subtend an angular range $45° < 2\theta < 115°$.

The sample, empty tube, and furnace data provide a portion of the information

required to extract the structure factor from the observed scattered intensity. In addition ,

another scattering experiment was done on a solid vanadium piece of the same

dimensions as the above sample tubes. Vanadium is a nearly completely incoherent scatterer, so the data obtained by scattering from a standard sample of the same geometry as the actual sample may be used to normalize the total scattered intensity. A standard data analysis package was used to treat the results. Corrections for the absorption of the furnace, tube and sample require input of the radii of the various annuli of the concentric cylindrical sample, container, and furnace, as well as the number density of scatterers in each material in order to calculate the multiple scattering and attenuation in these elements. A concentration weighted density of $\rho=0.063$ scatterers/$Å^3$ for liquid Cu_6Ce was used, as no experimental liquid density was available; this is slightly less dense than the crystalline Cu_6Ce density, about 0.065 scatterers/$Å^3$. A final portion of the analysis is to correct for inelastic scattering using Placzek corrections.

We choose to define the structure factor in terms of the Aschroft Langreth partial structure factors $S_{ij}(Q)$

$$S(Q) = \sum_{i,j=1}^{2} c_i c_j b_i b_j S_{ij}(Q)$$

where c_i is the atomic percentage of a given constituent, b_i is the neutron scattering length of the same constituent, Q is the momentum transfer, and

$$S_{ij}(Q) = (N_i N_j)^{1/2} \langle \sum_{l=1}^{N_i} \sum_{m=1}^{N_j} exp(-i Q \cdot (r_{il} - r_{jm})) \rangle - (N_i N_j)\delta_{Q,0}$$

In this expression, N_i is the number density of scattering centers, and r_{il} is the vector

between adjacent atoms, and again the vector nature of Q in S(Q) has been removed

because of the isotropy of the liquid. Figure 19 is the experimental structure factor

obtained from the measured cross section by

$d\sigma/d\Omega = \langle b \rangle^2 [S(Q)-1] + \langle b^2 \rangle$

where $<b> = c_1 b_1 + c_2 b_2$.

A fairly strong prepeak exists at Q ~ 1.6 Å^{-1}, and is followed by the main peak at

2.5 Å^{-1}. Although our scattering experiment involved only the total structure factor of

Cu_6Ce, the x-ray diffraction results of Waseda [46] for liquid Cu-Ce alloys display no

evidence of such a prepeak in any of the partial structure factors $S_{ij}(Q)$ even at the nearby

concentration 25 at. % Ce; this is significant in that by 25 at. % Ce, the temperature

coefficient of the resistivity has risen to positive values. In all of the partial S(Q)'s from

the work of Waseda, the main peak stays at essentially the same Q value for 20 at.%<Ce

content<80 at. %. It appears then that the intermediate range ordering indicated by the

prepeak at low momentum transfer is confined only to compounds around the highest

peak of the melting curve.

The pair correlation function may be obtained by fourier transform of the

experimental structure factor

$$g(r) = 1 + \frac{1}{2\pi^2 \rho_0} \int_0^\infty (S(Q)-1) \frac{\sin(Qr)}{Qr} Q^2 dQ$$

Here ρ_0 is the density in scatterers/ Å^3. In this case the integral is over all Q, but a real

experiment may have data only up to Q~40Å^{-1}. We have used a Lorch function to de-
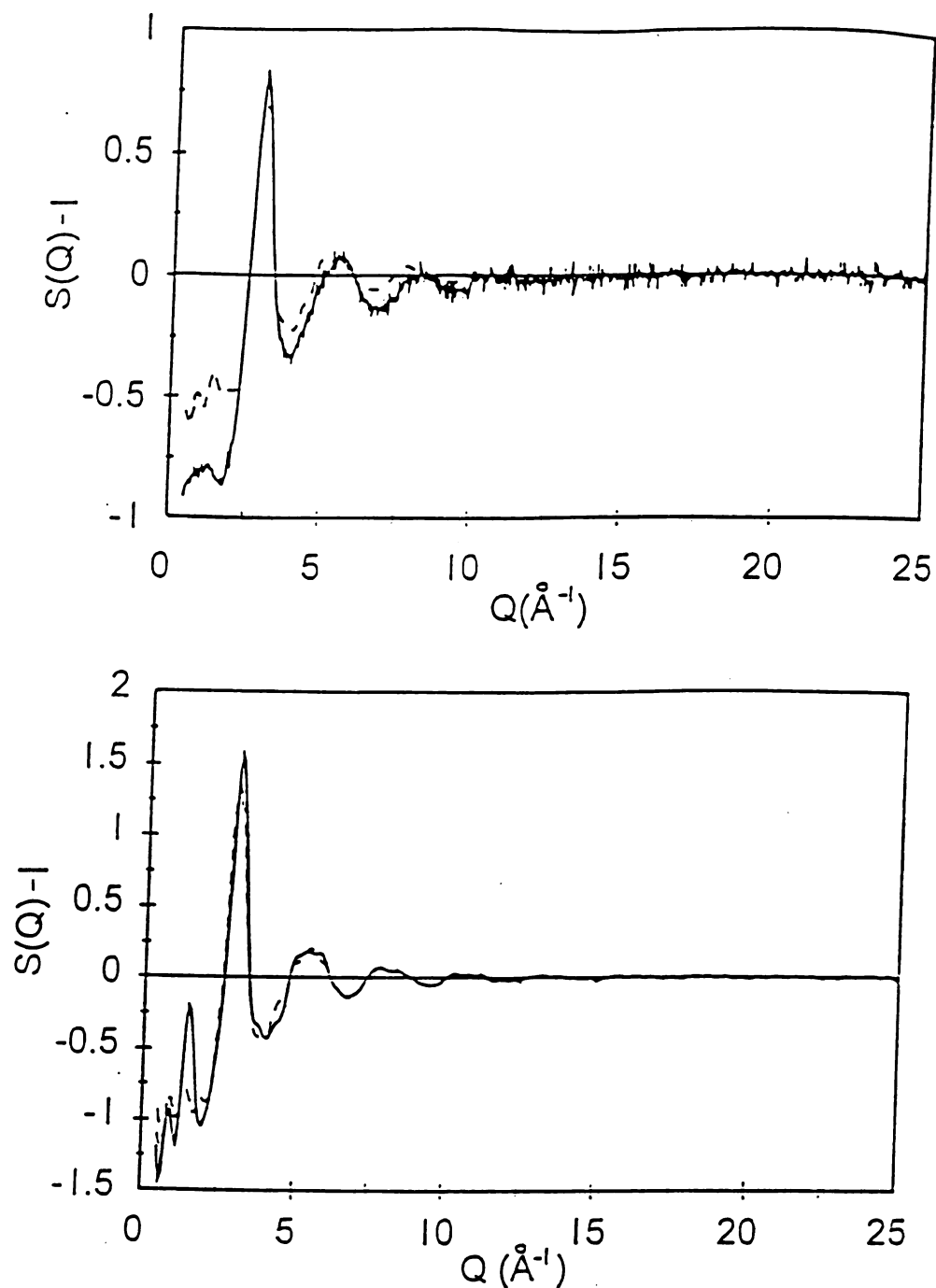
Figure 19 - (Top) The structure factor S(Q) -1 of Cu₆Ce, measured by neutron
diffraction. The solid line shows the experimental results, the
dashed line is the result of RMC analysis of the experimental data

Figure 21 - (Bottom) The RMC partial structure factor, $S_{CuCu}(Q)$. Here, the solid line is
the simulation started from the crystalline arrangement, and the
dashed line is that started from the random arrangement

emphasize the structure factor at high Q and to minimize the truncation errors in the integral. The pair correlation function may also be expressed as a sum of the partial pair correlations

$$g(r) = \sum_{i,j=1}^{2} c_i c_j b_i b_j g_{ij}(r)$$

with c and b the same as before.

The total correlation function, $T(r) = r*g(r)$ is shown in Figure 20. An inspection of the high r side of the main peak in $T(r)$ reveals a shoulder at roughly 3 Å, which is explained as follows. We have fit gaussians beneath $T(r)$; the difference curve between the fitted distributions and the experimental $T(r)$ is also shown in the figure, and illustrates that in the region below ~3.5 Å , 2 gaussians yield a very satisfactory fit. The shape of the gaussians indicates the distribution of interatomic separations. The area

$$C = 4 \pi \rho_0 \int_{r_{min}}^{r_{max}} r^2 g(r) dr$$

with ρ_0 being the density, and the limits of integration defined by the width of the gaussian, is related to the average number of atoms within $r_{min} < r < r_{max}$ around another atom by the following formula

$$C = \frac{1}{\langle \overline{b} \rangle^2} \sum_{i,j} c_i \overline{b_i} \cdot \overline{b_j} C_i(j)$$
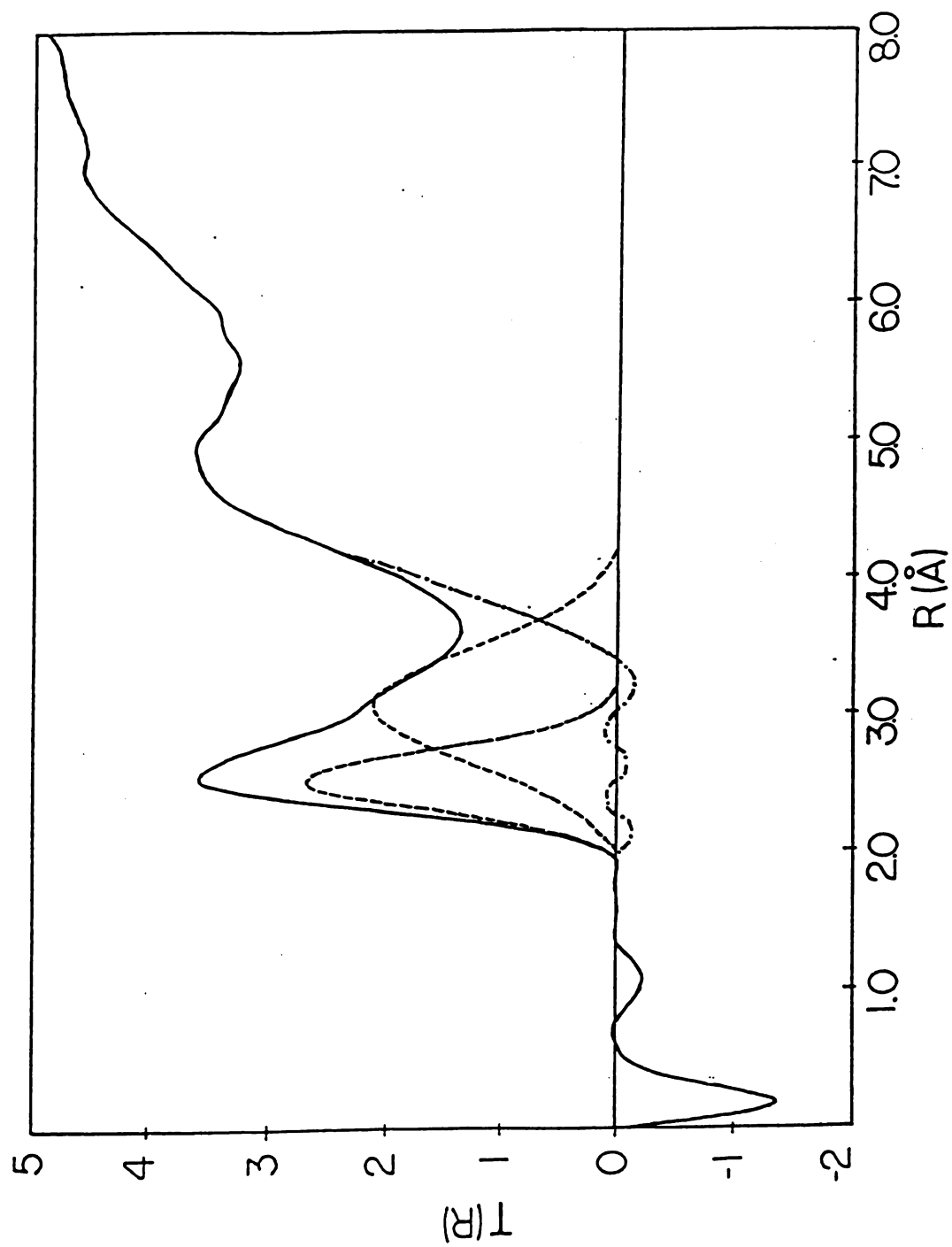
Figure 20 - $T(r) = r * g(r)$ of Cu_4Ce. The pair correlation function, $g(r)-1$, is the fourier transform of $S(Q)-1$.

where C_i is the coordination of the ith type of atom.

The first gaussian in our data is certainly due to Cu-Cu correlations exclusively, as in pure liquid copper the main peak in g(r) is at 2.5 Å. The second gaussian, fitted beneath the shoulder, probably contains both Cu-Cu and Cu-Ce correlations, as both types of pairs exist at distances of 3-3.4Å in the crystal; however, the scattering length of Cu is roughly twice that of Ce , and Cu is present in far greater numbers. If we consider the weight of the CuCe correlations in the second peak to be quite small, and the peak to consist solely of CuCu correlations, we calculate a CuCu coordination from the area of both of the gaussians to be 10.7, which compares favorably with the average coordination of Cu to Cu in the crystal, about 9.3. Proper accounting of the CuCe coordination represented in the second gaussian would of course bring the liquid coordination even closer to that seen in the crystal, and further from the 10-12 nearest neighbors seen in a typical close packed liquid. Certainly, varying the weighting of the partials is possible by either isotopic substitution and neutron scattering, or by combining our present neutron data with X-ray data. Neither option was viable at the time of this experiment. We have instead done a Reverse Monte Carlo (RMC) simulation on the total structure factor, which in previous studies on alloys has yielded a fair appraisal of the structure even from one set of scattering data [20].

E. RMC Procedure and Results

RMC is a program which considers the structure factor, as defined above, of a representative model ensemble of atoms. These atoms are moved singly in accordance with user specified constraints such as closest distance of approach and coordination

number, and after each move a comparison of the ensemble structure to the experimental

structure is made, with the move accepted if it results in a lessening of the difference

between the two, as measured by the quality of fit parameter

$$\chi^2 = \sum_{i=1}^{m} \frac{[S^C(Q_i) - S^E(Q_i)]}{\sigma(Q_i)^2}$$

It is also accepted with a probability $\exp[-(\chi 2-\chi'2)/2]$ if $\chi 2$ increases (χ' is the new χ),

but rejected if no change occurs. Here $S^C(Q_i)$ and $S^E(Q_i)$ are the computed and

experimental structure factors, respectively. The simulation is continued from the

modified ensemble, until $\chi 2$ varies randomly about a constant value. The ensemble is

then in a configuration that will yield the experimental structure factor, although this

ensemble is by no means the only configuration that can yield a particular structure

factor. The partial pair correlation functions $g_{ij}(r)$ are readily calculated from this

configuration of atoms. RMC has proven in some cases to yield results for partial pair

correlation that are nearly as good as those obtained by a proper isotopic substitution

experiment, but experience varies according to the quality of the data, and according to

the relative weighting of the partial components of the total structure factor. We expect

that the weighting factors will make the CuCu correlations most readily modeled, and

CuCe passably so; the weightings of the partials are as follows: Cu-Cu=.4375, Cu-

Ce=.0916, and Ce-Ce=.00479.

Two different initial configurations were selected for our simulations; these will

be referred to in what follows as case 1 and case 2. 1) A random arrangement of 1050

atoms of the stoichiometric concentration, with minimum distances of approach

r_{CuCu}=2Å, r_{CuCe}=2.55Å, and r_{CeCe}=2.85Å, which are very similar to the first peak positions

of liquid $Cu_{.75}Ce_{.25}$ according to the results of Waseda [45], but are less than the distances

r_{CuCu}=2.5 Å, r_{CuCe}=2.9Å, and r_{CeCe}=3.1Å seen in the crystalline solid. 2) A crystalline

configuration of Cu_6Ce [59], with 3500 atoms and with the minimum distances of

approach the same as above. The program fitted the configurations to the experimental

structure factor data; the results have been shown in Figure 19 by the dashed line. The

two simulations ultimately converged to $\chi 2$ values within 1% of one another, and both

simulations were successful in reproducing the prepeak.

The main peak of the total S(Q) was well reproduced in height, width, and

position for both starting configurations, although the following peaks were not modeled

as effectively. In both simulations, the prepeak is placed at the correct Q value, but as a

whole is rather too high, when compared to the main peak. The height of the pre peak in

the total structure factor agrees well with experiment, although is perhaps minimally

better modeled by case 2; the use of a larger configuration in an attempt to minimize the

ripples had no effect, so for the random arrangement a smaller configuration was used for

rapidity of convergence. In both cases, however, the prepeak is unmistakable in $S_{CuCu}(Q)$

(Figure 21) , and substantially larger, relatively speaking, than in the total S(Q), because

of a very deep minimum in $S_{CuCe}(Q)$ at the same Q. This serves to diminish the height of

the pre peak in the total structure factor.

The depth of this minimum in $S_{CuCe}(Q)$ is not significantly affected by varying the

minimum approach r_{CuCe} between 2.55Å and 2.9Å, although the post simulation partial

$g_{CuCe}(r)$ looks rather unnatural and non physical for r<2.9Å; by this we mean that although the distribution shows that a significant portion of the Cu-Ce pairs remain at distances 2.9Å in a comparatively broad peak, a spike appears in the distribution at the minimum distance of approach. The CuCe partial appears to be weighted just heavily enough to be adequately modeled. The Ce atoms collect artificially at the lowest allowed distance of approach because of the extremely small weighting of $S_{CeCe}(Q)$, and these correlations will not be discussed further. It is interesting that the variation of CeCe and CeCu minimum distances of approach had no noticeable effect on the position of the prepeak or the main peak in $S_{CuCu}(Q)$. To check whether this was plausible, we have examined a simple hard sphere, close packed arrangement according to the Percus-Yevick approach [see, for example, Waseda [46]). This calculation, like RMC, showed that the CuCu structure in a close packing scheme was unaffected by changes in the sphere diameter of Ce, but further was unable to reproduce the prepeak.

It is worth noting that for both case 1 and case 2, RMC $g_{CuCu}(r)$ (Figure 22) has a peak at 2.5 Å, and that the high r side of this peak is significantly less sharply inclined than the low r side, which is rather suggestive of a distribution of CuCu nearest neighbor distances with significant numbers at about 2.9Å, in agreement with the shoulder seen in the experimental g(r). We have calculated the average CuCu coordination number from RMC, using the same r_{max} for the limit of the integral in each case, and have found each copper to have 12.8 neighbors for the simulation starting from case 1, and 12.1 for case 2. Table 1 shows that although the average coordination of these cases after simulation are very similar, careful consideration of the coordination of each individual Cu atom will
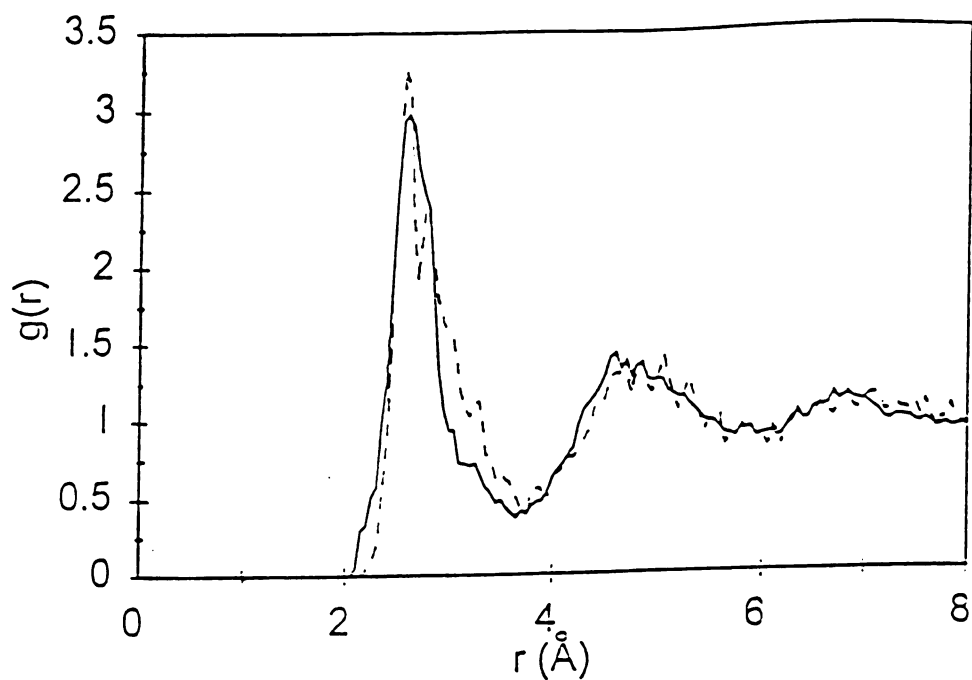
Figure 22 - The partial pair correlation function, $g_{CuCu}(r)$. Solid and dashed lines are the same as for Figure 21.
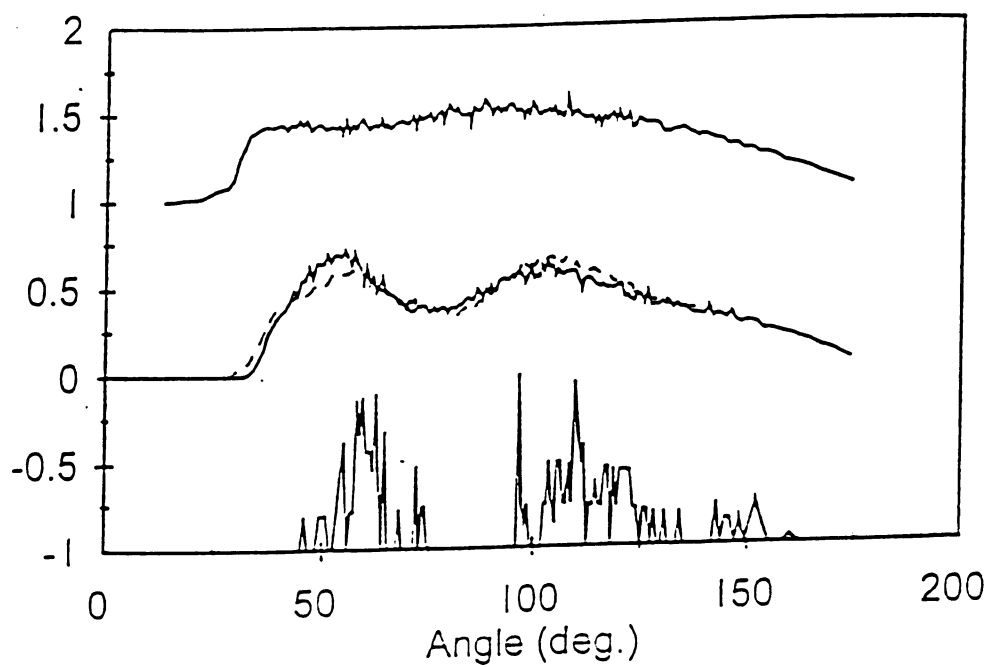
Figure 23 - The RMC bond angle distribution for random (top), post simulation (middle), and crystalline (bottom) Cu_6Ce.

Table 1 - The RMC nearest neighbor distribution for Cu-Cu coordinations, including the results of the simulations started from a random (column 2) and a crystalline (column 3) arrangement. The first column is the coordination number, the remaining columns express the percentage of Cu atoms with the associated coordination. The coordination is calculated by counting Cu atoms within a spherical shell centered on a Cu atom, of outer radius 4 A, and inner radius 2 A. It is seen that there is less spread in the coordination number for the simulation started from crystalline arrangement, and that the average coordination is lower, although the quality of fit parameter for both simulations was nearly equal.

Coordination	Percent of Total, Case 1	Percent of total, Case 2
5	0.1	0
6	0.3	0
7	1.0	0
8	3.0	0
9	4.9	1.5
10	9.8	10.1
11	11.4	23.8
12	13.3	26.5
13	16.6	21.4
14	14.3	11.6
15	12.0	4.5
16	6.7	0.5
17	4.7	0.1
18	1.2	0
19	0.7	0
Average Coordination	12.8	12.1

reveal that a greater percentage of the case 2 Cu atoms are lower coordinated than case 1 Cu atoms. This is a possible reason for the slightly stronger prepeak in the case 2 $S_{CuCu}(Q)$.

RMC may also yield information on experimentally unobtainable bond angle distributions in the liquid, and herein lies one of the strongest pieces of evidence for CSRO in liquid CuCe. Figure 23 shows the CuCuCu bond angle distributions, measured for atoms up to 4Å away from one another to include all of the atoms presumed held in the second gaussian in T(r). Shown are the initial crystalline arrangement, the post simulation ensembles of case 1 and 2, and the initial random arrangement subjected only to moveout of atoms to minimum distances of approach . A completely random arrangement of atoms will have a flat distribution, and this is what we see for the initial random arrangement. After the simulation, for both cases 1 and 2, there are obviously preferred angles in the liquid; the bond angle distribution has rather broad peaks of roughly the same magnitude at 55° and at 105°, which correspond nicely to the sharper distribution of peaks shown for the crystal. The crystalline Cu_6Ce arrangement is shown in Figure 24; it is apparent from this that 105° is not merely ~2*55°, but rather that the angles are independent of one another, and serve to define the corners of a parallelogram of 4 coppers, with the sides of the parallelogram of the lengths seen in the CuCu g(r).

F. Discussion

A first sharp diffraction peak in S(Q) at low momentum transfer (0.7-1.0 Å⁻¹) has in many studies of molten materials been associated with the presence of clustering, and is very often associated with extrema in the electronic properties, the nuclear magnetic
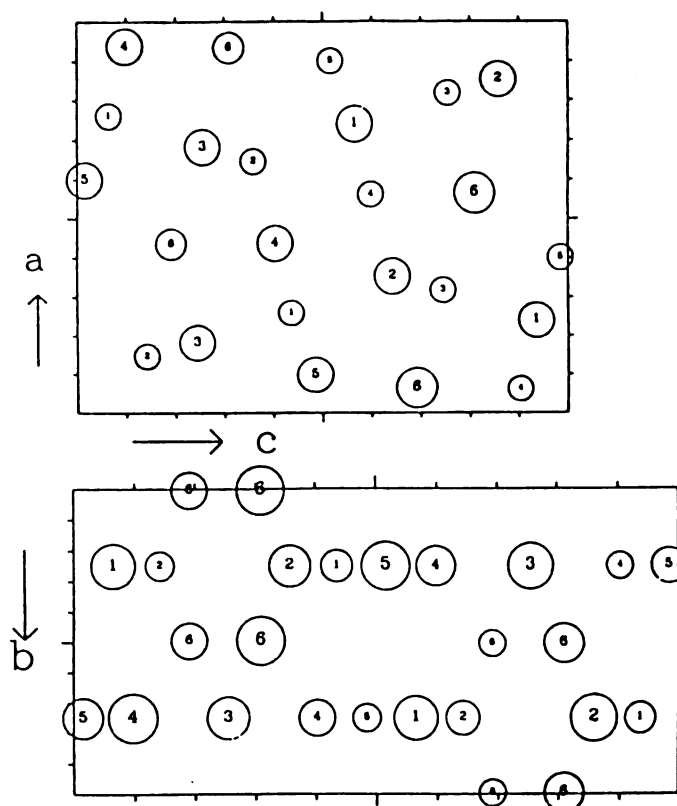
Cell content

Number	Atom	Coordinates		
		x	y	z
1	Ce	.7602	1/4	.0646
		.2602	1/4	.4354
		.7398	3/4	.5646
		.2398	3/4	.9354
2	Cu1	.1467	1/4	.1418
		.6467	1/4	.3582
		.3533	3/4	.6418
		.8533	3/4	.8582
3	Cu2	.1821	3/4	.2450
		.6821	3/4	.2550
		.3179	1/4	.7450
		.8179	1/4	.7550
4	Cu3	.9381	3/4	.0976
		.4381	3/4	.4024
		.5619	1/4	.5976
		.0619	1/4	.9024
5	Cu4	.5986	3/4	.0154
		.0986	3/4	.4846
		.9014	1/4	.5154
		.4014	1/4	.9846
6	Cu5	.4354	.0042	.1908
		.4354	.4958	.1908
		.9354	.4958	.3092
		.9354	.0042	.3092
		.0646	.5042	.6908
		.0646	.9958	.6908
		.5646	.5042	.8092
		.5646	.9958	.8092

Figure 24 -   The crystal structure of Cu_6Ce (From [62])

resonance spectrum, and even in the density . For example, resistivity measurements

coupled with neutron diffraction by Xu [58] has revealed what is thought to be the

presence of clustering in equiatomic alkali-Sn and alkali-Pb compounds, so called Zintl

alloys. In these cases, it is proposed that covalently bonded tetrahedral clusters of $(Pb_4)^{4-}$

form, which are separated by the alkali ions. The peak at low Q in S(Q) is a result of

the inter-cluster distance; the other peaks are interpreted as the intra-cluster distances.

There are also documented cases where a smaller peak is located on the low Q

side of the main peak at perhaps slightly higher Q values than the clustering features

defined previously, and these compounds are often thought to display chemical short

range order. For example, the liquid compound Mg-Bi, discussed briefly in the Ag-Te

section, displays in the structure factor of the stoichiometric compound Mg_3Bi_2 a prepeak

at 1.8 $Å^{-1}$, very similar to the position of our prepeak (1.6 $Å^{-1}$). Guo et.al. [20] have

shown that RMC analysis of a single total structure factor (in this case as well as ours,

an isotopic substitution experiment wasn't possible), with a starting configuration

modeled after the fast ion conducting high temperature β phase of the material, shows

that the prepeak is present in the Mg-Mg partial structure factor, and is significantly

decreased in height in the total structure factor by a deep minimum in S_{MgBi} (Q). These

precise structural characteristics have been identified by Enderby and Barnes [1] to signal

heterocoordination in numerous ionic liquids, and are similar to the outcome of our own

RMC analysis. It is quite difficult to consider Cu-Ce ionic; we suggest that the

proposed ordering in our system is probably due to covalent bonding that is not

sufficiently strong to open an energy gap or pseudo gap in the density of states, and thus
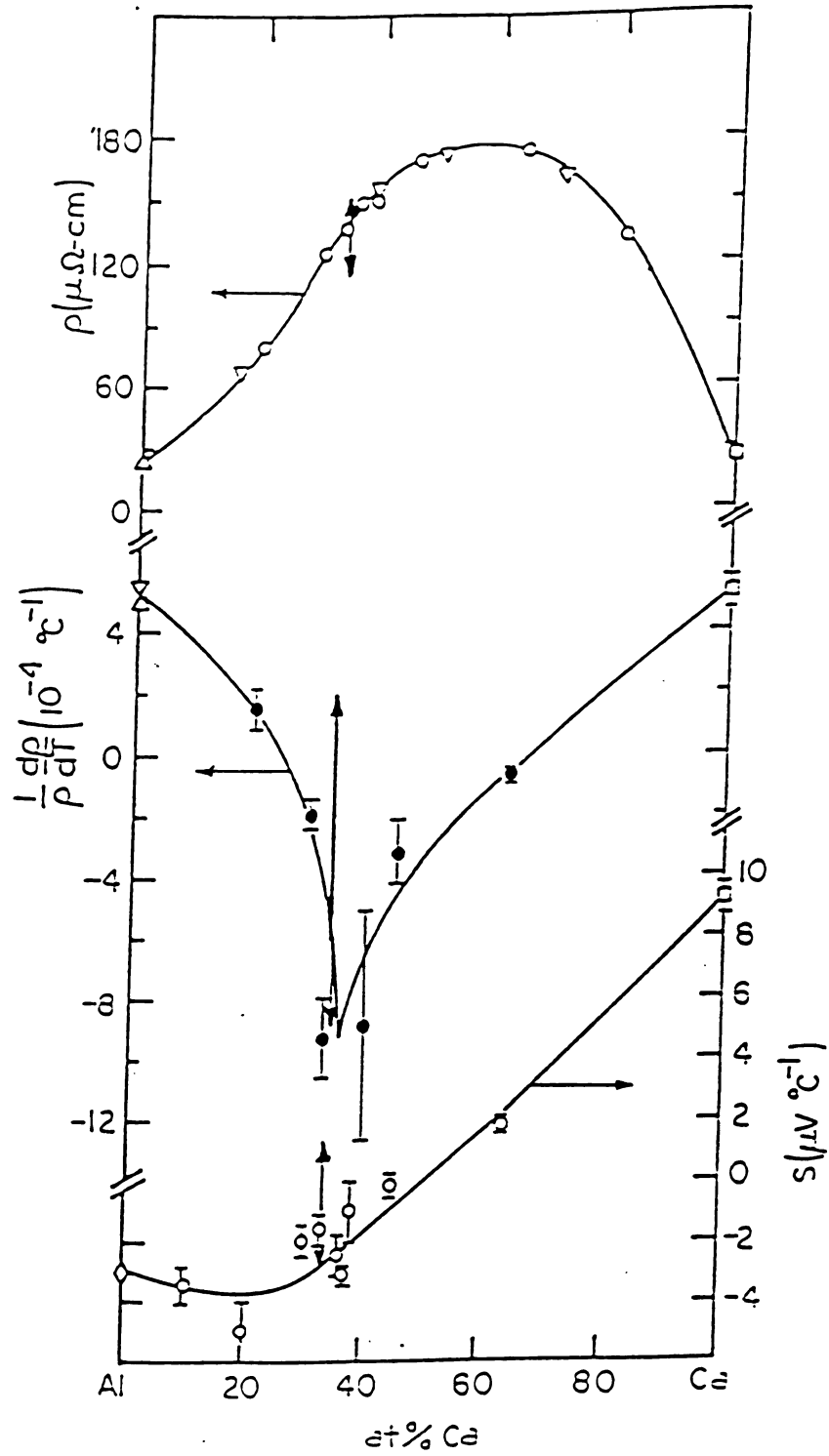
Figure 25 - The resistivity, thermopower, and temperature coefficient
of the resistivity for Al-Ca alloy from Zuo et.al. [60], evaluated at
T=1079°C.

Al-Ca Phase Diagram
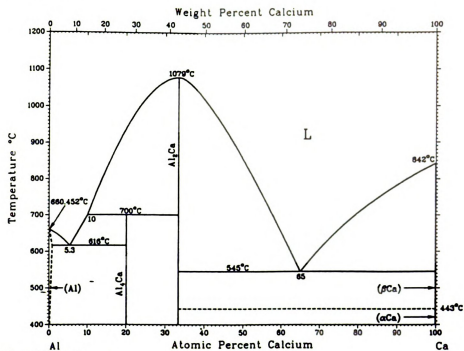
Ca-Ga Phase Diagram
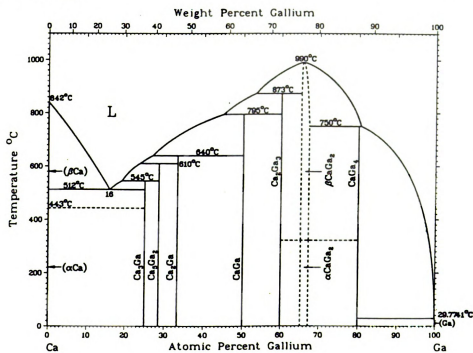
Figure 26 -   The phase diagram of Al-Ca and Ga-Ca (From [59]).

measurably effect either ρ or S. Evidence for liquid compounds is often seen near melting curve peaks; the phase diagram for Cu compounds with La, Ce, Nd, and Pr are very similar to one another, and all do form congruently melting solid compounds at Cu_6RE.

We suggest that α is perhaps a more sensitive indicator of CSRO in liquid alloys than either ρ or S, and in alloys where short lived temperature dependant covalent bonds are suspected, inspection of α for extrema may be the preferred method for identification of liquid covalent compounds. We present as further evidence of the effectiveness of α as an indicator of CSRO, an earlier study by Zuo et.al. [61] on liquid Al_2Ca. Al-Ca also possesses small ρ (150 $\mu\Omega$ cm) and NTC (-9 x10^{-4} C^{o-1}) at stoichiometry (Figure 25) (The stoichiometric alloy is a congruently melting solid with a high melting point (Figure 26).), but no visible extrema in ρ or S. A study of the substitutional alloy $Ga_xAl_{67-x}Ca$ by You et.al. [62] shows that $|\alpha|$ is fairly rapidly diminished as x is increased (Figure 27), suggesting that the Al_2Ca association is broken quickly as Ga is added, and that complexes of AlGaCa do not form. The percentage change in α is far larger as CSRO is disrupted than the change in either ρ or S, although in this case it does change by 15 % as the Al_2Ca complexes are disrupted by the additional Ga (Figure 28).

A further result of You's study is that CSRO does not necessarily result in NTC, but can certainly lead to *depressed* temperature coefficient, when compared to values at surrounding concentrations . A systematic study of liquid Ga-Ca alloys has not been done, but we do notice that as Ga is substituted for Al in the ternary alloy, dα/dc displays a marked change from linearity several atomic percent Ga before all of the Al had been
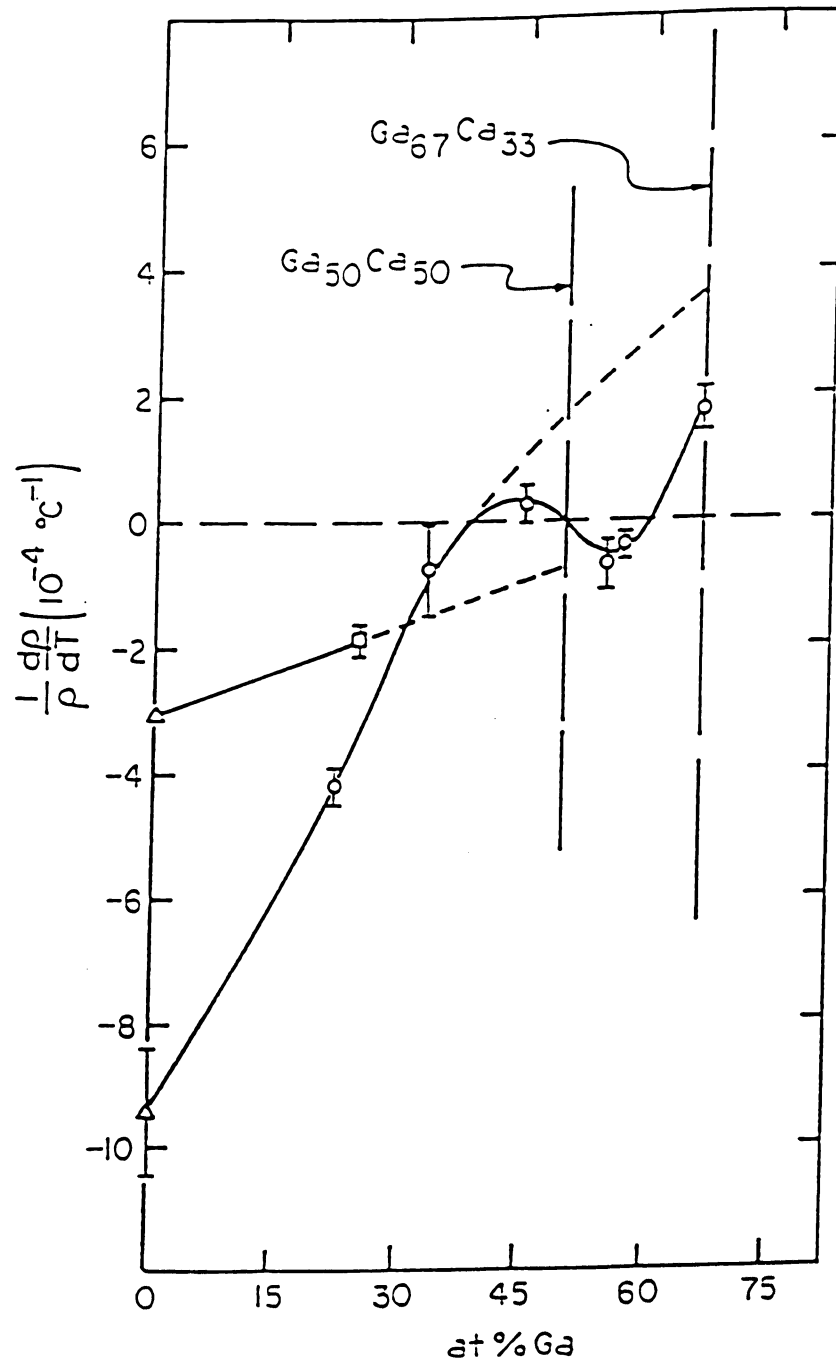
Figure 27 - The temperature coefficient of the resistivity of $Al_{1-x}Ga_xCa$ as a function of concentration of Ga from You et.al. [61], evaluated at $T=1079°C$.
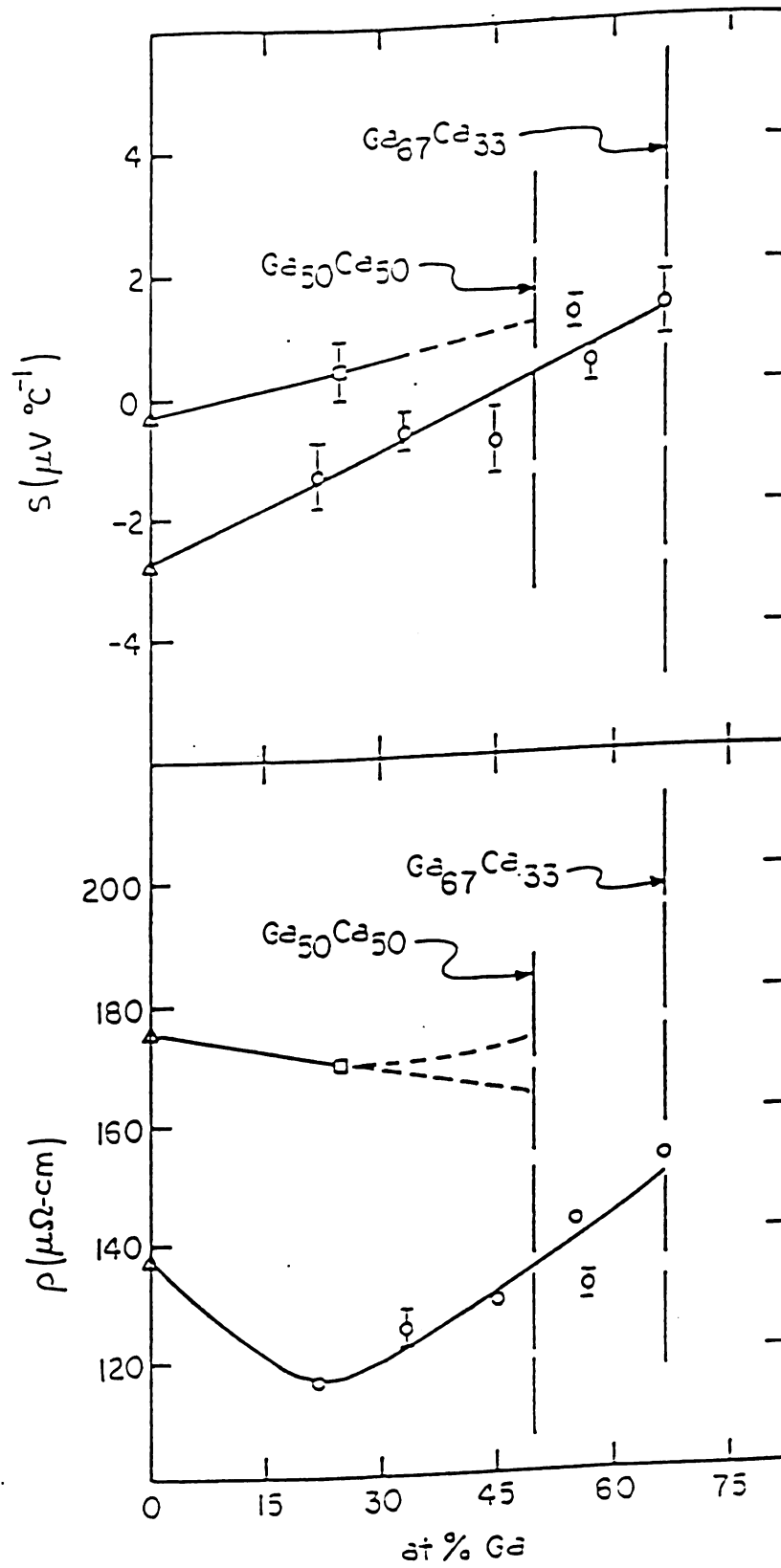
Figure 28 -   The resistivity and thermopower of $Al_{1-x}Ga_xCa$.

replaced. Furthermore, α for Ga_2Ca is significantly lower than an extension of this line would suggest. We compare this case of depressed temperature coefficient to our data for liquid Cu_6La, and even to the data of Busch for Cu_6Nd; for both, α is positive, but clearly at a minimum.

We have presented significant evidence that CSRO is responsible for the NTC in liquid Cu-Ce; although structural studies have not been carried out on Ag-Ce, we expect the same explanation to be valid in that system. Perhaps the strongest argument in favor of CSRO in liquid Cu_6Ce is the close similarity of the CuCuCu bond angle distributions for the RMC generated data and the crystalline material, as they emerge without special provocation from the simulation.

V. CONCLUSIONS

It is apparent from our work that one must move only slightly away from simple liquids or ionic liquids, the end points of the bonding spectrum, before theoretical inadequacy results. Cu-RE, Ag-RE, Si, and Ge are several of a growing set of liquids that demonstrate weak covalency, and are only marginally described by Ziman theory. At the other extreme, some authors have suggested that Ag-Te will only be adequately described using covalent corrections to complete ionicity. Unfortunately, it is obvious that such covalent considerations lend considerable difficulty to the theoretical description.

We may look with cautious optimism to the relatively new ab-initio techniques that consider the electronic and ionic motion on an equal basis, and have thus achieved some success in modeling the atomic structure, density of states, and conductivity. The method is vulnerable, however, in that it uses the local density approximation, which may be invalid at critical concentrations like Ag_2Te. It is also tremendously computationally expensive, especially for situations where higher shell electrons must be considered; f-electron compounds are currently beyond reach, and d-electrons have only recently been considered for the first time.

We expect that more weakly bonded liquids will be revealed as experimental methods and material purity improve, and make visible the somewhat subtle electronic effects. The increasingly intense X-ray and neutron sources, when used in conjunction, are capable of revealing the full structure of the liquids. It is apparent even from the data in this dissertation that any description of weak bonding in liquids will hinge on both of these important experimental data sets.

BIBLIOGRAPHY

BIBLIOGRAPHY

1.   J.E. Enderby, A.C. Barnes, 1990, Rep. Prog. Phys. **53**, 85.

2.   J.M. Ziman, 1961, Phil. Mag. **6**, 1013

3.   R. Evans, D.A. Greenwood. P. Lloyd, 1971, Phys. Lett. **35A**, 57.

4.   D.A. Greenwood, 1958, Proc. Phys. Soc. **71**, 585.

5.   J.P. Gabathuler, S. Steeb, 1979, Z.Naturf. **34**, 1314.

6.   Y. Waseda, K. Suzuki, 1975, Z. Phys. B **20**, 339.

7.   R.B. Roberts, F. Righini, R.C. Compton, 1985, Phil. Mag. B **52**, 1147.

8.   M. Yao, H. Endo, 1996, J. Non. Cryst. Solid, **205-207**.

9.   F. Kirchoff, J.M. Holender, M.J. Gillan, 1996, Europhys. Lett. **33**, No. 8, 605.

10.   S. Ohno, A.C. Barnes, J.E. Enderby, 1990, J. Phys.: Condens. Matter **2**, 7707.

11.   S. Ohno, A.C. Barnes, J.E. Enderby, 1994, J. Phys.: Condens. Matter **6**, 5335.

12.   E. Dancy, 1965, Trans. Metall. Soc. AIME **233**, 270.

13.   T. Okada, F. Kakinuma, S. Ohno, 1983, J. Phys. Soc. Jpn. **52**, 3526.

14.   S. Ohno, Y. Mizushina, T. Okada, M. Togashi, 1996, J. Phys. Soc. Jpn. **65**, no.7, 2182.

15.   D. Price, M.-L. Saboungi, S. Susman, K. Volin, J. Enderby, a. Barnes, 1993, J. Phys.: Condens Matter **5**, 3087.

16.   Y. Tsuchiya, 1996, J. Phys.: Condens. Matter **8** , 1897.

17.   H. Endo, M. Yao, K. Ishida, 1980, J. Phys. Soc. Jpn. **48**, 235.

18. A.C. Barnes, S. B. Lague, P.S. Salmon, H.E. Fischer, 1997, J. Phys.: Condens. Matter **9**, 6159.

19. J. Kooistra, K. Dreyer, J.B. VanZytveld, 1988, J. Phys. F: Metal Phys. **18**, 1225.

20. S. G. Cook, M.S. Laubitz, 1976, Can. J. Phys. **54**, 928.

21. A.C. Barnes, 1993, J. Non-Cryst. Solids **156-158**, 675.

22. C. Guo, A.C. Barnes, W. S. Howells, 1996, J. Phys.: Condens. Matter **8**, 10823.

23. S. Ramasesha, 1982, J. Solid State Chem. **41**, 333.

24. J. Fortner, M.-L. Saboungi, J.E. Enderby, 1994, Phys. Rev. Lett. **74**, 1415.

25. P. Junod, H. Hediger, B. Kilchor, J. Wullschleger, 1977, Phil. Mag. **36**, No. 4, 959.

26. A.C. Barnes, C. Guo, W. S. Howells, 1994, J. Phys.: Condens. Matter **6**, L467.

27. T. Koslowski, 1996, J. Phys.: Condens. Matter **8**, 7031.

28. G. Indelkofer, P Oelhafen, R. Lapka, H. J. Guntherodt 1988 Z. Phys. Chem. **157**, 465.

29. S.M. Rahman, 1986, Philos. Mag. B **53**, No. 5, 391.

30. Y. Kita, J. B. VanZytveld, Z. Morita, T. Iida, 1994, J. Phys.: Condens. Matter **6**, 811.

31. M.A. Howe, R.L. McGreevy, L. Pusztai, I. Borzsak, 1993, Phys. Chem. Liq **25**, 205.

32. I. Stich, R. Carr, M. Parrinello, 1991 Phys. Rev. B **44**, No. 9, 4262.

33. K. Siefert, J. Hafner, G. Kresse, 1996, J. Non-Cryst. Solids **205-207**, 871.

34. R.E. Chaney, C. J. Varker, 1976, J. Electrochem. Soc. **123**, 846.

35. G. Lenters, S. Platt, S. Remillard, J. Kooistra, J.B. VanZytveld, 1994, J. Phys.: Condens. Matter **6**, 3653.

36. N. Cusack, P. Kendall, 1958, Proc. Phys. Soc. **72**, 898.

37. J. VanZytveld, <u>Thermoelectricity in Metallic Conductors</u>, Ed. F. Blatt, P. Schroeder, 1978, Plenum Publishing Corp, USA.

38. H. Sasaki, Y. Anzai, X.M. Huang, K. Terashima, and S. Kimura, 1995, Jpn. J. Appl. Phys. **34**, 414.

39. N. Koubaa, J.G. Gasser, 1990, J. Phys.: Condens. Matter **2**, 2297.

40. H. Sasaki, A. Ikari, K Terashima, S. Kimura, 1995, Jpn. J. Appl. Phys, Part 1, **34**, 3426.

41. V.M. Glazov, V. B. Koltsov, V.A. Kurbatov, 1986, Sov. Phys. Semicond. **20**, 1351.

42. G. B. Bachelet, D.R. Hamann, M. Schluter, 1982, Phys. Rev. B, **26**, 4199.

43. G. Kresse, J. Hafner, 1994, Phys. Rev. B **49**, No. 20, 14251.

44. P. Vashishta, K. S. Singwi, 1972, Phys. Rev. B **6**, 875.

45. S. Ichimaru, K. Utsumi, 1981, Phys. Rev. B **24**, 7385.

46. Y. Waseda, <u>The Structure of Non-Crystalline Materials</u>, 1980, McGraw Hill, USA.

47. R.V. Kulkarni, W. G. Aulbur, D. Stroud, 1997, Phys. Rev. B **55**, no. 11, 6896.

48. J.E. Enderby, S. Ansell, S. Krishnan, D.L. Price, M.-L. Saboungi, 1997, Appl. Phys. Lett **71**, 116

49. G. Busch, H. J. Guntherodt, h. U. Kunzi, H.A. Meier, Electronic Structure of Liquid Transition and Rare Earth Metals and their Alloys, in : <u>The Properties of Liquid Metals</u>, edited by s. Takeuchi , 1973, Taylor and Francis, London.

50. J. Katerberg, S. Niemeyer, D. Penning, J.B. VanZytveld, 1975, J. Phys F.: Metal Phys. **5**, L74.

51. F. Steglich, J. Aarts, C.D. Bredl, W. Lieke, D. Meschede, W. Franz, H. Schafer, 1979, Phys. Rev. Lett. **43**, 1892.

52. K. Suzuki, K. Sumiyama, Y. Homma, H. Ameno, T. Hihara, 1993, J. Non-Cryst. Solids, **156-158**, 328.

53.   J. M. Ziman, 1970, Proc. R. Soc. Lond. A **318**, 401.

54.   P. Terzieff, J. G. Gasser, 1994, J. Phys: Condens. Matter **6**, 603.

55.   P. Terzieff, J. G. Gasser, 1996 J. Phys.: Condens. Matter **8**, 7041.

56.   L. Schlapbach, 1974, Phys. Condens. Matter **18**, 189.

57.   R. Fresard, H. Beck, M. Itoh, 1990, J. Phys.: Condens. Matter **2**, 8827.

58.   R. Xu, 1993, Ph.D. Thesis, University of Gronigen, The Netherlands.

59.   Binary Alloy Phase Diagrams , Ed. T. Massalski, ASM International, Materials Park, OH, 1986.

60.   D. Zuo, T. Vos, H. Nymeyer, L. Reynolds, H.S. Schnyders, J. B. VanZytveld, 1996, J. Non-Cryst. Solids **205-207**.

61.   D. You, H.S. Schnyders, J.B. VanZytveld, 1997, J. Phys. Condens. Matter **9**, 407.

62.   Atlas of Crystal Structure Types for Intermetallic Phases, ASM International, Materials Park, OH, 1991.

APPENDICES

Electrical resistivity and thermopower of liquid Ge and Si

H S Schnyders† and J B Van Zytveld‡

Physics Department, Calvin College, Grand Rapids, MI 49546, USA

Abstract. The electrical resistivity ρ and thermopower S of pure liquid silicon and pure liquid germanium have been carefully measured. For silicon, a new containment material was used, namely high-density graphite. This graphite has a low thermopower (6 μV $^{\circ}$C^{-1} at 1500 $^{\circ}$C) a high resistivity (1000 $\mu\Omega$ cm at 1500 $^{\circ}$C), and little or no reaction with Si, making it an ideal containment material. The results for each liquid show a metallic value of resistivity, a small but positive temperature coefficient of the resistivity and a small thermopower. In particular, for liquid Si, $\rho = 75.2 \pm 0.6$ $\mu\Omega$ cm, $d\rho/dT = (1.7 \pm 0.9) \times 10^{-2}$ $\mu\Omega$ cm $^{\circ}$C^{-1} and $S = -2.1 \pm 0.6$ μ V $^{\circ}$C^{-1} and, for liquid Ge, $\rho = 66.8 \pm 0.2$ $\mu\Omega$ cm, $d\rho/dT = (2.7 \pm 0.2) \times 10^{-2}$ $\mu\Omega$ cm $^{\circ}$C^{-1} and $S = -0.3 \pm 0.5$ μ V $^{\circ}$C^{-1}; all values are for the respective melting temperatures of Si and Ge. We also report a calculation of the resistivity of each liquid, using the Ziman formalism, with a recent pseudopotential and an experimental structure factor. Both our experimental and our calculated results are compared with other work.

1. Introduction

The properties of liquid Si (ℓ-Si and liquid Ge (ℓ-Ge) have recently become the focus of new attention with the advent of successful new computing techniques which are yielding results previously unavailable. Among the unusual characteristics of these liquids which the new theoretical methods address are neutron and x-ray structure factors $A(Q)$, with a substantial shoulder on the high-Q side of the main peak, yielding a radial distribution function with a first-nearest-neighbour coordination as low as 5 [1]; a value of approximately 12 is normally associated with a close-packed simple liquid structure. This low co-ordination implies an open structure and perhaps indicates that some remants of the crystalline tetrahedral network remain. Early attempts to explain the structure factor of these liqids with multiple-diameter hard-sphere modelling [2] reproduced the first peak of $A(Q)$ fairly well, but became worse at higher Q. Other attempts suggests two kinds of coordination, with some of the atoms being fourfold co-ordinated and some being close packed [3]. More recently, Jank and Hafner [4] calculated the structure of these liquids, using pseudopotential perturbation theory (PPT) with a simple local Ashcroft pseudopotential; they concluded that the unusual coordination numbers of ℓ-Si and ℓ-Ge are a result of Freidel oscillations superimposed on the repulsive hump of the interatomic potential, and that the balance of volume energy and this potential leads to the splitting of the first coordination shell. The results for this calculation of the structure factor are in good agreement with the especially interesting new work of Stich *et al* [5], who have followed an *ab-initio* approach, working from local density functional

10875

(LDF) theory and using standard equations of motion for the ionic and for the electronic degrees of freedom. In addition to $A(Q)$, their model yields information on the electronic charge density dynamics; this displays a build-up of charge between neighbouring atoms in ℓ-Si that is interpreted with the aid of the triplet coordination function as the remnants of tetrahedral bonding in the liquid. Further study of ℓ-Ge by Kresse and Hafner [6] using the LDF has validated the earlier PPT study [4] and has also produced a self-diffusion coefficient that agrees well with experiment.

These computer models have also shown that the density-of-states (DOS) function of silicon becomes metallic and nearly free electron like upon melting in spite of the unusual coordination [4,7], losing the sharp features associated with sp^3 bonding in the solid. Although measured ultraviolet photoemission spectra have shown that the DOS for ℓ-Ge has a minimum between the s and p states [8], the minimum is well away from E_F (calculated from nearly-free-electron theory) and is not expected to affect the electronic transport properties.

Evidence such as this would suggest that the Ziman [9] theory, with an adequate pseudopotential and an accurate structure factor, could provide a relatively good calculation of the electronic transport properties for these liquids. In the Ziman formulation, the resistivity ρ for a pure liquid metal may be written

$$\rho = \frac{3\pi}{e^2\hbar v_F^2}\frac{N}{V}\frac{1}{4k_F^2}\int_0^{2k_F} Q^3 A(Q)|u(Q)|^2 \, dQ \tag{1}$$

where $u(Q)$ is the screened pseudopotential, $A(Q)$ is the structure factor and Q is the magnitude of the scattering vector. The thermopower is related to the logarithmic derivative of the resistivity:

$$S = \frac{+\pi^2 k_B T}{3|e|}\left(\frac{\partial\{\ln[\rho(E)]\}}{\partial E}\right)_{E=E_f}. \tag{2}$$

Improving theoretical (including molecular dynamics) techniques and more satisfactory pseudopotentials have created a demand for higher-quality measurements of the electronic properties of ℓ-Si and ℓ-Ge. Differences of about 20% between measured values of these properties by various workers make new and accurate measurements desirable. Here we present new measurements of ρ and S for these liquids that carry uncertainties of less than 1% for ρ and less than 0.6 μV°C^{-1} for S.

2. Experimental method

The experimental method used to study ℓ-Ge has been described in detail elsewhere [10]. The only modification to this is the addition of graphite plugs, used to seal the contact holes in the containment tubes; these more securely contain the liquid and allow electrical contact to be made to the sample. ℓ-Ge can be contained easily in high-density Al$_2$O$_3$ tubes with no evidence of attack, as is apparent from visual inspection, from the stability of the meaurements and from the ease of separation of the solid sample from the post-experiment tube. The resistivity was measured by the four-probe DC technique. The thermopower of germanium was measured relative to chromel counterelectrodes; $S(T)$ for chromel is from [10].

Numerous attempts have been made to measure the resistivity of ℓ-Si; we attribute some of the great disparity in the measurements to contamination of the samples due to containment in Al$_2$O$_3$ crucibles; we consider that all such measurements should be treated with caution because of serious corrosion that we have noted in our tests of ℓ-Si in Al$_2$O$_3$.

One recent measurement of p was done on a sample held in a boron nitride container [11]; we expect that this should provide a much better result. We find only one attempt to measure the thermopower of l-Si [12]; this measurement was conducted in an Al_2O_3 container and must therefore also be treated with care.

Because of the great difficulty usually experienced in containing l-Si, we shall describe our method in some detail. We found that we were able to contain this liquid very well within high-density graphite, which allowed us to sidestep the oxidation problems that plague experiments done in quartz or alumina containers. Other workers have found that conventional machined graphite rods immersed in l-Si experience a change in radius due to corrosion of only about 1.02×10^{-3} cm h^{-1} [13]; for our experimental containers this would result in about a 2% change in the cross-sectional area of the sample over the course of an average experiment. Further, these workers discovered that x-ray diffraction measurements on the boundary between l-Si and graphite display no evidence of diffraction peaks that would indicate the presence of silicon carbide [13]. (If an insulating layer of SiC were to form at this interface, it would prevent measurement of the transport properties.) In a separate test, we have measured the resistance of a graphite–l-Si–graphite junction for as long as 12 h and have seen no increase in the resistance, implying no measurable formation of SiC.

The previous tests done by other workers (noted above) were on graphite prepared by an unknown method and characterized only by some indication of its hardness (6–7 on the Mohs scale) and low porosity. Our graphite was supplied by ESPI, and was their Aeromet grade. This is the hardest, least porous graphite that they make and appears to be at least as good for containing l-Si as the previously tested material.

Not only are the containment properties of this graphite very good, but its electronic properties make it a nearly ideal sample holder at these temperatures. In particular, this material has a low thermopower (about 6 μV °C^{-1} at 1500 °C) and a high resistivity (about 1000 $\mu\Omega$ cm at 1500 °C). Tests of the resistivity and thermopower of Aeromet-grade graphite from room temperatures 1600 °C were conducted on numerous rods of different batch numbers, and several individual graphite rods were tested throughout the full range of temperature several times. Although the resistivity varied by about 10% from one rod to the next, the ratio $p(T)/p$ (room temperature) was highly reproducible. The thermopower of the graphite, however, was consistent to within ± 1 μV °C^{-1} on all rods tested. Standard curves were established on the basis of these tests so that a calibration for each tube constant could be done with mercury at room temperature, and the parameters of the tube at high temperatures could be computed. Plots of the calibration data are presented in figure 1.

To form each graphite tube, a graphite rod was drilled with a special hollow core drill, leaving a wall thickness of about 0.76 mm; triangular grooves for placement of contact wires were machined around its surface to a depth of about 0.20 mm. Voltage leads for resistivity measurements were made with Mo wires of nominal 0.102 mm diameter placed in these grooves and held in place with alumina clamps. The uncertainty introduced into the measurement by the machining of the grooves was estimated at below 0.1%. The thermocouples used for temperature measurement were W–5% Re and W–26% Re, were supplied in matched lengths by Omega Engineering Inc. and were quoted to be accurate to ± 1%. The W–26% Re leg also served as the counterelectrode for measurement of S, and its thermopower was measured to 1500 °C against Pt, using the results of Roberts *et al* [14] for Pt. Further calibration of W–26% Re below 1200 °C was conducted against chromel, with the thermopower of chromel taken from [10]. Moreover, these calibrations were also compared with data obtained from the thermocouple voltage curve for W versus W–26% Re published by Omega Engineering Inc, using data from Roberts *et al* [14] for
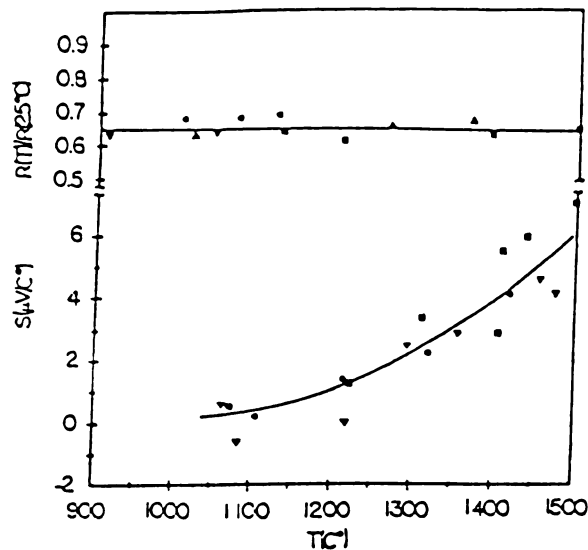
Figure 1. $R(T)/R$ (room temperature) and thermopower of ESPI Aeromet-grade high-density graphite. The thermopower was measured with W–26% Re counterelectrodes. The various symbols signify different graphite rods tested in separate experiments.

$S(T)$ for W. Our best fit to these data for W–26% Re is

$$S_{W-Re}(T) = -3.98582 + 6.91069 \times 10^{-2}T - 2.93294 \times 10^{-6}T^2 \ \mu V \, ^{\circ}C^{-1} \tag{3}$$

for the range of temperatures from 1000 to 1500 °C. We estimate the uncertainty in S to be $\pm 0.5 \ \mu V \, ^{\circ}C^{-1}$ for this material.

Values for ρ and S for ℓ-Si were extracted from measured data by considering the ℓ-Si and the graphite tube as parallel conductors. A 'small-thermal-gradient method' was used to obtain the relative thermopower dV/dT of the parallel combination. The thermopower S of the liquid was then obtained from the relation

$$S_1 = (1 + B)(S_x + dV/dT) - BS_t \tag{4}$$

where S_x is the thermopower of the counterlectrode (here W–26% Re), S_t is the thermopower of the graphite tube and

$$B = \rho_1 A_t / \rho_t A_1 \tag{5}$$

where A_t and A_1 are the cross-sectional areas of the tube and the sample, respectively, and ρ_t and ρ_1 are their resistivities. Because of the dimensions chosen for the tube and because of its electronic properties, the value of B in these experiments was only about 0.02; the contribution of B to the measured thermopower of the parallel system was therefore also very small, only about 0.12 $\mu V \, ^{\circ}C^{-1}$. As a result, uncertainties in the tube parameters contributed minimally to the final values obtained for S for ℓ-Si.

Germanium and silicon sample materials were supplied by Aesar–Johnson Matthey Co. and were of 99.9999% and 99.99% purity, respectively. All measurements were done in a system baked under vacuum and backfilled with argon.

89

3. Results

Our experimental results for *l*-Ge are shown in figures 2 and 3 and those for *l*-Si are shown in figures 4 and 5; these are also summarized in table 1, with some previous results. Both *l*-Si and *l*-Ge have the characteristics of metallic behaviour: fairly small values of resistivity, positive temperature slope of the resistivity and small thermopower. We made measurements on three separate samples of *l*-Ge; as can be seen in the figures, all the results are very consistent with one another. By making a least-squares linear fit to *all* our data we find ρ(*l*-Ge) at the melting point (938 °C) to be 66.8 ± 0.2 $\mu\Omega$ cm and $d\rho/dT = (2.7 \pm 0.2) \times 10^{-2}$ $\mu\Omega$ cm °C^{-1}. These values agree exceptionally well with the most recent results reported by Koubaa *et al* [15] (see table 1); we note also that these workers contained their sample in alumina and measured resistivity with the direct-contact four-probe technique. In addition, our results for the thermopower, (-0.3 ± 0.5) μV °C^{-1}, are also in good agreement with those of the same workers, as well as other recent work (see table 1).
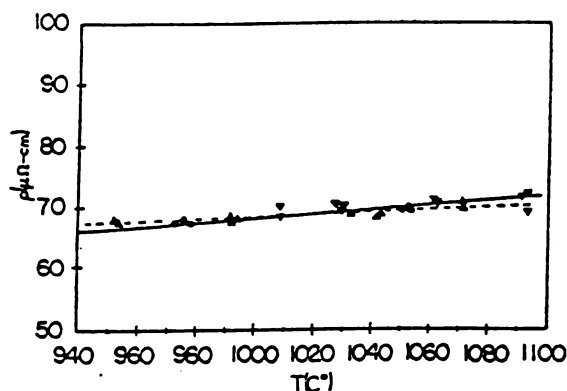

Figure 2. The electrical resistivity of *l*-Ge. Only a fraction of our resistivity points are shown for better graphical clarity, and different symbols signify separate samples. The results of Koubaa and Gasser [15] are shown as a broken line.

Our value of ρ(75.2 ± 0.6 $\mu\Omega$ cm at $T_{mp} = 1410$ °C) for *l*-Si, also obtained by a least-squares fit to all data, is very close to the recent value of Sasaki *et al* [11], who also used a four-probe measurement technique with boron nitride containment. As is evident in figure 4, one of our sets of measurements of resistivity of *l*-Si was somewhat higher than the others; the uncertainty and final value quoted include all the data. Using all our measurements of *l*-Si, the slope of the resistivity is $(1.8 \pm 0.9) \times 10^{-2}$ $\mu\Omega$ °C^{-1}. The measured thermopower of *l*-Si was very consistent through all experiments (three different samples); our value of -2.1 ± 0.6 μV °C^{-1} differs substantially from the earlier work of Glazov *et al* [12], however. We consider this difference a result of our improved containment method. (Containment for this ealier mearurement was Al$_2$O$_3$.)

4. Discussion

It is clear that our primary goal in this research, that of obtaining high-quality measurements of ρ and S for the *l*-Ge and *l*-Si, has been met. It will now be interesting to discover
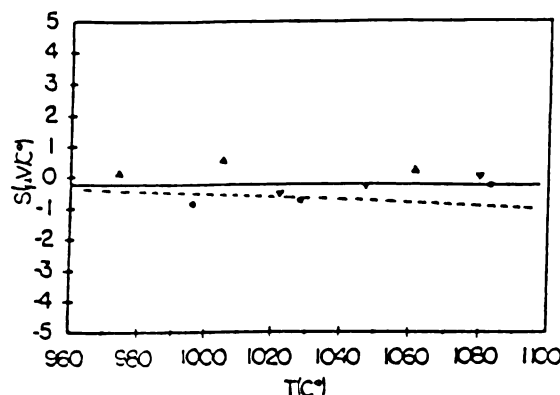
H S Schnyders and J B Van Zytveld

Figure 3. The thermopower of *ℓ*-Ge. The results for the three samples are shown with different symbols. The experimental thermopower of Koubaa and Gasser [15] is shown as a broken line.
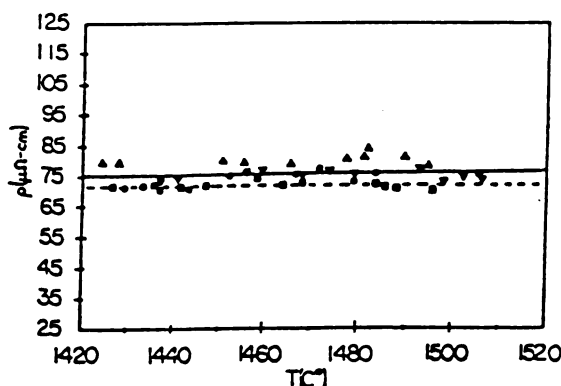

Figure 4. The electrical resistivity of *ℓ*-Si. Again, only a fraction of the resistivity points taken are shown, and results from four samples measured by the same method are shown as different symbols. For comparison, the results of Sasaki *et al* [11] are shown as a broken line.

how successfully various theoretical methods can reproduce these values for the electronic transport parameters. (Numerical results of these calculations are shown in table 2.)

Some early calculations of ρ and S for *ℓ*-Ge and *ℓ*-Si [16, 17] were relatively successful, utilizing the Ziman method and either a modified hard-sphere structure factor [17] or an experimental structure factor [16]. (In [16] the Ge $A(Q)$ was used in the calculations for Si; the results for this calculation of ρ and S were not nearly so good.) Their success is somewhat surprising, especially in the case of Rahman [17], since the softened hard-sphere structure factor used in that work inadequately describes the shoulder seen in the experimental scattering data [18, 19]. Other workers [11, 18, 20] have used the extended Ziman formulae, a t-matrix method developed especially to address the transition metals, and an experimentally determined $A(Q)$. The results of these calculations come very close to the measured values of these parameters in each case (see table 2).

Koubaa and Gasser [15] have recently attempted a calculation for *ℓ*-Ge, again utilizing a pseudopotential in the Ziman formalism, but have chosen the Bachelet–Haman–Schluter
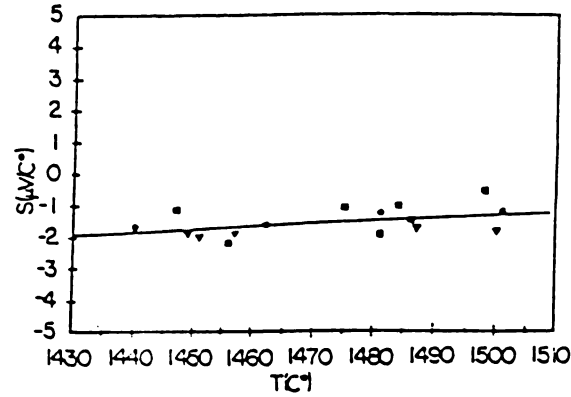
Figure 5. The thermopower of ℓ-Si. The different symbols denote different samples.

Table 1. Experimental values for ρ, $d\rho/dT$, S and dS/dT for ℓ-Ge and ℓ-Si at their respective melting temperatures. (The numbers in the square brackets identify the references.)

Metal	ρ ($\mu\Omega$ cm)	$d\rho/dT$ ($10^{-2}\ \mu\Omega$ cm $^{\circ}C^{-1}$)	S ($\mu V\ ^{\circ}C^{-1}$)	dS/dT ($10^{-3}\ \mu V\ ^{\circ}C^{-2}$)
Ge	66.8 ± 0.2 [present]	2.7 ± 0.2 [present]	−0.3 ± 0.5 [present]	0 ± 5 [present]
	67.8 [15]	1.3 [15]	−0.4 [15]	−4 [15]
	66 [26]	≃ 1.5 [28]	−0.5 [20]	−3.3 [20]
	85 [27]		0 [27]	
	80 [28]			
Si	75.2 ± 0.6 [present]	1.7 ± 0.9 [present]	−2.1 ± 0.6 [present]	9.1 ± 5.3 [present]
	72 [11]	(non-linear) [11]	−14 [12]	
	60 [27]			
	80 [26]	≃ 6 [12]		
	84 [12]			

(BHS) [21] non-local pseudopotential, one that is widely recognized currently for its broad utility. They also use the screening function of Vashishta and Singwi [22]. In separate calculations, with either a hard-sphere or an experimental structure factor, they have noted that the use of the experimental structure factor improves their results by 8 $\mu\Omega$ cm over the calculation employing hard spheres; their best calculation, however, is still 20% below our experimental value for ρ for ℓ-Ge (see table 2). Their calculated value for S for ℓ-Ge is relatively good (-2.2 $\mu V\ ^{\circ}C^{-1}$, compared with an experimental value of about -0.3 $\mu V\ ^{\circ}C^{-1}$).

In order to understand better the limitations of this pseudopotential method, and to extend its application to ℓ-Si, we have also calculated ρ for ℓ-Ge (and for ℓ-Si) using the BHS pseudopotential [21], the experimental structure factor of Waseda [23], and the screening function of Vashishta and Singwi [22]. (We did not pursue a thermopower calculation because of the sensitivity that we discovered in the calculation of ρ to the input parameters.) In the range of Q required for calculation of transport properties, the x-ray diffraction structure factor reported by Waseda [23] compares well with other work, including the recent x-ray data of Kita et al [1], and the neutron data of Gabathuler and Steeb

Table 2. Calculated values of ρ and S for ℓ-Ge and ℓ-Si near their respective melting temperatures. (The numbers in the sequence brackets identify references.)

Metal	ρ_{exp} ($\mu\Omega$ cm)	ρ_{calc} ($\mu\Omega$ cm)	S_{exp} (μV ^{2}C^{-1})	S_{calc} (μV $^{\circ}$C^{-1})
Ge	66.8 [present]	41.2 [present]	−0.3 [present]	−2.2 [15]
		55 [15]		−3.3 [20]
		66.2 [18]		−6.4 [16]
		45.5 [20]		−1.4 [17]
		75.9 [16]		−3.2 [18]
		57.4 [17]		
Si	75.2 [present]	66.6 [present]	−2.1 [present]	−3.6 [18]
		57 [5]		−1.1 [17]
		69 [11]		−10.1 [16]
		67.3 [18]		[Ge $A(Q)$]
		46.3 [17]		
		180 [16] [Ge $A(Q)$]		

[19]. The BHS pseudopotential also includes relativistic effects on the valence electrons by the atomic core region. This treatment has been validated by close agreement between calculations [21] and experiment for such properties as bulk moduli and phonon frequencies. Si and Ge have been specifically noted as two elements well described by this formulation [21]. (Stich *et al* [5] and Kresse and Hafner [24] have also used BHS potentials in their calculations recently. These potentials were modified slightly to lessen the number of high-frequency components in the potential and to ease its use in LDF calculations, but these modifications appear mostly above $Q = 2k_F$ and are outside the area of importance for calculation of transport properties by the Ziman formula.) For our purposes the non-local BHS pseudopotential should be fully adequate.

The value that we calculate for ρ for ℓ-Si, 66.6 $\mu\Omega$ cm, is rather close to the experimental value, but the result for ℓ-Ge is not nearly so good (41.2 $\mu\Omega$ cm). We found that, if we used the screening function of Itchumaru and Utsumi (IU) [25] in this calculation, even though it differed rather little from that of Vashishta and Singwi, we obtained a value for ρ for ℓ-Ge that was even lower by about 15 $\mu\Omega$ cm. (The small difference between the two screening functions occurs mainly in the range of Q where $A(Q)$ is large and contributes substantially to the calculation of ρ.) The calculation of ρ for ℓ-Si is affected much less by use of the IU screening function, lowering ρ by only 4 $\mu\Omega$ cm. Nonetheless, because of these sensitivities, we do not report calculations of thermopowers for these liquids.

It would now be especially interesting to see the results of applying the recently developed and highly successful *ab-initio* molecular dynamics methods of Car and Parrinello [7] to a calculation of the transport properties of ℓ-Ge and ℓ-Si. Some work along these lines has begun. As noted above, Stich *et al* [5] have successfully used optimally smooth BHS pseudopotentials to calculate numerous properties of ℓ-Si, including the structure factor and DOS; additionally, an extrapolation of AC conductivity to the DC limit for ℓ-Si gives a resistivity of 57 $\mu\Omega$ cm, in reasonable agreement with the measured value. Kresse and Hafner [6] have calculated the DOS for ℓ-Ge with the same method and this is in very good agreement with experiment, although no estimate of resistivity was given. Now that good experimental data are available for ρ and S for ℓ-Ge and ℓ-Si, it would be especially interesting to apply these new methods to the calculation of these parameters.

p and S of l-Ge and l-Si   10383

Acknowledgment

References

[1] Kita Y, Van Zytveld J B, Morita Z and Iida T 1994 *J. Phys.: Condens. Matter* **6** 811
[2] Zeng X 1989 *Phys. Chem. Liq.* **19** 69
[3] Ferranti A and Tosi M P 1989 *J. Phys.: Condens. Matter* **1** 1679
[4] Jank W and Hafner J 1990 *Phys. Rev.* B **41** 1497
[5] Stich I, Car R and Parrinello M 1991 *Phys. Rev.* B **44** 4262
[6] Kresse G and Hafner J 1994 *Phys. Rev.* B **49** 14251
[7] Car R and Parrinello M 1988 *Phys. Rev. Lett.* **60** 204
[8] Indlekofer G, Oelhafen P, Lapka R and Guntherodt H J 1988 *Z. Phys. Chem.* **157** 465
[9] Ziman J M 1961 *Phil. Mag.* **6** 1013
[10] Walhout H, Haarsma L and Van Zytveld J B 1989 *J. Phys.: Condens. Matter* **1** 2923
[11] Sasaki H, Ikari A, Terashima K and Kimura S 1995 *Japan. J. Appl. Phys.* Part 1 **34** 3426
[12] Glazov V M, Koltsov V B and Kurbatov V A 1986 *Sov. Phys.—Semicond.* **20** 1351
[13] Chaney R E and Varker C J 1976 *J. Electrochem. Soc.* **123** 846
[14] Roberts R B, Righini F and Compton R C 1985 *Phil. Mag.* B **52** 1147
[15] Koubaa N and Gasser J G 1990 *J. Phys.: Condens. Matter* **2** 2297
[16] Bose G, Gupta H C and Tripathi B B 1974 *J. Phys. Chem. Solids* **35** 595
[17] Rahman S M 1986 *Phil. Mag.* B **5** 391–8
[18] Waseda Y and Suzuki K 1975 *Z. Phys.* B **20** 339
[19] Gabathuler J P and Steeb S 1979 *Z. Naturf.* a **34** 1314
[20] Bath A, Hugel J and Kleim R 1985 *Phys. Status Solidi* **128** 761
[21] Bachelet G B, Hamann D R and Schluter M 1982 *Phys. Rev.* B **26** 4199
[22] Vashishta P and Singwi K S 1972 *Phys. Rev.* B **6** 875
[23] Waseda Y 1980 *The Structure of Non-crystalline Materials* (New York: McGraw-Hill)
[24] Kresse G and Hafner J 1994 *Phys. Rev.* B **49** 14251
[25] Ichimaru S and Utsumi K 1981 *Phys. Rev.* B **24** 7385
[26] Busch G and Guntherodt H J 1974 *Solid State Physics* vol 29, ed H Ehrenreich, F Seitz and D Turnbull (New York: Academic) p 235
[27] Cusack N E 1963 *Rep. Prog. Phys.* **26** 361
[28] Busch G and Tieche Y 1963 *Phys. Kondens. Mater.* **1** 78

The electronic transport properties of liquid Ag–Te

H S Schnyders†‡, J Hahn†, D Streutker† and J B Van Zytveld†§

† Physics Department, Calvin College, Grand Rapids, MI 49546, USA
‡ Department of Physics and Astronomy, Michigan State University, East Lansing, MI 48824, USA

Abstract. We have systematically measured the conductivity and the thermopower of the Ag–Te system for concentrations in the neighbourhood of Ag$_2$Te. Our ability to stir the sample while taking measurements has allowed us to accurately study the immiscible region below 31 at.% Te and to measure the complete extent of the p–n transition in the thermopower as stoichiometry is crossed. Our results are compared to the recent experimental results of Ohno *et al* [1], and are found to be largely in excellent agreement for thermopower and conductivity; however, in our data approximately at stoichiometry, a previously unseen feature in the conductivity is observed, and a significant deviation from the thermopower data of Ohno *et al* is also seen. This conductivity feature is consistent with, but much smaller than, peaks that have been observed in the conductivities in liquid Ag$_2$Se and Ag$_2$S. We also include data for $d\sigma/dT$ and dS/dT that have not been previously available. Our results are discussed in terms of the Kubo–Greenwood equations, and are compared to the highly unusual systems Ag–Se and Ag–S.

1. Introduction

Silver chalcogenide systems have been the subject of intense scrutiny in recent years because of the observation in Ag$_2$Se [2] and Ag$_2$S [3] of an unexpected rise in the conductivity, σ, to a sharp peak at stoichiometry. At temperatures of about 1000 °C, the peak has been observed to be about 100 Ω^{-1} cm^{-1} in height, approximately 6 at.% wide, and centred on stoichiometry. The peak in conductivity is accompanied in this narrow concentration range by a negative temperature coefficient; further from stoichiometry on either side, the temperature coefficient is positive. In the same range the thermopower, S, undergoes a p–n transition; for example, the thermopower of Ag$_2$Se changes from -60 to $+120$ μV °C^{-1}. Although a p–n transition is seen in a multitude of liquid semiconducting systems ($\sigma < 500$ Ω^{-1} cm^{-1}), the conductivity in these two unusual systems departs from the more regularly observed sharp minimum and positive temperature coefficient at stoichiometry. In this way, Ag–Se and Ag–S are unique among all liquid semiconductors. It is also interesting to consider whether these phenomena might be related to the fast-ion conducting character of Ag$_2$S and Ag$_2$Se in the high-temperature solid and in the liquid [4].

Perhaps just as curious as the feature in liquid Ag$_2$Se and Ag$_2$S is the apparent lack of such a phenomenon in the similar liquid alloy Ag$_2$Te. Early measurements of the conductivity of Ag–Te by Dancy [5], relying on convection alone to stir the sample, showed no evidence of the Ag–Se type conductivity behaviour, but rather displayed the

§ Present address: M J Murdock Charitable Trust, PO Box 1618, Vancouver, WA 98668, USA.

more conventional sharp minimum at stoichiometry, associated with a positive temperature coefficient. The immiscible region below 31 at.% Te prevented the complete measurement of the conductivity and the p–n transition in the thermopower in previous experiments. Later results by Okada *et al* [6] were also measured only above 31 at.% Te, and the 31–40 at.% region was largely untouched.

Following these results, the apparent difference in behaviour between Ag_2Te and Ag_2Se was addressed at a structural level via neutron diffraction by Price *et al* [7], who found that in both liquid alloys the structure was very similar. Ag_2Se displayed a prepeak at $Q \sim 1.8$ Å^{-1}, which was found in a later analysis by *ab initio* simulations to be the result of Se–Se coordinations not unlike those seen in the fast-ion conducting solid. It was noted that the prepeak was absent in Ag_2Te, but this was expected to be a result of the similarity of scattering lengths of the two materials. Most importantly, there was no noticeable structural change as the concentration of selenium was varied in a narrow range about stoichiometry, suggesting that structure was not responsible for the anomalous peak in the conductivity.

Very recent results by Ohno *et al* [1] have sampled the neighbourhood of stoichiometry in more closely spaced concentration steps, and have again found no special features. No mention is made, however, of the stability of the liquid at temperatures below the miscible–immiscible boundary at Te concentrations between 9 and 31 at.%, although measurements appear to have been made at these temperatures. Such a boundary is seen in roughly the same concentration range in both Ag–S and Ag–Se, and the earlier studies have considered only data taken at higher temperatures, in the miscible region.

Additionally, the experimental thermopower data taken at concentrations and temperatures within the immiscible portion of the phase diagram suggest by the asymmetry of the p–n transition that the slopes of the valence and conduction bands are highly asymmetric, following the formalism of Enderby *et al* [8]. But rigid band modelling, comparing experimental data to those generated by numerical integration of the Kubo–Greenwood equations, is incapable of reproducing even the general features of the conductivity and the thermopower. We have therefore studied Ag–Te once more in the neighbourhood of stoichiometry, proceeding in even finer concentration steps, and examining only the well stirred liquid.

2. Experimental details

The experimental apparatus used to study liquid Ag–Te has been described in detail elsewhere [9]. The only modification is the addition of graphite plugs, used to seal the contact holes in the alumina containment tubes; these more securely contain the liquid and allow electrical contact to be made with the sample. The alloy showed no evidence of attack on the Al_2O_3, and the solidified sample separated easily from the post-experiment tube. The tubes were open at the top to allow stirring, and all of the samples were agitated repeatedly during the experiments. Even in Te rich samples, the cool upper inside of the sample tube was free from condensed Te after the experiments, leading us to believe our concentrations were largely unaffected by evaporation. Conductivity was measured with the four-probe DC technique, and thermopower was measured with a chromel counterelectrode, with $S(T)$ for chromel from [10]. Our calibration for chromel is in excellent agreement with that of Cook and Laubitz [11], and we estimate the uncertainty in the absolute thermopower of chromel to be ±0.2 μV°C^{-1}. The sample concentration was not varied continuously during the experiment to avoid any possibility of progressive contamination; the majority of the samples were independently prepared in different alumina tubes from pure Ag and Te, making most data points completely independent of all others.
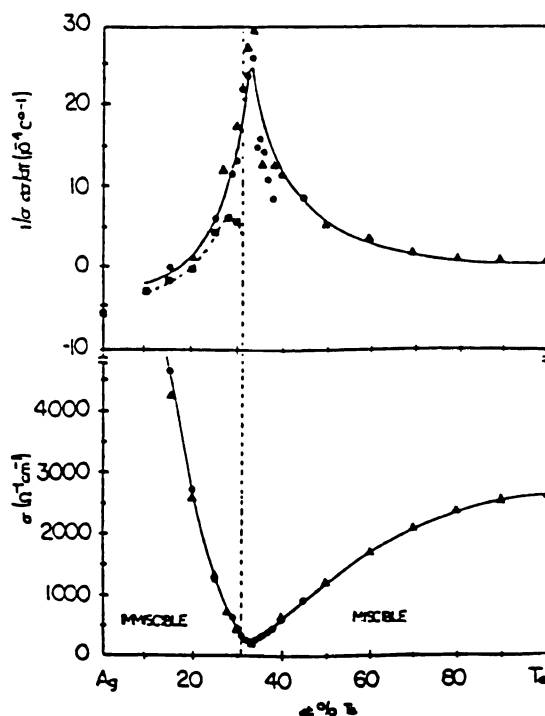
Figure 1. Measurements of σ and $1/\sigma \, d\sigma/dT$ fr $\cdot$ liquid Ag–Te. ●, current results as a function of Te concentration on the isotherm $T = 960\,^\circ C$; ▲, results of Ohno *et al* [1] for Ag–Te, $T = 1000\,^\circ C$; ■, results for Ohno *et al* [2] for Ag–Se. The upper concentration boundary of the immiscible region, 31 at%. Te, is denoted by a dashed vertical line; the other boundary is at 9 at.% Te. The uncertainty in σ is smaller than the extent of the points.

Silver and tellurium sample materials were supplied by Aesar–Johnson Matthey Co. and were of 99.99% and 99.999+% purity, respectively. The samples were prepared in air, but all measurements were made in a system that was baked under vacuum, and maintained during the experiment under 1 atmosphere of argon.

3. Results

Our results for the conductivity of Ag–Te as a function of Te content are shown in figure 1, and are seen to be in good general agreement with the results of Ohno *et al* [1]. Our points result from the evaluation at 960 °C of a linear fit to all of the data at each concentration. We also provide our data for the temperature coefficient of the conductivity, which also agree well with the limited data of Ohno *et al* [1], and appear to be rather asymmetric. Also shown on this graph are the boundaries of the immiscible region, according to Massalski [12]; the immiscible region extends from 31 at.% Te to 9 at.% Te, with a very sharply concentration dependent temperature boundary.

Figure 2 shows a curve fit to our data outside the immediate neighbourhood of stoichiometry. This curve falls below our data close to stoichiometry, and would suggest that our conductivity data do form a peak approximately at stoichiometry, extending from
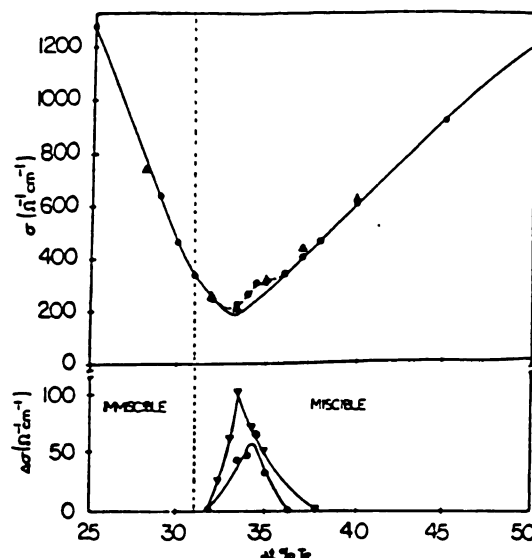
Figure 2. The conductivity of Ag–Te for a narrow range of Te concentrations, shown with a line drawn as a guide to the eye. Symbols are the same as for figure 1, and the immiscible boundary is again marked by a dashed line. The lower portion of the graph is the difference between the curve extrapolated from the experimental data at higher Te concentrations and our data near stoichiometry. ●, present data; ▲, data for Ag–Te from Ohno et al [1]; ▼, similar difference curve for Ag_2Se, from Ohno et al [2].

roughly 32 at.% to 36 at.% Te, with a maximum height of about 65 Ω^{-1} cm^{-1}. Also included on this graph is the difference between this curve and our experimental data; for comparison, similar difference data at 1000 °C for the peak in the Ag–Se system have been plotted as well (data from Ohno et al [2]). The peak in the conductivity of Ag–Te begins at roughly 32 at.% Te, and extends to roughly 36 at.% Te. It is quite similar to the peak in Ag–Se, which begins at roughly 31 at.% chalcogenide, and extends to 37 at.%, and which shows a significant broadening toward higher Se content as temperature is increased.

Figure 3 shows a graph of the conductivity at 30 at.% Te, which we have included to demonstrate the apparent lack of any mixing difficulties within the immiscible region. Our graph includes data for two different 30 at.% samples, both of which were measured during repeated stirring at temperatures above and below the boundary of the immiscible region. The Ag–Te phase diagram indicates the boundary is at roughly 1075 °C for this concentration, indicated with an arrow in the figure; the conductivity varies smoothly through this temperature. At no temperature in any of the Te alloys in this region is there a dramatic change of the slope or the magnitude of the conductivity which would indicate the presence of a mixed–unmixed boundary. In particular, the temperature coefficient is quite small and positive over all temperatures surveyed, in contrast to the very large positive slopes displayed by the unmixed Ag–Se and Ag–S alloys, which change to small positive slopes when the miscibility boundary is crossed. Furthermore, at various temperatures within the immiscible region, the sample was stirred, measured, and allowed to settle for several hours, at which time more measurements were taken. There was no time dependence of the electronic properties, which makes us believe that these components separate far more slowly in the immiscible region than in the other silver chalcogenide alloys.
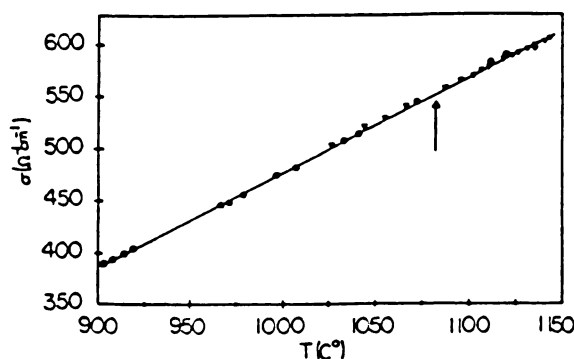
Figure 3. The conductivity for 30 at.% Te as a function of temperature. All of the data are current data, but different symbols denote separate experiments. Only a fraction of the data is shown of graphical clarity. The arrow denotes the temperature of the immiscible–miscible boundary of the liquid.

Our thermopower data (figure 4) we are generally in good agreement with Ohno *et al* [1]. Our study includes thermopower measurements in the immiscible region, and has verified that the thermopower extends at its lowest point to only $-13 \, \mu V \, °C^{-1}$. The dramatic dip in the thermopower seen in Ag–Se or Ag–S between 29% and 32% chalcogenide is absent in our Ag–Te data. Interestingly, the concentration dependence of our thermopower data through stoichiometry is very close to that in Ag_2Se, about $20 \, \mu V \, °C$ at.%$^{-1}$. (Measurements on Ag–S were not completed in this region because of miscibility problems.) The zero of the thermopower is at the same concentration as in the data of Ohno *et al* [1], 31.5 at.% Te, and less than the 36 at.% zero seen in Ag_2Se; it is not surprising that this is at a lower chalcogen concentration than in Ag–Se, as the deeply negative thermopower is not seen in our data. Additionally, our data recognize a small positive temperature coefficient of the thermopower at stoichiometry, in contradiction to the earlier study of Endo *et al* [4]. A positive temperature coefficient is also seen in Ag_2Se and Ag_2S.

It is interesting to note that while the data of Ohno *et al* [1] lie consistently $3–4 \, \mu V \, °C^{-1}$ below ours outside the neighbourhood of stoichiometry, perhaps due to their different counterelectrode material, in the area from ~34 at.% Te to 40 at.% Te their thermopower is above ours by as much as $25 \, \mu V \, °C^{-1}$. The difference between these measurements is well beyond the error quoted for their measurements (~$10 \, \mu V \, °C^{-1}$), and far greater than our estimated errors, about $3–5 \, \mu V \, °C^{-1}$. These concentrations are crucial to the definition of the curvature on the conductivity graph as stoichiometry is approached from the tellurium rich side, and ultimately to the identification of the peak in σ at stoichiometry.

4. Discussion

For the majority of liquid semiconductors, an analysis according to the method of Enderby *et al* [8] can yield a good qualitative agreement with experimental data. This method involves the numerical integration of the Kubo–Greenwood equations

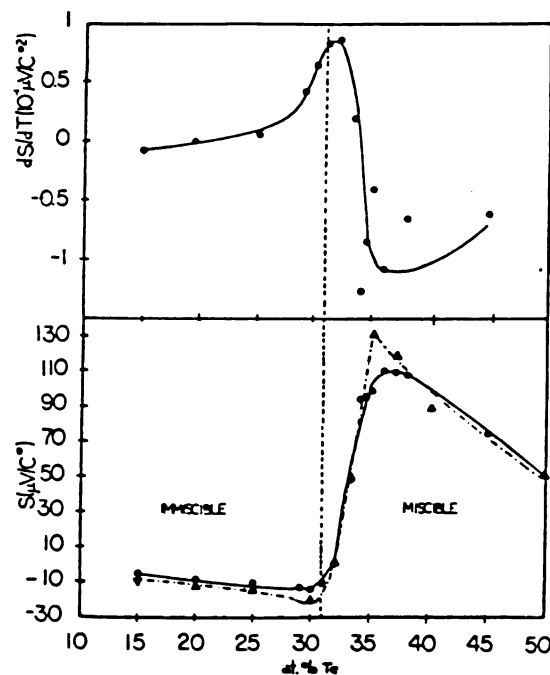$$\sigma = -\int_0^\infty \sigma(E) \frac{df}{dE} \, dE$$

Figure 4. The thermopower, S, and temperature coefficient of the thermopower, dS/dT, for liquid Ag–Te. Again, ●, current results at $T = 960\,°C$; ▲, results of Ohno *et al* [1] for Ag–Te, $T = 950\,°C$. Estimated uncertainties in S are 3–5 $\mu V\,°C^{-1}$. Again, the boundary of the immiscible region is marked by a vertical dashed line.

$$S = -\frac{k_B}{|e|} \int_0^\infty \frac{\sigma(E)}{\sigma} \frac{E - E_f}{k_B T} \frac{\delta f}{\delta E}\, dE$$

where f is the Fermi function, k_B is Boltzmann's constant, and E_f is the Fermi energy. $\sigma(E)$ is the energy dependent conductivity, and the valence and conduction band contributions may be expressed generally as

$$\sigma_c(E) = a_c(E - E_c) \qquad (E \geqslant E_c)$$
$$\sigma_v(E) = a_v(E_v - E) \qquad (E \leqslant E_v)$$

where E_c and E_v are the energies that denote the edges of the bands. The variables a_c and a_v may be calculated using the band width, the atomic separation, and the total number of electron states per unit volume in the band.

Our new data would suggest that the behaviour of AgTe around stoichiometry is rather more complex than a simple $\sigma(E)$ could explain. A consideration of the overall shape of $\sigma(c)$ for Ag–Te, neglecting the feature near stoichiometry, and of the behaviour of $S(c)$ on the Te rich side of stoichiometry would suggest that $\sigma(E)$ falls rather steeply to a gap or pseudogap within a few atomic per cent of stoichiometry. Using the random phase approximation and a model $\sigma(E)$ according to Barnes [13], with bandwidths from a calculation of the density of states for liquid Ag_2Te by Koslowski [14], we have calculated $a_c \sim 1300\ \Omega^{-1}\,cm^{-1}\,eV^{-1}$, in reasonable agreement with the choice of Ohno *et al* of $2000\ \Omega^{-1}\,cm^{-1}\,eV^{-1}$ [1]. A choice of $a_c = 2a_v$ for Ag–Te, similar to that chosen for Ag–Te [1], does indeed reproduce the asymmetry and magnitude of $\sigma(c)$ about stoichiometry, and

the thermopower rises to a maximum of roughly 100 $\mu V \,^\circ C^{-1}$. However, no choice of a_c, a_v, or band gap ΔE could reproduce the shallow $S(c)$ and steep $\sigma(c)$ in this concentration range simultaneously. A small feature can indeed be reproduced in the conductivity and the thermopower on the tellurium rich side of stoichiometry with a more detailed $\sigma(E)$ similar to that suggested by Enderby *et al* [8] for Cu_2Te, but only with the same inability to reproduce even the general shape of both $\sigma(c)$ and $S(c)$. We conclude that a rigid band model is not appropriate for liquid Ag–Te.

A neutron diffraction study by Price *et al* [7] indicates a prepeak exists in liquid Ag_2Se at $Q \sim 1.8\ \text{Å}^{-1}$, which has been determined experimentally by partial structure factor analysis to be most substantially composed of a contribution from the comparatively immobile Se ions. There is no apparent change in structure as concentration of Se is scanned through stoichiometry, making it unlikely that a structural change is the source of the unusual conductivity peak. Price *et al* also note the strong similarity of liquid Ag_2Se structure to liquid Ag_2Te; an absence of the prepeak in Ag_2Te is attributed to the similarity in scattering lengths of Ag and Te. It should be noted that all three silver chalcogenides have been shown to be fast-ion conductors.

It is therefore interesting that a recent neutron diffraction study of liquid Mg_3Bi_2 by Guo *et al* [15] indicates an ordering in the liquid similar to the fast-ion conducting solid phase of the same material. Furthermore, the structure shows broad similarity to that of Ag_2Se, including the presence of a prepeak at low wavenumber. Reverse Monte Carlo analysis suggests that the Bi–Bi distances generate the prepeak in Mg_3Bi_2, and that a shallow first minimum in the Mg–Mg real space distribution indicates that Mg ions are indeed quite mobile. Additionally, transport studies of Mg–Bi have shown that the inadequacy of a rigid $\sigma(E)$ is not limited to the silver chalcogenides. Guo *et al* find that fast-ion conducting liquid Mg_3Bi_2 is also difficult to explain using the Kubo–Greenwood formalism with any simple model $\sigma(E)$, because the conductivity drops to a sharp minimum while $|S| < 10\ \mu V \,^\circ C^{-1}$ around stoichiometry. By changing the concentration by only 1.5 at.% on either side of stoichiometry, the conductivity rises to values expected of a material with a shallow pseudogap.

In the absence of a structural explanation for the conductivity anomaly in Ag–Se, Ohno *et al* [3] suggested that the density of states in Ag_2Se may be modelled by rigid band behaviour, but that a sudden change in $d\sigma(E)/dE$ may be responsible for the unusual peak in the conductivity which spans the concentration range 31–37 at.% Se. The change in $\sigma(E)$ is believed to occur as a result of changes in mobility; magnetic susceptibility measurements indicated $N(E)$ was at a minimum at stoichiometry. The susceptibility measurements are in agreement with the conclusions of Koslowski [14], who calculated the density of states for all three silver chalcogenides using a simple tight-binding method, and found that with sufficient introduction of chemical bonds, the Fermi energy was indeed located in a pseudogap located between the silver s and tellurium p bands. Guo also postulated a change in $N(E)$ *and* the mobility to explain the small dS/dc through stoichiometry and shallow $d\theta/dc$ away from stoichiometry in Mg_3Bi_2, and further pointed to the work of Fortner *et al* [16] which suggests a possible link between mobile ions and enhanced mobility. Our new data, and the similarity in structure and transport to other similar alloys, suggest that a similar dramatic change in mobility or density of states occurs in Ag_2Te around stoichiometry.

At least four liquid fast-ion conductors have now been identified as being inadequately explained by the Kubo–Greenwood equations. Our study has revealed the presence of a peak in the conductivity near stoichiometry similar to that seen in the other silver chalcogenides, though smaller in magnitude. Ag–Te has also been studied at temperatures above and below

the immiscible boundary, and found at temperatures inside this region to be a surprisingly stable liquid.

Acknowledgment

References

[1]   Ohno S, Mizushina Y, Okada T and Togashi M 1996 *J. Phys. Soc. Japan* **65** 2182
[2]   Ohno S, Barnes A C and Enderby J E 1990 *J. Phys.: Condens. Matter* **2** 7707
[3]   Ohno S, Barnes A C and Enderby J E 1994 *J. Phys.: Condens. Matter* **6** 5335
[4]   Endo H, Yao M and Ishida K 1980 *J. Phys. Soc. Japan* **48** 235
[5]   Dancy E 1965 *Trans. Metall. Soc. AIME* **233** 270
[6]   Okada T, Kakinuma F and Ohno S 1983 *J. Phys. Soc. Japan* **52** 3526
[7]   Price D, Saboungi M-L, Susman S, Volin K, Enderby J and Barnes A 1993 *J. Phys.: Condens. Matter* **5** 3087
[8]   Enderby J E *et al* 1990 *Rep. Prog. Phys.* **53** 85
[9]   Walhout M, Haarsma L and Van Zytveld J B 1989 *J. Phys.: Condens. Matter* **1** 2923
[10] Kooistra J, Dreyer K and Van Zytveld J B 1988 *J. Phys. F: Met. Phys.* **18** 1225
[11] Cook S G and Laubitz M S 1976 *Can. J. Phys.* **54** 928
[12] Massalski T 1986 *Binary Alloy Phase Diagrams* (Metals Park, OH: American Society for Metals)
[13] Barnes A C 1993 *J. Non-Cryst. Solids* **156–158** 675
[14] Koslowski T 1996 *J. Phys.: Condens. Matter* **8** 7031
[15] Guo C, Barnes A C and Howells W S 1996 *J. Phys.: Condens. Matter* **8** 10823
[16] Fortner J, Saboungi M-L and Enderby J E 1994 *Phys. Rev. Lett.* **74** 1415

Diffraction Electronic Transport and Neutron Evidence for Chemical Short Range Order in Liquid Cu$_6$Ce.

Harold S. Schnyders*

J.B. VanZytveld**

Physics Department, Calvin College, Grand Rapids, MI 49546 USA

*Also at: Physics and Astronomy, Michigan State University, East Lansing, MI 48824, USA
**Also at: M J Murdock Charitable Trust, PO Box 1618 ,Vancouver WA 98668

Abstract

We have measured the electronic resistivity and thermopower of liquid $Cu_{1-c}Ce_c$, $Cu_{1-c}La_c$, and $Ag_{1-c}Ce_c$ alloys for c<0.4. In all of the alloys the resistivity is very similar, rising smoothly and steeply as x increases, but at all times remaining less than 200 $\mu\Omega$-cm.. The thermopower is also featureless and metallic. However, the temperature coefficient, a=1/p dp/dt, displays in the Cu alloys a minimum at Cu_6RE (RE=Rare Earth), which furthermore is negative in Cu_6Ce; a negative temperature coefficient is also seen at Ag_3Ce. We also present the results of neutron diffraction scattering from liquid Cu_6Ce, and of a Reverse Monte Carlo (RMC) analysis of the structure data, which shows evidence for ordering in the liquid, with characteristics similar to crystalline Cu_6Ce. We discuss several possible explanations for the negative temperature coefficient in both Ag and Cu alloys, and conclude that it's origin the presence of Chemical Short Range Order (CSRO).

Introduction

The resistivities of liquid copper alloys with Rare Earths (RE) were first studied by Guntherodt *et.al.* [1]. All of the alloys studied, including those with La, Ce, Nd, and Pr, show remarkably similar behavior up to 40 at. % RE. Furthermore, the highest resistivity of the alloys, approximately at the equiatomic concentration, is still metallic in magnitude. In addition, the temperature coefficient of the resistivity, a=1/p dp/dT , was in all alloys at all concentrations determined to be small and positive. A simple description seemed in order, due to the apparent lack of effect on p or a of the additional f electrons contributed by the RE's; weak scattering Faber-Ziman theory seemed appropriate because magnitude of the resistivity was far less than in divalent liquid Ba (p=338 $\mu\Omega$-cm [2]), which was successfully modelled by the theory.

In later structure measurements by anomalous X-ray diffraction, Cu-Ce was determined by Waseda [3] to be unremarkable across a wide range of rare earth concentrations; these authors suggested that the alloy was most likely a simple random mixture of Ce and Cu atoms, based on the apparent invariability with respect to Ce content of the peak positions in the partial structure factors. However no structure measurements were made below 20 at. % Ce.

Additional recent interest in some RE-alloys stems from the fact that they are Heavy Fermion compounds. This is also true for Cu_6Ce. Sputter deposited amorphous Cu_6Ce was discovered comparatively recently by Suzuki *et.al.* [4] to display at low temperatures

the -log(T) dependance of the resistivity characteristic of Heavy Fermion behavior, and similar to the behavior recorded previously in Cu_6Ce crystal [5]. The amorphous alloy shows a continued linear temperature dependance of p with negative a up to the highest temperature surveyed, about 300 K. The absence of thermopower data for liquid Cu-RE compounds, the availability of high purity materials, and the unusual negative temperature coefficient (NTC) in the amorphous solid have prompted us to systematically study these liquid materials. We have for comparison measured the electronic transport properties of liquid Ag-Ce; we believe these are the first electronic transport measurements on this liquid system. In addition, we have conducted a neutron diffraction study of liquid Cu_6Ce, and have also done a Reverse Monte Carlo (RMC) analysis. The results of the transport measurements and the structure measurements are discussed in separate sections below.

Transport Properties: Experimental details

We obtained sample materials from AESAR/Johnson Matthey: lot analyses of La and Ce yielded impurity levels of 60 and 200 ppm (wt), respectively; Ag and Cu, from the same supplier, were of 99.99% and 99.999% purity. Samples were prepared and handled under an argon atmosphere in an evacuable glove box to avoid contamination. During measurements, our alloys were held in high density Al_2O_3 tubes, and were stirred vigorously to ensure uniformity. Sample material separated easily from the wall of the post experiment tube, and no reaction is thought to have occurred. (For a more detailed description of the sample containment see Walhout et.al. [6]). The resistivity was measured using a standard 4 probe technique, and the thermopower was measured against chromel counterelectrodes [7]; the uncertainty in the absolute thermopower of chromel is estimated to be + 0.2 μV/°C. The error in the resistivity and the thermopower are calculated from a least squares fit to all of the data, and in the majority of cases do not exceed 0.5 μΩ cm and 0.3 μV/°C, respectively.

Results

Our results for the resitivity of liquid Cu-Ce are shown in figure 1, along with our data for Cu-La and Ag-Ce, and Cu-Nd data from Guntherodt and Zimmerman[8]. All data points shown are from a linear fit to all of the data, evaluated at 950° C, except for the Ag alloys, which were evaluated at 1050° C . In all cases, the resistivity rises smoothly from pure

Cu(Ag) as rare earth content is increased. The resistivity of the different alloys is remarkably similar up to 35 at. % RE; none of the alloys show any features in the resistivity, even at Cu_6RE or Cu_2RE, or at Ag_3Ce, which are the concentrations of congruently melting crystalline compounds, and correspond to peaks in the melting curve. Even near the equiatomic concentration and the highest resistivity in the alloys, all of the materials hold values of the resistivity which are well within the bounds of metallic conduction.

Figure 2 displays the concentration dependance of the thermopower; in all cases, dS/dc is quite steep from pure Cu(Ag) to ~30 at. % rare earth; again, S is featureless and smooth, and at all concentrations examined holds a value which is decidedly metallic and between the values of S for the pure constituents.

Figure 3 shows the concentration dependance of the temperature coefficient of the resistivity, a. In Cu-Nd , a is quite small and positive over a wide range of RE concentration, but appears to have a very shallow minimum at Cu_6Nd. In both Cu_6Ce and Cu_6La, a is markedly depressed compared to surrounding concentrations, and furthermore is negative in Cu_6Ce. It is highly unusual to see structure in a and not in the resistivity or thermopower; furthermore, to our knowledge, this is the lowest resistivity in a liquid alloy, about 95 $\mu\Omega$-cm, associated with NTC. Our value of a= $-1.8*10^{-4}$ $C^{\circ -1}$ is comparable to that seen in the divalent pure liquid elements like Sr and Zn, and in the divalent alloy SnCe. In Ag_3Ce, a = $-1.6*10^{-4}$ $C^{\circ -1}$, but again, no features are seen in p or S .

In all of the studied materials, the minima in a correspond to peaks in the melting curve. Cu_6RE, for RE= La, Ce, Pr, and Nd all possess the same crystal structure and melt congruently from an orthorombic structure; Ag_3Ce melts from a hexagonal crystal structure. It is interesting that the minimum in a around stoichiometry is most pronounced in Cu_6Ce, which has the highest melting point of the Cu-RE compounds studied, and is least pronounced in Cu_6Nd, the lowest melting point compound. With this in mind, we have conducted a neutron diffraction study of liquid Cu_6Ce.

Neutron Diffraction: Procedure

The neutron diffraction study was performed on the GLAD (Glass, Liquid, and

Amorphous Diffractometer) at the Intense Pulsed Neutron Source (IPNS) at Argonne National Laboratory. Sample material of the purity noted earlier was prepared in an argon atmosphere, as above, and was initially melted and stirred in an alumina tube under argon, prior to being sealed under argon in a vanadium tube for the scattering experiment. The alloy sample was not at any time exposed to the atmosphere. The experiment was conducted at 1000 C° within a cylindrical vanadium furnace in a vacuum. Data for the empty tube, and for the furnace, were subtracted from the experimental spectra before analysis.

Diffraction results

The experimental structure factor, $S(Q)$, is shown in figure 4. A significantly robust prepeak is seen at 1.6 Å^{-1}; in other alloys, a prepeak in the structure factor at low Q value has been interpreted [9] as evidence of CSRO.

Fourier transform of the data up to $Q=25\text{Å}^{-1}$, using a Lorch window to truncate, leads to the pair correlation function $g(r)$. The total correlation function, $T(r)=r*g(r)$, is shown in figure 5. The main peak in $T(r)$ is at 2.5 Å, and a shoulder is seen on the high r side at 3.05 Å. Because of the relative concentrations of Cu and Ce, and because the scattering length of Cu is nearly twice that of Ce, the structure seen in $T(r)$ is most significantly composed of Cu-Cu correlations. The total structure factor may be calculated according to the following formula

$$S(Q) = \sum_{ij} c_i \, c_j \, b_i \, b_j \, (S_{ij}(Q)-1)$$

where c_i is the concentration of constituent i, b_i is the scattering length, and $S_{ij}(Q)$ is the partial structure factor. For our alloy, the weightings of the partials are as follows: Cu-Cu=.4375, Cu-Ce=.0916, Ce-Ce=.0048.

The coordinations may be calculated from the area of gaussians fitted beneath the $T(r)$ curve. The first gaussian is certainly Cu-Cu correlation exclusively; the second, however, is probably a combination of CuCu and CuCe coordinations, mostly CuCu. If we take the total area under both Gaussians as CuCu, we calculate Cu coordination of 10.7, which compares favorably with the average coordination of Cu to Cu in crystalline Cu_6Ce calculated out to 4 Å, about 9.3. However, CuCe distances of ~3-3.4 Å also exist in the crystal, and almost certainly comprise a portion of the second gaussian. To continue this analysis, we have utilized RMC to further examine the structure factor, and to shed

light on the origin of the prepeak.

Two different initial configurations were selected for our simulations; 1. A random arrangement of 1050 atoms of the stoichiometric concentration. The following minimum distances of approach were used: r_{CuCu}= 2Å, r_{CuCe}= 2.55Å, and r_{CeCe}=2.85Å, very similar to the first peak positions of liquid $Cu_{.75}Ce_{.25}$, according to the anomalous x-ray diffraction results of Waseda [3]. 2) A crystalline configuration of Cu_6Ce[10], with 3500 atoms, and with the minimum distances of approach the same as above. The program fitted the calculated S(Q) to the experimental structure factor data; the results are shown in figure 4. The quality of fit parameter, c2 , of the simulation started from the initial crystalline configuration, and of the simulation started from a random initial arrangement ultimately converged to within 2% of one another; both simulations were successful at reproducing the prepeak.

The main peak in S(Q) is very well reproduced in height, width, and position for both starting configurations, but for the second and following peaks the RMC fits were less effective. The baseline against which the height of the prepeak may be measured appears to have been set rather too high by the simulation. However, for both simulations, the height of the peak in S(Q) with regards to this baseline is in good agreement with the height of the experimental peak, but it is only as pronounced as the experimental prepeak in the simulation starting from the crystalline arrangement. The prepeak is found in both cases in the CuCu partial structure factor; and is centered at 1.6 $Å^{-1}$ (figure 6). At the same momentum transfer, there is a deep minimum in the CeCu partial, which in spite of it's significantly lower weighting in the total structure factor serves to diminish the height of the prepeak . We find that essentially the same quality of overall fit as measured by c2 is achieved for minimum approach values 2.55Å< r_{CuCe}<2.9Å, although inspection of the post simulation CuCe partial g(r) shows that for r_{CuCe}<2.9Å, the partial looks rather unnatural and probably non-physical; we believe that the weighting of the CuCe partial is just large enough to yield an adequate fit. S_{CeCe}(Q), on the other hand, was not well modelled by RMC due to the relative lack of information about it in the experimental S(Q), and will not be discussed further . The main peak of the CuCe partial S(Q) is at 3 $Å^{-1}$, and the CuCu peak is at 2.5$Å^{-1}$.

Fourier transformation of the RMC partial structure factor of CuCu yields g_{CuCu}(r) with a main peak at 2.5Å (figure 7); the high r side of this peak is significantly less sharply inclined than the low r side, and perhaps indicates the presence of a shoulder, or nearby

smaller peak at a value of about 2.9Å, in agreement with the gaussians fitted to the experimental g(r). The next peak at 4.4Å is still quite strong, and is precisely a CuCu distance in the crystalline solid. The RMC partial $g_{CuCe}(r)$ (not displayed) is peaked at 2.9 Å, close to the CuCe distances of 3Å-3.4 Å seen in the crystalline solid.

RMC analysis has also allowed an examination of the bond angle distributions; we expect the simulated CuCuCu bond angles to be most reliable because of the exceptional weight of CuCu correlations in S(Q). An examination of the pre-simulation bond angle distribution for the initial random configuration subjected only to moving out of the particles to minimum distances of approach, and using an atom-atom separation cutoff of 4Å, showed a rather flat distribution (figure 8), indicative of a random arrangement. The post simulation angle distribution with a similar cutoff shows a peak at about 55°, and a somewhat more broad peak at around 105°; interestingly, crystalline Cu_6Ce has bond angles in a range of angles around 60° and 110°, but a lack of bond angles in between; the post simulation bond angle distribution reflects a lesser number of bonds in this same region. There is, however, no evidence in the liquid of the much less common 140° angles also seen in the crystal.

Discussion

Several possible explanations for NTC in alloy systems exist, but the results for these systems appear to provide an unusual challenge. Divalent pure liquid metals and liquid alloys often display a NTC. This behavior for pure metals occurs as a result of the temperature dependance of the main peak in the structure factor, S(Q), and is seen uniquely for divalent liquids because of the relative positions of $2k_f$ (where k_f is the Fermi wave vector) and this primary peak in S(Q) [11]. A similar situation occurs for liquid alloys. This characteristic NTC has been seen for liquids with rather low values of p, as in our . alloys, but is seen only if the effective valence of the liquid is close to 2 [12]. If we assume that La and Ce each contribute 3 electrons per atom to the conduction band, and Cu and Ag contribute 1, the Z_{eff} = 1.3 for Cu_6Ce and Cu_6La and 1.5 for $CeAg_3$, rather too far from 2 to show divalent character.

NTC's are also expected and observed for liquid and amorphous metals and alloys for which E_f falls approximately at a fairly deep minimum in the Density of States (DOS). Fresard, Beck, and Itoh [13] examine this model and further assume non-degeneracy of

the conduction electrons (ie: that df_{FD}/dE evaluated at E_f cannot be approximated by a d-function, an assumption that is particularly important at high temperatures, where f_{FD} is the Fermi-Dirac distribution function) but take only elastic scattering into account, and find that they obtain NTC at high temperatures even in this case, but only for p > 400 $\mu\Omega$-cm. They take this to be a possible explanation (at high temperatures) of the behavior that has come to be called the Mooij Correlation: NTC associated with large p. However, they also found that in such cases the thermopower is especially sensitive to features in the DOS. Our experimental thermopower and resistivity show no signs of the behavior predicted by this model.

If NTC results from the release of electrons into the conduction band from covalent or ionic bonds as the temperature increases, one often observes a negative minimum in a(c) accompanying a maximum in p(c). These NTC's also tend to be quite sharply concentration dependant and to occur at compositions corresponding to maxima in the respective melting curves, and to rather strongly bound crystal structures in the solid alloy. While the NTC's that we see in liquid Cu-Ce and Ag-Ce do occur at maxima in their melting curves, and these also do correspond to preferred solid crystal structures, no feature is apparent in p(c) at these compositions that would reflect evidence for bound clusters in these liquids. Moreover, p at these compositions is quite low (~100 $\mu\Omega$ -cm), and reaches it's peak at much higher RE-concentrations.

Salmon [9] has discussed the importance of the position, width, and height of the first sharp diffraction peak in liquids. Significantly, the width of the peak has proved in several cases to be directly related to the r space distance over which CSRO is present, and the height of the peak to the amplitude of the density fluctuations in g(r). The height of the prepeak in the RMC $S_{CuCu}(Q)$ suggest that the concentration fluctuations are not large. Also, the width implies that the order tapers quickly in the liquid. Such weak order is quite consistent with the absence of features in p or S. We suggest that a is perhaps a more sensitive indicator of CSRO than p or S, and that the NTC in Cu-Ce and Ag-Ce is indicative of ordering in those systems. We turn for an example of this sensitivity to the liquid Al_2Ca system [14], which also possesses small p (< 150$\mu\Omega$-cm) and a NTC (a= -9 x 10^{-4} C° $^{-1}$). The resistivity in this case is also featureless and metallic, as is the thermopower; however, the substitution of Ga for Al gives strong evidence that clusters of Al_2Ca do exist in this system.

Perhaps the strongest single argument in favor of CSRO in liquid Cu_6Ce is the

close similarity of the CuCuCu bond angle distributions for the RMC generated data and the crystalline material. (Figure 8). The cluster of bond angles in the liquid near $55°$ compares well with the crystalline configuration, which is peaked slightly closer to $60°$. It is unlikely that these angles result merely from close packing in the liquid because of the substantial size difference between Cu and Ce atoms (about 50%). It is also clear from examination of the arrangement of atoms in the crystal that bond angles near $115°-120°$ at least for the crystal are quite independent of those at $60°$ (not necessarily $2 \times 60°$). Perhaps those near $110°$ in the liquid are similarly independent.

We have argued that CSRO does occur in liquid Cu_6Ce. This implies that CSRO can be seen even in liquid alloys with $p < 100 \ \mu\Omega$ -cm. The magnitude of the NTC and the height and width of the prepeak in the structure factor indicate that perhaps only a small fraction of the atoms participate in clustering on average, which could explain the lack of discernible features in p or S. It is significant that no signs of a prepeak are seen in $S_{CuCu}(Q)$ for liquid $Cu_{.75}Ce_{.25}$ [3], even at this concentration comparatively close to Cu_6Ce. A shallow minimum can be seen in Waseda's partial $S_{CeCu}(Q)$ at $1.6 \ Å^{-1}$, but it cannot compare in depth to the minimum modelled in our RMC calculations. It might be reasoned that weak ordering occurs in a reasonably narrow concentration range around stoichiometry; this is consistent with the narrowness of the minimum in a. The chemical similarity with other Cu alloys with the light rare earths, and similarity of a for liquid Cu-La, invite further study into possible ordering in these alloys, and possibly RE alloys with other noble metals.

[1]   G. Busch, H.J. Güntherodt, H.U. Künzi and H.A. Meier, Electronic Structure of Liquid Transition and Rare Earth Metals and their Alloys, in: The Properties of Liquid Metals, edited by S. Takeuchi (Taylor and Francis, London, 1973), p. 263-276.

[2]   J.B. Van Zytveld, 1977, Inst. Phys. Conf. Ser. No. 30, p. 212.

[3]   Y. Waseda, The Structure of Non-Crystalline Materials; Liquids and Amorphous Solids, 1980, McGraw-Hill Inc., USA.

[4]   K. Suzuki, K. Sumiyama, Y. Homma, H. Ameno, and T. Hihara, 1993, J. Non-Cryst. Solids, 156-158, 328.

[5]   F. Steglich, J. Aarts, C.D. Bredl, W. Lieke, D. Meschede, W. Franz, and H. Schäfer, 1979, Phys. Rev. Lett. 43, 1892.

[6]   M. Walhout, L. Haarsma, and J.B. Van Zytveld, 1989, J. Phys.: Condens. Matter 1, 2923.

[7]   J. Kooistra, K. Dreyer, and J.B. Van Zytveld, 1988, J. Phys. F.: Met. Phys. 18, 1225.

[8]   H.-J. Güntherodt and A. Zimmermann, 1973, Phys. Kondens. Materie 16, 327.

[9]   P. Salmon, 1994, Proc. R. Soc. Lond. A, 445.

[10]   "Atlas of Crystal Structure Types for Intermetallic Phases", ASM International, Materials Park, OH, 1991

[11]   L. Rottman, J.B. Van Zytveld, 1979, J. Phys. F: Met. Phys. 9, 2049-56.

[12]   J.M. Ziman, 1970, Proc. R. Soc. Lond. A 318, 401.

[13]   R. Fresard, H. Beck, and M. Itoh, 1990, J. Phys.: Condens. Matter 2, 8827.

[14]   D. You, H.S. Schnyders, and J.B. Van Zytveld, 1997, J. Phys.: Condens. Matter 9, 1407- 15 .

[15]   J. Van Zytveld, "Liquid Metals and Alloys", Handbook on the Physics and Chemistry of Rare Earths, Vol. 12, edited by K.A. Gschneidner Jr, and L. Eyring, Elsevier Science Publishers B.V., 1989.

112

Figure 1: ρ as a function of atomic fraction, c, of RE, for the liquid alloys: Cu-Ce, Cu-La, Cu-Nd, Ag-Ce. Present results: ● -Cu-Ce;   ■ -Cu-La;   ▼ -Ag-Ce.   ▲ -Cu-Nd, reference [8]. In all cases, the error bars are encompassed by the point.

Figure 2: S as a function of atomic fraction, c, of RE, for the liquid alloys: Cu-Ce, Cu-La, Ag-Ce. Present results: ● -Cu-Ce;   ■ -Cu-La;   ▼ -Ag-Ce.   Unless shown, error bars are to be considered smaller than the extent of the point.

Figure 3: $1/\rho \, d\,\rho/dT$ as a function of atomic fraction, c, of RE, for the liquid alloys: Cu-Ce, Cu-La, Cu-Nd, Ag-Ce. Present results: ● -Cu-Ce;   ■ -Cu-La;   ▼ -Ag-Ce.   ▲ -Cu-Nd, reference [8];   data for pure liquid Ce, La, Nd from [15].

Figure 4: The experimental total structure factor, $S(Q) - 1$, for liquid Cu_6Ce (solid line), shown with the converged Reverse Monte Carlo fit started from the crystalline configuration of 3500 atoms (dashed line).

Figure 5: The total correlation function, $T(r) = r * g(r)$; $g(r)$ is obtained by fourier transform of the experimental structure factor $S(Q)$ for liquid Cu_6Ce. The dashed lines result from a Gaussian deconvolution of $T(r)$.

Figure 6: The RMC partial structure factor, $S_{cucu}(Q) - 1$, for liquid Cu_6Ce: dashed line - simulation results starting from a random initial configuration;   solid line- simulation results starting from the crystalline initial configuration.

Figure 7: The RMC partial pair correlation function, $g_{cucu}(r)$, for liquid Cu_6Ce: dashed line - simulation results starting from a random initial configuration;   solid line- simulation results starting from the crystalline initial configuration.

Figure 8: The RMC CuCuCu bond angle distribution for Cu_6Ce. Uppermost line: Bond angle distribution of the initial random arrangement. Middle line: Bond angle distribution at the conclusion of RMC simulation for initially random arrangement (solid line), and initially crystalline arrangement (dashed line). Bottom line: Bond angle distribution for initial crystalline configuration
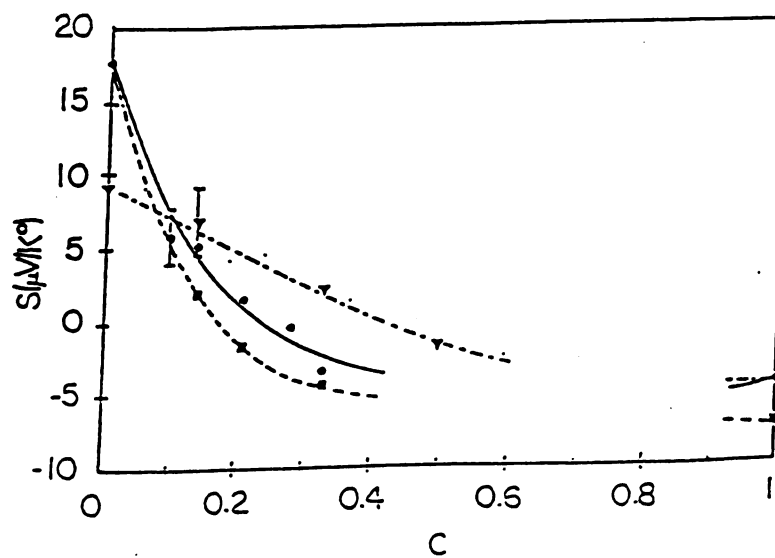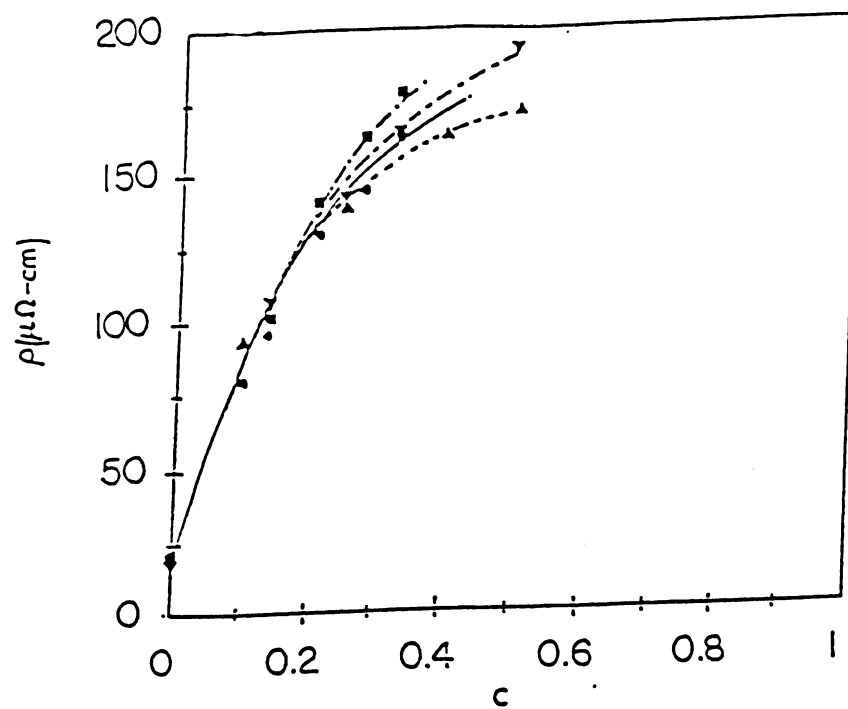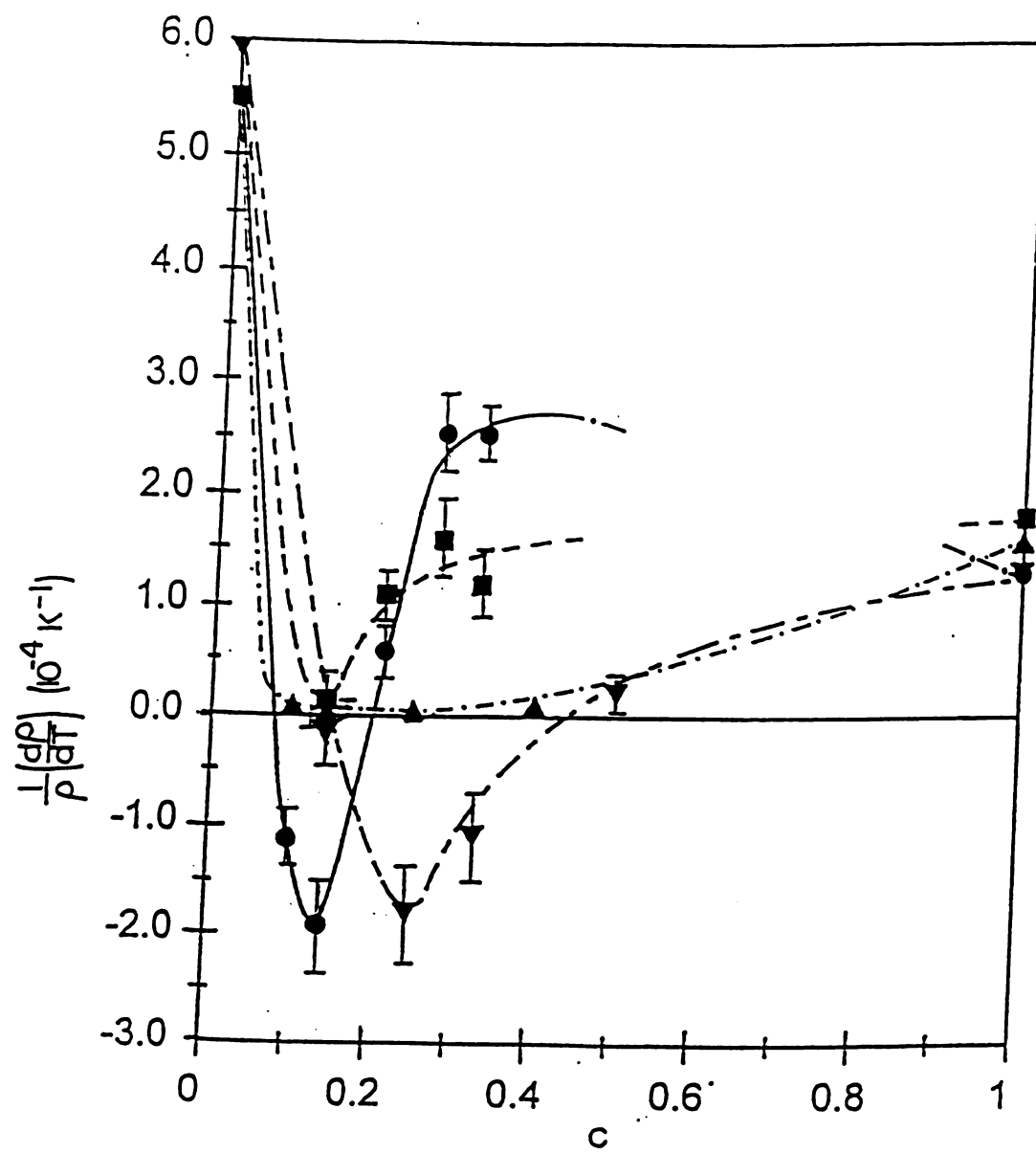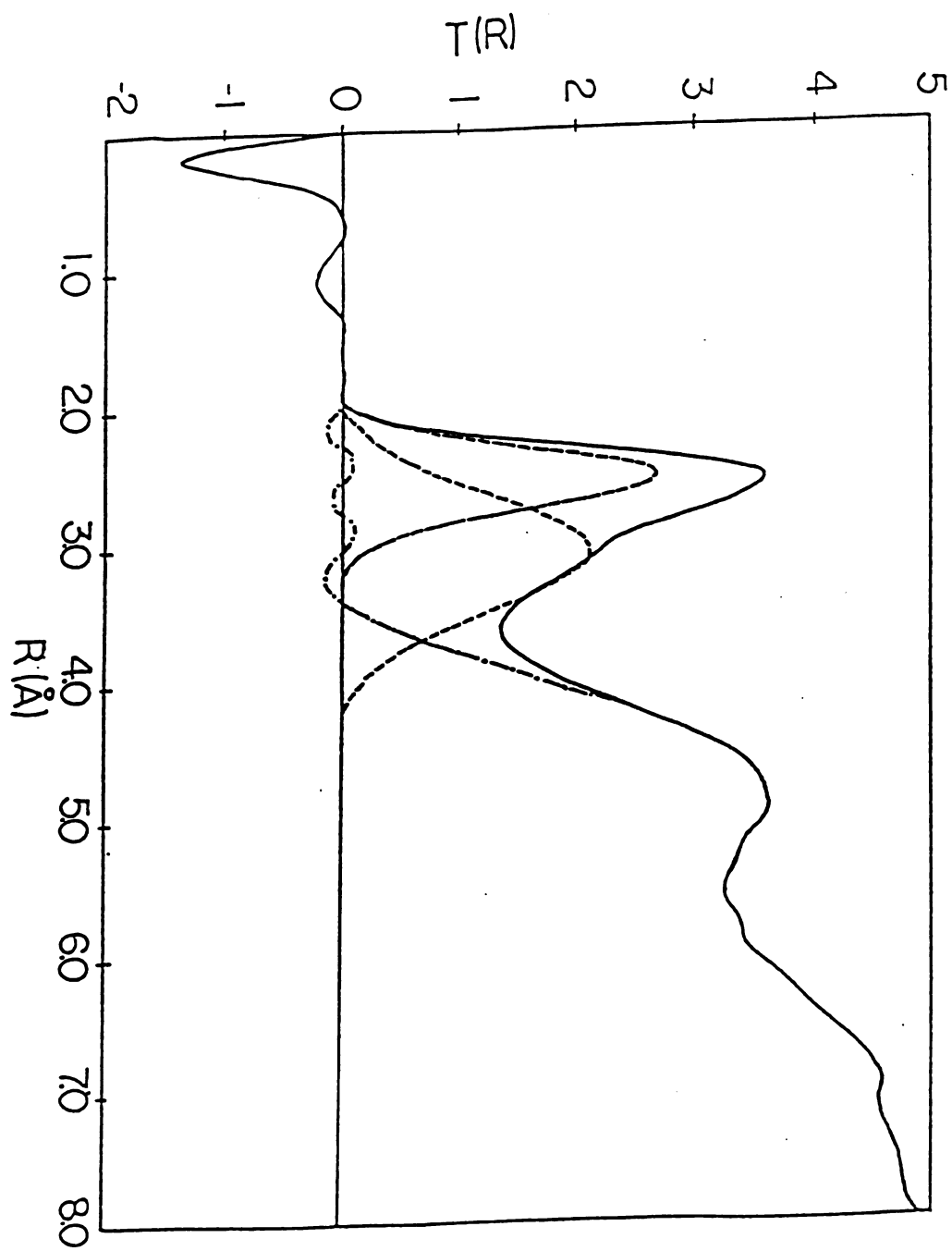
Figure 1   Figure 2

Figure 3

Figure 5
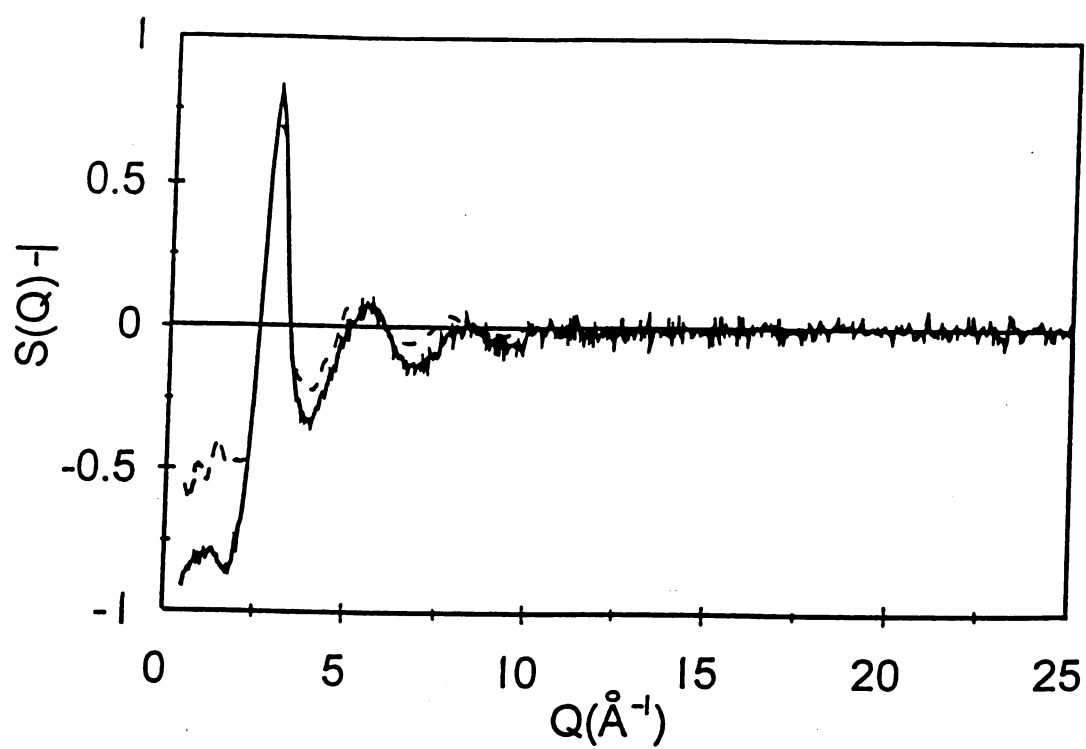
Figure 4
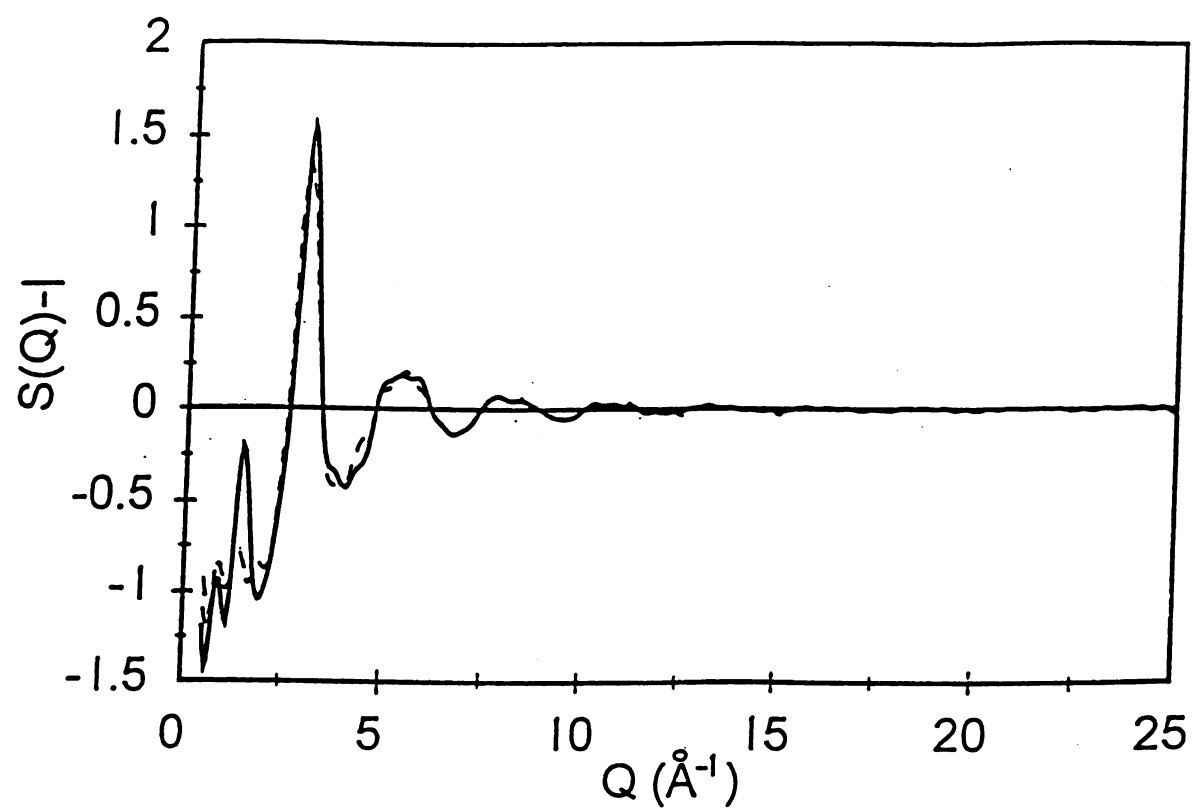
Figure 6

Figure 7

Figure 8